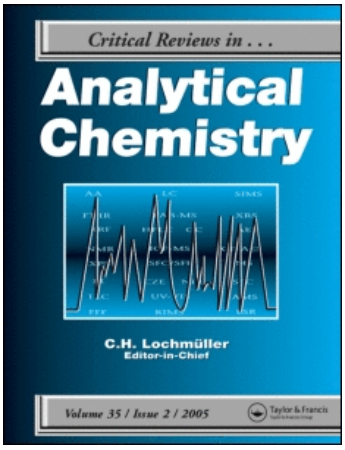

Critical Reviews in Analytical Chemistry
Publication details, including instructions for authors and subscription information:
http://www.informaworld.com/smpp/title~content=t713400837

Advances in the Application of X-Ray Photoelectron Spectroscopy (ESCA) Part I. Foundation and Established Methods

Tery L. Barr[a]
[a] Departments of Materials, Laboratory for Surface Studies, University of Wisconsin, Milwaukee, WI

To cite this Article Barr, Tery L.(1991) 'Advances in the Application of X-Ray Photoelectron Spectroscopy (ESCA) Part I. Foundation and Established Methods', Critical Reviews in Analytical Chemistry, 22: 1, 567 — 635
To link to this Article: DOI: 10.1080/10408349108055027
URL: http://dx.doi.org/10.1080/10408349108055027

TABLE OF CONTENTS

PART I

Critical Reviews in Analytical Chemistry, 22(1,2):567—635 (1991)

Advances in the Application of X-Ray Photoelectron Spectroscopy (ESCA) Part I. Foundation and Established Methods

Tery L. Barr

Department of Materials, Laboratory for Surface Studies, University of Wisconsin—Milwaukee, Milwaukee, WI 53201.

ABSTRACT: X-ray photoelectron spectroscopy (XPS or ESCA) has reached a state of maturity in which some of its common uses may be considered routine. There is a danger, however, in the possible over-interpretation of this status. (Consider, for example, the hundreds of incorrect ESCA analyses in high T_c superconductivity.) Thus, although recent advances in instrumentation have simplified general operations, they have also clearly identified a variety of previously undetected or misunderstood features in the technique that seem to suggest the potential of a more powerful analysis tool. These new areas require a much more sophisticated understanding of the photoelectron process and its potential uses. In the present article we provide a description of the background, present status, and possible future uses of some of these features of photoemission spectroscopy, including: (1) the charging shift and Fermi edge referencing, (2) valence band analysis, (3) XPS induced loss spectroscopy, (4) surface-to-bulk chemical shifts, (5) small cluster analysis, (6) photoelectron microscopy, (7) inverse photoemission, (8) resonance photoemission, (9) photoemission of adsorbed xenon, (10) photoelectron diffraction, and (11) liquid phase photoemission. (Some prejudicial discretion has been exercised in the degree of emphasis on each of these topics.) Novel analyses are described of various oxides (including zeolites and high T_c superconductors), inert hydrocarbon polymers, carbon filled metal ceramics, supported metals catalysts, unique structures, and a variety of other systems. This review is divided into two parts. The first part treats the developmental and theoretical background of ESCA in detail, including established ESCA procedures (up to recent studies of the causes and uses of loss spectroscopy in ESCA), laying the basis for the description and elaboration of promising new directions in ESCA given in part two of this review. This two-part work is intended to serve as a useful treatise defining the underlying characteristics and broad capabilities of the ESCA technique.

* Written, in part, while the author was associated with The Faculty Research Participation Program in the Chemistry Division, Argonne National Laboratory, under the following Federal Grant US DOE BES-Materials Sciences, under contract W-31-109-Eng 38.

KEY WORDS: X-ray photoelectron spectroscopy, ESCA.

I. INTRODUCTION

A. Introductory Statement

The following is intended as a review of recent advances in the science of photoelectron spectroscopy, particularly the branch now commonly labeled as X-ray Photoelectron Spectroscopy (XPS) or Electron Spectroscopy for Chemical Analysis (ESCA). The review is primarily aimed at the analytical user (or potential user) of the spectroscopy, and not the ESCA expert in either the instrumental or theoretical areas. Although the presentation is primarily focused on descriptions of the more recent advances, it was felt that the proper perspective for the nonexpert would be aided by also reviewing the history, methods of practice, basic equipment, and fundamental theory involved. Thus, in the present review, the latter topics are used to set the stage for the principal themes to follow. Some emphasis is placed on several of the problems inherent in the methodology, particularly as *raisons d'etre* for some of the recent developments. This discussion of problems should not be construed as criticisms of the spectroscopy. The nearly 1000 ESCA units in operation throughout the world are obvious testimony to the viable

1040-8347/91/$.50

utility of the spectroscopy as the premier method for chemical analyses of surfaces.

B. Historical Perspective

The photoelectron effect had its birth in controversy. Discovered by Heinrich Hertz, in 1887,[1] as part of his monumental attempt to experimentally verify the implications of Maxwell's relations, the production of photoelectrons did the opposite, demonstrating that the (then) theory of radiation was incomplete. Numerous scientists tried diligently to mend this crack in the foundation of classical physics, but all of the good experiments merely reinforced Hertz's initial observation.[2] The theoretical explanation of the photoelectron effect awaited "The Dawn Of A New Light" as Hoffmann[3] has described the year 1905, and the contributions therein by Albert Einstein. In one of Einstein's major achievements,[4] he brilliantly employed the new quantum of energy concept of Planck[5] to explain how radiation of low intensity, but high frequency, could eject electrons from metal foils, whereas the converse might fail to produce any electrons. As a result Einstein logically evolved a consistent, single relationship that (in slightly modified form) is still today the basis of photoelectron spectroscopy, i.e.,

$$h\upsilon = 1/2\ mv_e^2 + E_b + q\Phi \qquad (1)$$

where υ i the frequency of the incoming quanta (later dubbed as "photons" by Lewis[6]), h is Planck's constant, $1/2\ mv_e^2$ the kinetic energy of the outgoing "photoelectron" of mass m and velocity v_e, q a reference charge, Φ the work function of the emitting material, and E_b the so-called "Binding Energy," expressed here against the Fermi level of the material. It is the latter feature, of course, that is the back-bone of the spectroscopy we describe in this review. Had Einstein left the argument at this point, his paper would have still been very famous, and perhaps not nearly so controversial. Unable, however, to accept the political view in place of the correct view (as he saw it), Einstein added a section to his paper challenging the totality of the Maxwellian wave theory of radiation, and suggested the possibility of a wave-particle duality.[4] Even Planck hated these "alterations" of his original concepts, and the disputes over the latter half of Einstein's paper (that ushered in the Quantum Theory of Radiation) were not completely resolved until the advent of Quantum Mechanics in the mid 1920s.[2] In fact, although Einstein's 1921 Nobel Prize was granted primarily for this paper, it specifically mentions only the first half—the laws of the photoelectron effect. To the ever honest Einstein and his growing band of followers, the dispute was illogical, as you "can't have one half of this paper without the other." In any case, all attempts (pro and con) to challenge the validity of Einstein's interpretation of the photoelectron effect succeeded instead in verifying it, culminating in the beautiful confirmation studies of Milliken.[7] Following these studies, scientists turned to attempts to use this new phenomenon, particularly as a form of spectroscopy. Preeminent in these early studies were the investigations of Robinson,[8] who easily verified that an elemental spectrum could be realized, but found that so many difficulties were inherent to these measurements that the studies did as much to discourage the evolution of this spectroscopy as to promote it. The lack of availability of a continuous, high vacuum capability, the inability to control stray interfering fields, and the unrealized need for integrated, stable electronics caused most scientists of the 1930s and 1940s to ignore the prospect of a "useful" photoelectron spectroscopy.

These problems were eventually rectified in the laboratories of Kai Siegbahn in Uppsala, Sweden.[9] Professor Siegbahn and his colleagues were initially attempting to develop a spectroscopy to examine β decay, but they soon realized that a similar version could be employed to examine photoelectrons. Using giant Helmholtz coils to "deflect" all outside fields, they achieved their first spectrum in 1955. Soon thereafter they made a dramatic discovery. The binding energy, E_B, detected for the C(ls) lines in several different carbon containing systems was (reproducibly) found to exhibit different values. The same feature was found for the two chemically different sulfurs in a thiosulfate. Thus, accurately measured photoelectron spectroscopy was found to produce *Chemical Shifts!* Professor Siegbahn and

his group were able to produce similar shifting effects for many other compounds, both in the gas state[10] and as solids.[11] They noted, as we now expect, that the photoelectrons from atoms in a more electropositive state are emitted with less kinetic energy (greater E_B), and vice versa for atoms that are made more negative. Thus, the use of photoemission to map changes in oxidation state and other chemical details seemed to be a viable possibility. Realizing the potential impact of these observations, Siegbahn dubbed his new technique, Electron Spectroscopy for Chemical Analysis, or ESCA.[12] Some other scientists have preferred to identify the method with both the nature of the excitation source and the emitted particles, thus calling it various types of photoelectron spectroscopy (e.g., XPS, when X-rays are employed as the emitting photons, and Ultraviolet Photoelectron Spectroscopy, or UPS, when UV radiation is used). The latter process was developed as a companion technique soon after the Swedish development in a number of labs, particularly those of Turner[13] and Price.[14]

Obviously the choice of radiation frequency, υ, is a matter that depends upon the experimental parameters (as long as $h\upsilon$ exceeds the so-called threshold energy, $E_b + q\Phi$). In point of fact, it is often advantageous to have available the ability to employ variable energies, such as provided by many synchrotron radiation centers. In the following, however, we will concentrate upon the area often reserved for the term ESCA (i.e., that employing X-ray emission, [XPS]). We do this for brevity, and to emphasize that area that has had, by far, the largest impact in analytical chemistry, particularly in the applied (industrial) setting. We will, however, where warranted, refer to interconnects with other radiation sources.

II. THE ESCA PROCESS

A. Basic Principles and Procedures

Although rather simple in appearance, it soon became apparent that certain difficulties prevented the ready, experimental implementation of Equation 1. One of the difficulties results from the fact that the threshold energy ($1/2\ mv_e^2 = 0$) is defined with respect to a zero at the sample vacuum level. (The vacuum level may be defined as that point in energy space that if exceeded by an electron, the latter will be completely [energetically] disassociated from its origin materials system.) This is a useful energy point for a gas (for which $\Phi = 0$), but for a solid ($\Phi \neq 0$) this reference point provides significant problems. The reason is that those features that define E_b are expressions of the atomic* chemistry of the system (i.e., $E_b = 0$ in Equation (1) defines the Fermi edge [or in the case of certain wide band gapped systems, the pseudo Fermi edge] of that part of the solid material). The work function, Φ, on the other hand, may be totally independent of that original chemistry, but does depend upon certain influences of the surrounding material units. Thus, for example, different structural faces of a particular crystal may produce different values of Φ. A figurative rendition of these properties is presented in Figure 1. Unfortunately, although measurements of E_b or Φ are relatively straight-forward, simultaneous measurements of both are not readily achieved. In order to circumvent this difficulty, Siegbahn and his group noted a very interesting feature of many solid systems.[12] If the sample to be examined is a conductor, then it can be placed in the ESCA spectrometer such that the sample is conductively coupled (in thermal and electronic equilibrium) with the conductive probe of the spectrometer. An energetic expression of this situation is displayed in Figure 1. In this arrangement the energy of the photoelectron detected by the β spectrometer may be measured against the vacuum level, E_{VL}^{SP}, of the spectrometer. The work function of the latter, Φ_{SP}, is accurately predetermined by measuring the energy of photoelectrons emitted from a particular level in a reference sample with a well established E_b (e.g., Au $4f_{7/2} = 83.96$ eV). Thus, this measurement determines the Fermi level of the spectrometer, E_F^{SP}. If the spectrometer system is reasonably stable, this value may be retained for a substantial period of time, and reevaluation, when needed, should be relatively simple. Thus, the binding energies of all conductive samples may be measured, because of the Fermi

* We refer herein to the basic unit site in the solid as *atomic*, although in reality this fundamental chemical component may be molecular or even a solid unit cell.

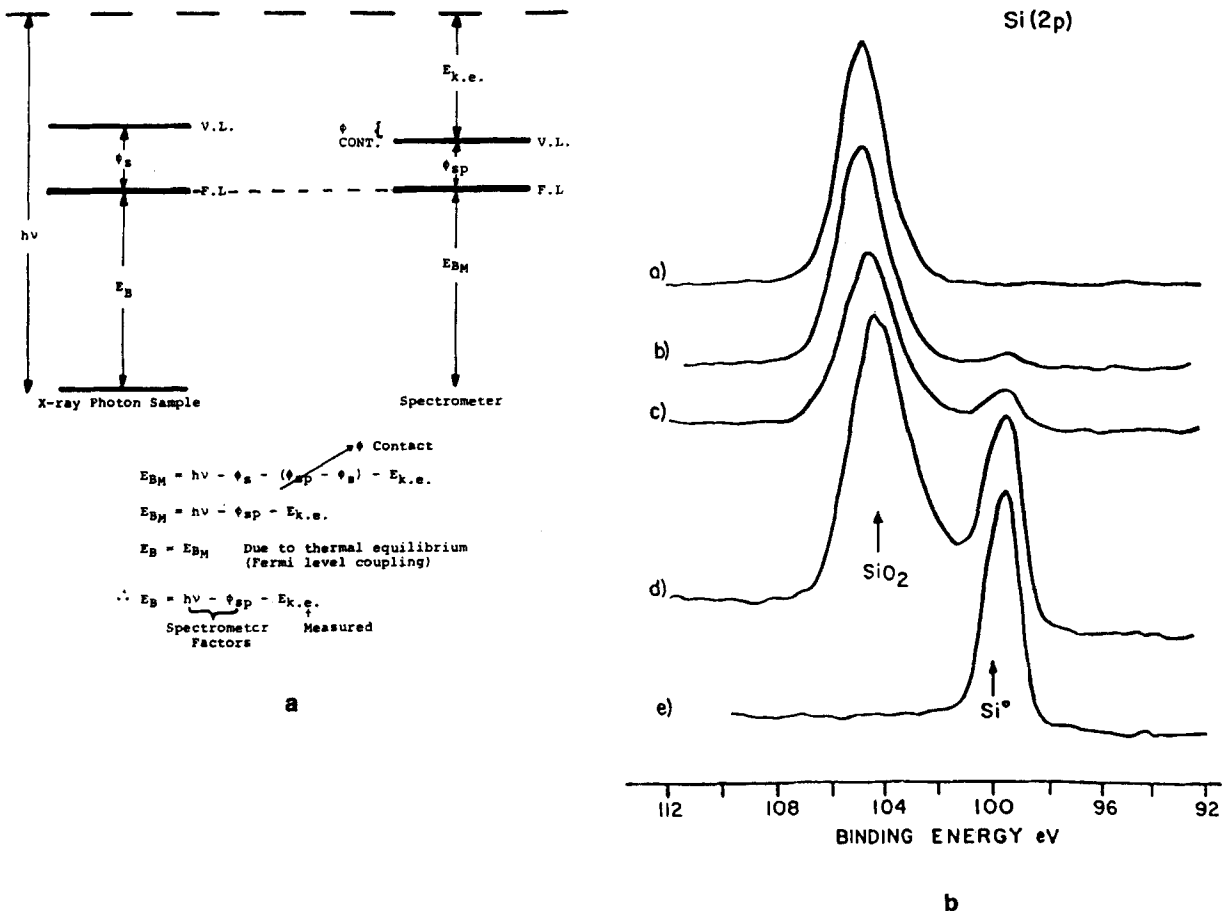

FIGURE 1. (a) ESCA binding energies and chemical shifts for conductive samples: energy level scheme (based on Siegbahn coupling of Fermi edges). (b) ESCA binding energies and chemical shifts for conductive samples: representative binding energies and chemical shifts.

edge coupling relative to the spectrometer work function value, Φ_{SP}, see Figure 1.

Viewed in terms of Figure 1b, the aforementioned chemical shifts arise due to the small changes in E_b that may often occur (even for core level peaks) as a result of changes in the chemical (electronic state) environment of an atom, designated here as A, as registered by its jth state. Thus, the energy change, $\Delta E^m_{A(j)}$ $(1 \rightarrow 2)$ from state $1 \rightarrow 2$, is given by

$$\Delta E^m_{A(j)}(1 \rightarrow 2) = E^m_{bA(j)}(2) - E^m_{bA(j)}(1) \quad (2)$$

B. Problems: Relaxation and Satellites

All of this would appear to be very straightforward, and indeed the measurement of these, so-called, chemical shifts, for many materials, is easily accomplished. Thus, we find ready production of chemical shift data, such as that reported in Table 1. The problem, however, is that any ready interpretation that $\Delta E^m_{A(j)}$ $(1 \rightarrow 2)$ is caused only be the chemical changes experienced by atom A in going from situation 1 to 2 may be incorrect.

There are several reasons for the latter qualifying statement. All of these reasons obviously detract from the straightforward, simple analysis of ESCA results that many casual users would appreciate. Fortunately, it often turns out that even when such problems occur, they may be ignored. In addition, close scrutiny also reveals that an understanding of these problems may produce auxillary benefits, and several of the new analytical methods, to be described next, are direct offshoots of these observations.

TABLE 1
Representative Chemical Shift Data

Element	Probable oxidation state and compound	PMEP[a]	BE and selected line widths[b] for PMEP	Oxide BE O(1s)	Hydroxide BE O(1s)
Pd	Pd^0	$Pd(3d_{5/2})$	335.45(1.00)		
	PdO	$Pd(3d_{5/2})$	336.9	530.1	
	PdO_2	$Pd(3d_{5/2})$	?	?	
	$Pd(OH)_4$	$Pd(3d_{5/2})$	338.55		?
	$PdSO_4$	$Pd(3d_{5/2})$	338.7[c]		
	$PdBr_2$	$Pd(3d_{5/2})$	337.7[c]		
Ni	Ni^0	$Ni(2p_{3/2})$	852.75		
	NiO	$Ni(2p_{3/2})$	854.6	530.0	
	Ni_2O_3	$Ni(2p_{3/2})$	855.7	530.0	531.7
	$Ni(OH)_2$	$Ni(2p_{3/2})$	856.45		531.95
	$NiSiO_3$	$Ni(2p_{3/2})$	856.9[c]		
	NiF_2	$Ni(2p_{3/2})$	857.4[c]		
Cu	Cu^0	$Cu(2p_{3/2})$	932.47(1.01)		
	CuO	$Cu(2p_{3/2})$	933.7	530.3	
	Cu_2O	$Cu(2p_{3/2})$	932.5(1.2)		531.7
	$Cu(OH)_2$	$Cu(2p_{3/2})$	934.75		
Si	Si^0	Si(2p)	99.15		
	SiO_2	Si(2p)	102.5	531.7	
	$Si(OH)_4$	Si(2p)	103.0		531.9
Zr	Zr^0	$Zr(3d_{5/2})$	179.6		
	ZrO_2	$Zr(3d_{5/2})$	182.2	529.9	
	$Zr(OH)_4$	$Zr(3d_{5/2})$	183.6		531.2
Mo	Mo^0	$Mo(3d_{5/2})$	227.95		
	Mo_2O_5	$Mo(3d_{5/2})$	231.6	?	
	MoO_3	$Mo(3d_{5/2})$	232.3	530.5	531.9
	MoO_3XH_2O	$Mo(3d_{5/2})$	232.6	530.4	
S	NiS	S(2p)	162.8[d]		
	Na_2SO_3	S(2p)	166.6[e]		
	$CuSO_4$	S(2p)	169.1[d]		

[a] Principal metal ESCA peak.
[b] Line widths are enclosed in parentheses.
[c] Wagner, C. D., Gale, L. H., and Raymond, R. H., *Anal. Chem.*, 51, 466, 1979.
[d] Wagner, C. D. and Taylor, J. A., *J. Electron Spectrosc., Relat. Phenom.*, 20, 83, 1980.
[e] Wagner, C. D. and Taylor, J. A., *J. Electron Spectrosc., Relat. Phenom.*, 28, 211, 1982.

Source: Except as footnoted, all values from: Barr, T. L., *J. Phys. Chem.*, 82, 1801, 1978. With permission.

In order to understand these problems, it is important to note that the measured binding energy, E_b^m, is, in fact, determined as an energy difference between that for the N electron system in question immediately before measurements, $E_I(N)$, and that for the state of the $N-1$ electron system at the point of photoelectron detection, $E_F(N-1)$, i.e.,

$$E^m_{A(j)}(1) = E_F(N-1) - E_I(N) \qquad (3)$$

where I is our designation for the appropriate

premeasurement, initial state, and F designates the corresponding post measurement, final state, for atom A, in chemical environment 1 as measured (m). The measurement is accomplished using the photoemission from the jth electronic state. Displayed in these terms, it is not hard to see where the chemical argument arises. If we assume that we can represent our atom by typical "chemical" arguments (quantum mechanically, this means electrons in specific orbitals for models calculated [perhaps] to the Hartree-Fock limit). Then, in order for this chemical (only) shift to be true, it is necessary that one is able to associate the energy difference in Equation 2 with differences in specific, premeasurement, orbital energies, ϵ, i.e.,

$$E^{m}_{A(j)}(1) = -\epsilon_{A(j)}(1) \qquad (4)$$

where $\epsilon_{A(j)}(1)$ refers to the jth (usually core level) orbital energy for atom A in chemical state 1. Thus, in this model the measured *chemical shift* defined in Equation 2 is given simply by the energy difference experienced by a particular orbital state for atom A in two different chemical environments, i.e.,

$$\Delta E^{m}_{A(j)}(1 \rightarrow 2) = \epsilon_{A(j)}(2) - \epsilon_{A(j)}(1) \qquad (5)$$

Thus, the two ϵ's in Equation 5 may represent, for example, the C(ls) orbital energies for carbon in $FeCO_3$,(1), and FeC,(2), etc.

Those readers who are familiar with quantum mechanics will have already noted that this description is flawed or limited by our choice of the "one-electron" or orbital energy argument. In so doing, we have ignored the correlation energy,[15] but we have retained that feature labeled herein as the "chemical" environment. It turns out that this correlation deficiency is generally not very large, particularly when viewed from a qualitative perspective.[16]

Another feature is ignored in Equation 5 that is much more serious, at least from the standpoint of a fundamental understanding of ESCA. Close scrutiny of Equations 3 and 4 will show that inherent to these steps is the assumption that the N − 1 balance of electrons retained in the A system during, and following, photoelectron ejection are unaffected by that process, at least insofar as the time frame of the measurement process of the photoelectrons is concerned. In terms of the orbital, or one-electron, model this is often referred to as the *Frozen Orbital Model* (i.e., in this approach the orbital states of the N − 1 electrons remain frozen in their initial states during the photoelectron ejection and detection).[17] When the orbital picture has been "perfected" to the point of the Hartree-Fock limit this feature comes under the general heading of Koopman's theorem (KT),[18] and therefore one will find the designation:

$$E^{m}_{A(j)}(1) \cong -\epsilon^{KT}_{A(j)}(1) \qquad (6)$$

often appearing in the literature.[16] Unfortunately this model is fundamentally flawed, as all photoelectron measurements suffer from some degree of energy relaxation and/or secondary electron, satellite emissions as a result of the response of the N-1 electron set to the photoemission of the electron in question. As a result of these (final state) effects, it should be obvious that the totally initial state, chemical (Koopman's theorem) argument expressed in Equation 6 is incomplete. This complicates, to some degree, the interpretations of ESCA. In addition, these relaxation shifts and satellite peaks play an integral role in some of the new auxillary techniques described later in this review. Further discussion of the implications of these effects requires quantum mechanical considerations, which are presented in Section IV.

C. Problems: Introduction to Charging and Fermi Edge Coupling

Another difficulty in the ESCA measurement process results from the previous assertion of conductivity as a property needed for samples in order to apply the Fermi edge coupling-binding energy measurement process. This would seem to restrict ESCA to studies of reasonably good conductors. Fortunately this is not the case. One should note that the measurement process refers to the Fermi edge (thermal and electronic equilibrium) coupling with the conductive part of the probe at room temperature. It appears that all reasonable conductors (in most physical environments) and many narrow band gapped semicon-

ductors can generally be configured (as samples) to meet the latter criterion for ESCA. This is true because sufficient intrinsic conductivity and "stray" electrons are present in these materials to provide that coupling. In the case of wide band gapped semiconductors and insulators, however, the situation is different and energy measurement problems result. There is no obvious point where this differentiation of material-type occurs, except that the author has noted that he has been able to achieve Fermi edge coupling using a commercial ESCA system (Hewlett-Packard 5950A) for many configurations of elemental silicon (Si°), ($E_g \sim 1.1$ eV), whereas slight Fermi edge decouplings were found during similar ESCA investigations of thin films of InN ($E_g \sim 1.7$ eV), in the same system. It is readily apparent that a variety of micro and macromorphological factors substantially influence these decoupling results. For example, a thick wafer of alumina, Al_2O_3 ($E_g \sim 9.0$ eV), behaves as an obvious insulator and produces substantial decoupling,[19] with its ensuing problems, whereas the space charge or Schottky Barrier flow of electrons from conductor to nonconductor prevents decoupling in the first few monolayers of Al_2O_3 grown on top of conductive Al°.[19] All of this is considered later in more detail.

The most obvious problem that occurs as a result of Fermi edge decoupling is *charging*,[19,20] (see Figure 2). This is a multifaceted process, by which many nonconductive samples subjected to photoelectron (and related electron) emission build up macroscopic (surface and near surface oriented) clusters of positive charges that produce a Volta potential that results in a "drag" on the outgoing photoelectrons. As a result, a *charging shift* upfield (to higher binding energy) occurs in the measured binding energy scale. Numerous factors, including macromorphology, chemistry, uniformity of microstructure, etc., influence the size of this charging shift, which has been found to vary from a few tenths of an eV, to more than 100 eV. When significant charging occurs, it is never entirely uniform (i.e., there is always some form of differential charging across the sample),[20] and substantial (broadening-type) distortions of the ESCA peaks generally result (see Figure 3). Thus, the ESCA peaks may not only shift to an unrealistic, large, binding energy, they may also distort, sometimes beyond recognition. It is quite obvious that when the latter occurs some form of rectification is necessary. In fact, since the charging effect has varied, often nonchemical causes, there may be advantages in always trying to remove it.[20,21] This often may be (substantially) achieved using some form of low energy, electron source (e.g., an electron flood, or neutralization, gun). An example of this type of situation is presented in Figure 3.

Unfortunately, it often goes unrecognized that removal of the charging shift, even when totally successful, generally does not produce a "valid" binding energy by the previously described conventional measurement procedure.[20,22] This occurs because, as explained above, precise binding energy measurements in the conventional ESCA spectrometer require the coupling of the Fermi edge of the sample involved with that of the spectrometer. "Neutralization" of an insulating solid may leave its electronic energy scale still floating with respect to that of the spectrometer. In fact, it may be argued that an insulator does not even have a Fermi edge to use in this coupling process. (It is possible, however, to induce a Fermi edge into some insulators and promote the aforementioned coupling, but the procedure for doing this generally alters the physical and chemical status of the sample).[23]

The most common procedure for producing valid binding energies for nonconductive solids, therefore, has been to reference all binding energies to that for a particular constituent (or dopant) with a purportedly fixed, easily reproduced set of binding energies. Often, in fact, the C(ls) binding energy of the ubiquitous, adventitious carbon, generally deposited on all air exposed surfaces, is employed for this purpose[24] (see Section VI). Although generally utilized (and often correctly so) this "reference" method is fraught with potential problems, since such features as morphology, degree of dispersion, and other variable parameters may significantly alter the basis for these measurement procedures.[25] As a result, a variety of alternative techniques for the removal of charging and establishing the valid Fermi edge have been developed. None of the techniques appear to be a panacea, while most have at least specialized merit. Some of these newer techniques are outlined later in this review.

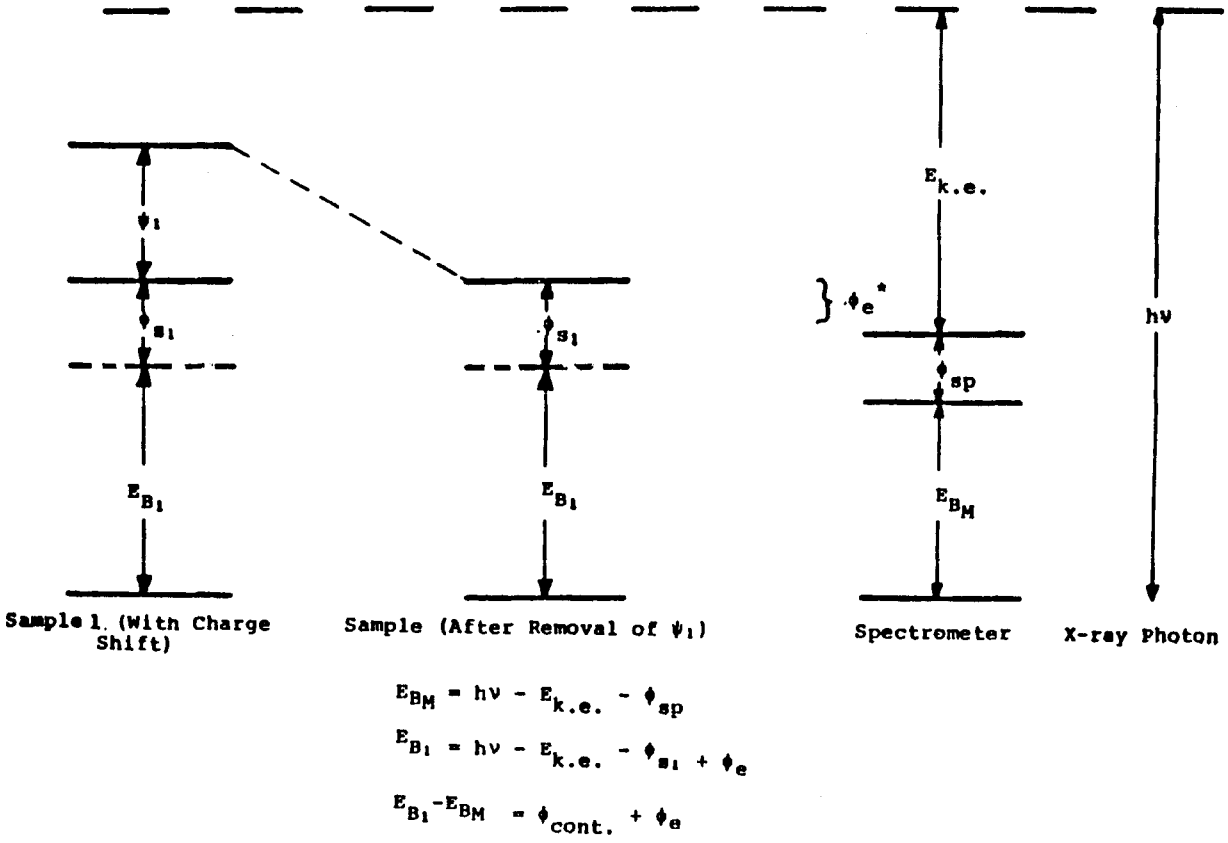

FIGURE 2. Energy level scheme for nonconductive sample.

Interestingly, in our own studies we have discovered that the variable presence of charging and decoupling (particularly of the differential type) actually provides an auxillary tool for materials analysis by ESCA that, in some cases, produces unique results.[20,26,27] Hence these studies are likewise described later in this review.

D. Summary of the Pros and Cons of Conventional ESCA

In summary, we have noted that the basic ESCA process provides a rather straightforward measurement procedure that generally produces readily identified peaks, particularly from core level emissions. Shifting patterns in the binding energies of these peaks were originally determined by the Siegbahn group to indicate changes in chemistry. In order to fix a common reproducible scale for these binding energies, the Siegbahn group recommended Fermi edge coupling between the (conductive) sample and the spectrometer.[12]

Unfortunately, several problems interfere with the total, ready use of these arguments and methods for all systems. Thus, we have suggested that the measurement process itself interferes with the actual measured binding energy values by mixing relaxation and/or satellite peak effects into the chemical (initial state) arguments. The latter would be preferred by those seeking a simple "chemical" shift. We also have shown that nonconductive materials may be subjected to Fermi edge decoupling and a charging shift following photoelectron ejection. As stated earlier, these effects tend to complicate the measured results.

Fortunately, as we have seen, it is often possible to ignore or remove these difficulties. In addition, we describe in some detail how various aspects of these "problem" phenomena may be used as important auxillary tools. First, however, it will be useful to describe the basic rudiments of the experimental systems, and the quantum concepts, that are the basis of the ESCA process.

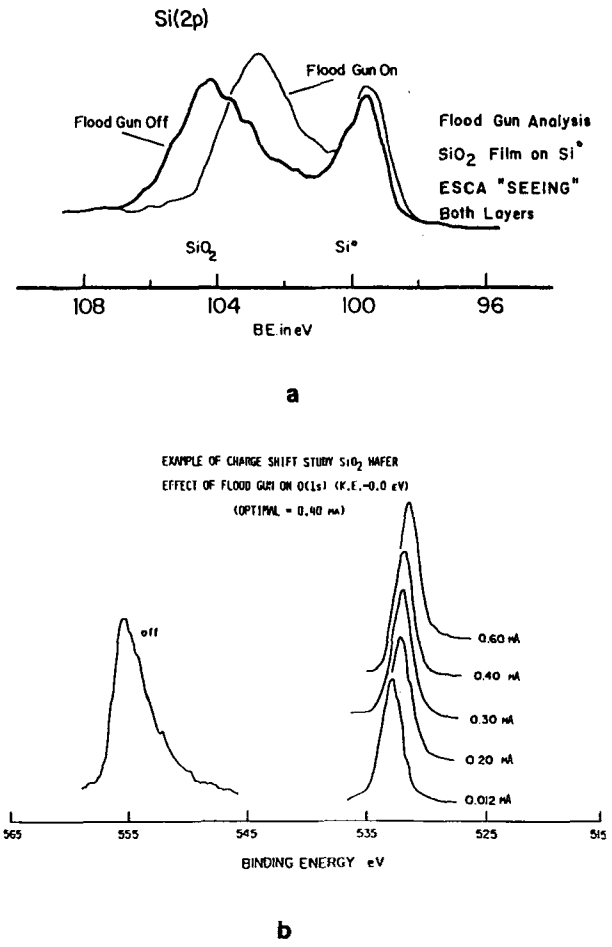

FIGURE 3. Representative charging case from ESCA: (a) SiO_2 film on Si°; (b) pressed wafer of SiO_2 powder.

III. THE ESCA SPECTROMETER

A. Introduction to the Basic System

The conventional commercial ESCA experiment generally employs either $Al_{k\alpha}$ (1486 eV) or $Mg_{k\alpha}$ (1254 eV) X-radiation. Whether utilized with direct "line of sight" from the X-ray anode, or a crystal monochromator, the incidence angle of the X-rays are typically in the range of 33 to 90 degrees, with respect to the sample normal. The ejected photoelectrons are often collected along this sample normal, although almost all angles down to the specular are employed. Initially, a variety of electron (or β) analyzers were employed to collect and energy sector the photoelectrons, with particular use of either hemispherical or cylindrical mirror systems. Many spectrometer manufacturers originally employed various arrangements of different sized slits to introduce and remove the photoelectrons from these analyzers. The lack of consistently satisfactory results also has generally led to the use of a variety of lens systems (electrostatic or magnetic) that are employed (often with slits) to focus the photoelectrons properly inside the analyzer. Recently most manufacturers have realized the superiority of the hemispherical analyzer for the ESCA process.[28] A typical arrangement of this type is displayed in Figure 4. A variety of detectors, often arranged into particular geometries, are employed to collect the final electron emissions. Successful detectors have included channeltrons, micro-channel plates, and resistive anode plates, often coupled with various arrangements of phosphor screens and high sensitivity TV cameras.

B. Extensions and Improvements

1. Monochromators—High Resolution and Acute Sensitivity

As mentioned earlier, conventional ESCA is still often accomplished employing direct impingement of the relatively soft X-rays from their anode source onto the sample of interest. This approach is generally simple to operate and permits the maximum use of the photon density, and thus the maximum "flexibility" with the *total* electron output. Early in the use of ESCA, however, the University of Uppsala group under Kai Siegbahn recognized that this simple approach often defeated some of the purported attributes of the ESCA technique.[29] To illustrate: (1) direct X-ray impingement with its accompanying thermal effects and additional "stray" particles (e.g., Bremsstrahlung, etc.) was sometimes found not to provide a "nondestructive" analytical method, as generally advertised (e.g., direct impingement ESCA cases were reported that beam reduced some samples [e.g., Cu^{++} to Cu^{+}],[30] and seriously chemically damaged various polymers);[31] (2) the secondary electron continuum mentioned above was often so large that it produced a signal to background that sometimes interfered with the detection of weak peaks; (3) concepts of optics dictated that the maximum electron output res-

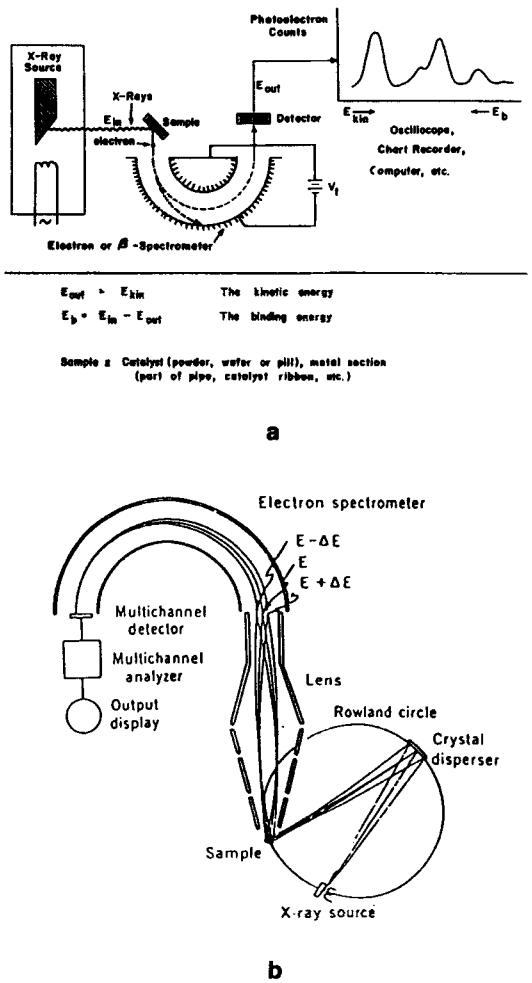

FIGURE 4. (a) Generalized schematic for ESCA spectrometer and typical results. (b) Figurative rendition of older monochromator based ESCA.

olution (minimum line width) could not exceed that of the input X-ray line; (4) all of the significant satellites exhibited by the impinging X-ray line also produce photoelectron peaks, sometimes in binding energy regions that screened the peaks of sparse species or interfered with chemical shift registration.

Faced with these difficulties, the Siegbahn group proposed,[29] demonstrated[32] and brought to general practice the use of monochromatically scattered X-rays. This led to the development and demonstration[33] of the use of geometrically rearranged silica (quartz) crystals, bent to produce the proper Bragg angle, such that a Rowland circle arrangement will permit the focus on the sample of a diffracted segment of the principal $Al_{k\alpha}$ X-ray peak. As a result, the beam damage is substantially curtailed,[33] line widths may be reduced (often by several times), and the general background may be sufficiently reduced to realize an improvement in signal-to-background of several orders of magnitude.

Unfortunately, however, the carefully worked out details of the Uppsala arguments were often not totally heeded. Thus, many manufacturers and practitioners failed to note that successful implementation of an X-ray monochromator often depends upon the care employed to couple it with the *proper* electron spectrometer (particularly, the right arrangement of lenses and hemispherical analyzer). Originally, for example, the Siegbahn group suggested a dispersion compensation arrangement for X-ray monochromator and electron lense, which could, theoretically, completely decouple the output resolution from that of the input.[32] This arrangement was successfully implemented in the Hewlett-Packard ESCA system marketed from 1971 to 1976.[33]

Most manufacturers have finally realized the importance of providing a satisfactory monochromatic option to the conventional direct impingement system. It is now not uncommon for systems to be equipped with both procedures, permitting the use of the faster, high intensity, moderate resolution in cases where sensitivity or resolution is not critical, with relatively easy conversion to a high resolution/acute sensitivity monochromatic mode.

2. Other Developments — Spacial Resolution

Several other recent improvements in ESCA technology deserve special mention. It is now possible to fine focus the X-ray beam before monochromatizating, thus permitting enhanced spacial resolution with further enhancement in energy resolution.[34] It is also possible to adroitly employ the lens and slit system to segment the spacial aspects of the photoelectron output. Focusing of the latter output would appear to permit even greater spacial resolution (1 μm or less is predicted) with rastering.[35] Fine focus of the X-rays, however, also permits a much more intense

(faster) small spot analysis. It should be apparent that all of these improvements have ushered in a period of intensive effort in spacial analysis, thus effectively removing one of the often mentioned shortcomings of ESCA — the statistical (relatively large x-y) nature of its analysis.[36] With recent alterations, one may now routinely switch many systems from "large spot" (analysis generally of the order of 1 to 5 mm in diameter) to small spot inside the same experiment, thus permitting the sequential realization of the advantages of both approaches. These small spot capabilities have naturally led to the successful beginnings of a form of "photoelectron microscopy" (see Section VIII.) with the obvious goal of providing a replacement (or at least supplement) for modest electron microscopy and/or Auger microscopy, in a mode that will simultaneously provide detailed chemical, as well as qualitative analysis.

C. The Present Performance Frontier

Subsequent developments in resolution and sensitivity have recognized not only the need to optimize the separate features of ESCA systems (e.g., source, monochromator, sample presentation and treatment capability, lenses, slits, hemispherical analyzer, detector, and data system), but have also noted that this improvement will depend particularly upon the ability of the spectrometer manufacturer to optimize most (if not all) of these features into a simultaneous, cohesive package.[37] On the commercial front this motivation is presently best represented by the new system being produced in Uppsala, Sweden by Scienta Instruments AB.[38] This system (depicted in Figure 5) begins with a fine focus electron gun that is employed to eject $Al_{k\alpha}$ X-rays from an anode that is electroplated onto the circumference of a high speed (~10,000 rpm) rotor (rotating anode). These X-rays are then focused onto 7+ strategically bent and placed quartz crystals, aligned on an adjustable backing plate. The monochromatic, diffraction scattered output of the latter is further focused onto a sample strategically placed to form the optimal Rowland circle geometry with both the anode and silica crystals. A multistaged, high resolution, electrostatic lens is employed to collect the photoelectron output, and channel it through a 650 mm diameter hemispherical analyzer using various intermediate slits. Final detection is achieved with a microchannel plate detector, phosphor and a computer interfaced CCD TV camera. The preliminary resolution achieved by this system (see Figure 6) exceeds that of any other commercial instrument, and the sensitivity enhancement appears to be more than an order of magnitude better (see Figure 7). All of this is achieved with minimal sample damage while collecting data at a rate that not only exceeds that of all other commercial systems but also most synchroton radiation sites. Such improvements are not cheap, of course, and in the view of some practioners, may not be necessary, particularly if the desired results fall into an area loosely labeled as "conventional" ESCA. It should be noted, however, that many of the more sophisticated techniques to be described later in this review (Sections VI to VIII) are substantially enhanced by technology, like that employed in the Scienta 300. Thus, the fact that both photons and electrons are focused in the Scienta system produced the resolution and geometry needed for some applications in surface-to-bulk photoemission, photoelectron diffraction and photoelectron microscopy (see Section VIII). It is also possible with adroit plating or rotor wheel choice to achieve reasonable monochromatic output from several X-ray sources at substantially different energies (e.g., $Al_{k\alpha}$ and $Cr_{k\beta}$). Thus, a system configured similar to the Scienta may, for some purposes, function as a reasonable "in house" alternative to synchroton radiation.

IV. QUANTUM MECHANICAL ARGUMENTS

A. Introduction to the Total (Primarily Elastic) Process

The quantum mechanics of the photoelectron process has been considered previously in detail by various researchers, particularly Feibelman and Eastman,[39] Cederbaum,[40] Penn,[41] Pendry,[42] and others.[43] As stated above, due to our primary analytical goal, we are not herein concerned with

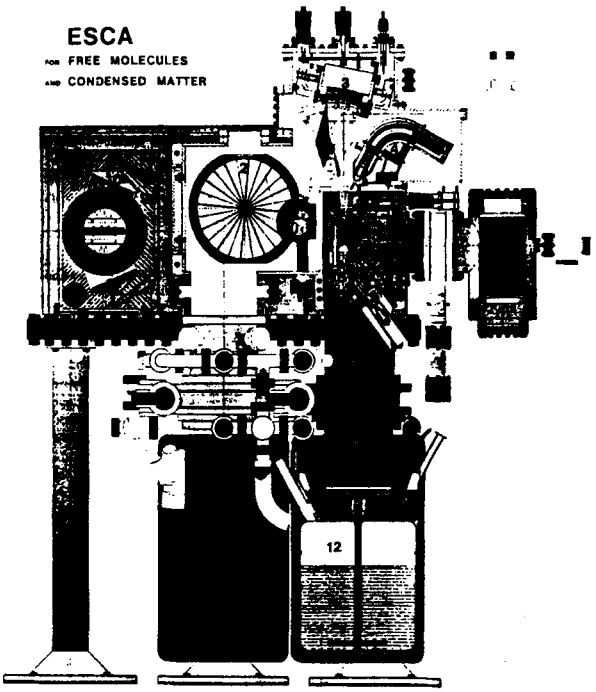

Vertical cross section through the instrument. The numbers show: 1. high power e^--gun; 2. rotating anode; 3. multicrystal monochromator; 4. monochromatic e^--source; 5. UV-source with grating; 6. fine focus e^--source; 7. electron lens system; 8. outer hemispherical electrode; 9. inner hemispherical electrode; 10. terminating electrodes; 11. multidetector; 12. cryopumps.

a

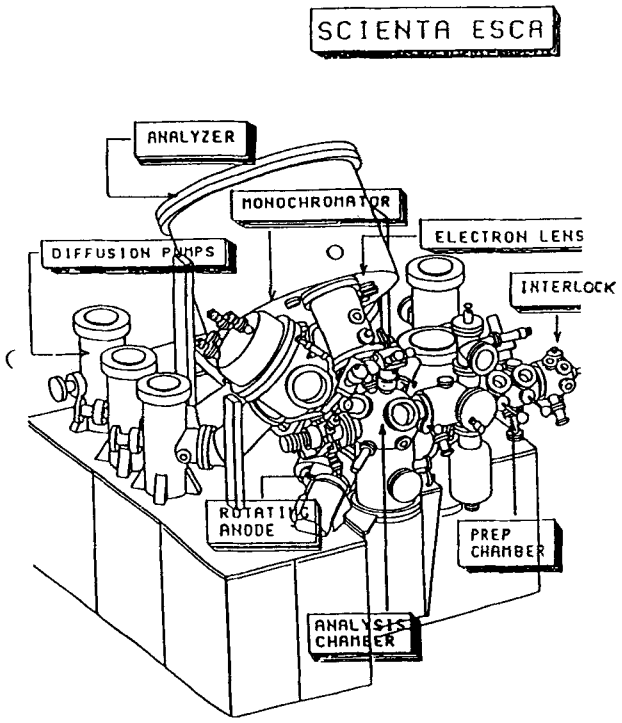

b

FIGURE 5. (a) Cutaway rendition of precursor to present commercial Scienta ESCA. (b) Pictorial representation of present day commercial Scienta ESCA.

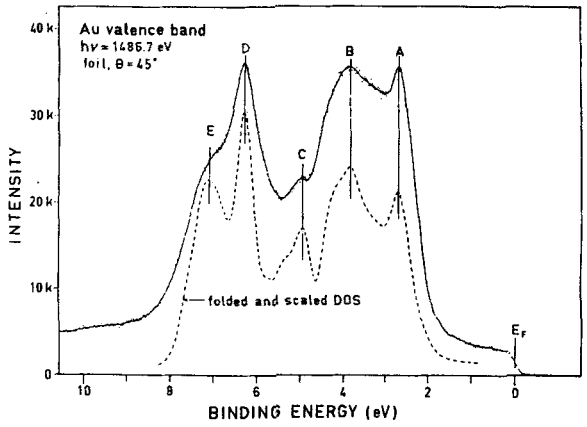

a

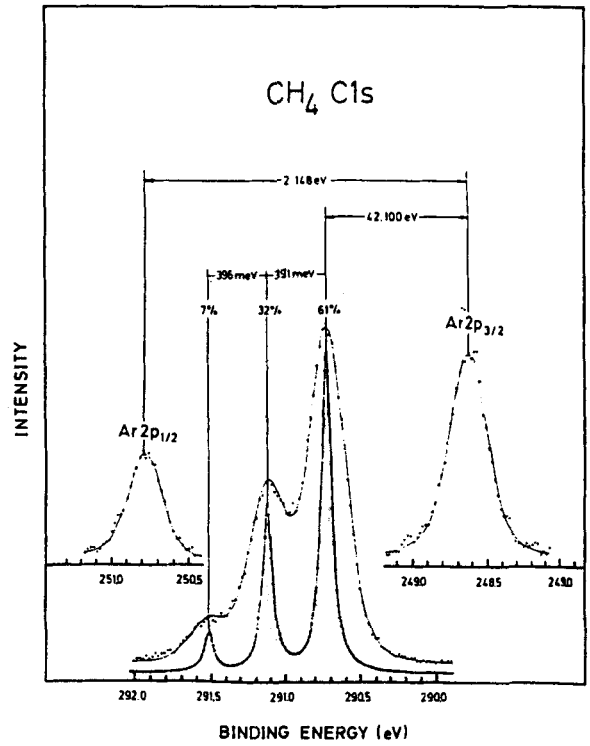

b

FIGURE 6. Typical set of high resolution valence band and gas phase core level result achieved with Scienta precursor.

these details; therefore, we present here only a cursory outline, paying particular attention only to those parts that deal specifically with several relatively new processes that are featured in this review (Sections VI to VIII).

A number of years ago, Spicer[44] developed a useful model of the photoelectron phenomenon as a three staged scattering process. In this review we follow the lead of Sunjic,[45] who has presented a particularly succinct version of this model. The three steps include

(1) In the first step we consider the electronic state of the solid material of interest to be described by a many-electron state function, $|\Psi_I\rangle$, which we hope to adequately model as a properly symmetrized set of product functions of one electron orbitals. Thus, this system is often described as an initial state in which correlation is being ignored.[46] The incoming (X-ray) photon that is nearing the surface of the solid may be described by a vector potential $\vec{A}$ (r,w). As pointed out by Sunjic, during stage 1 this potential is already being altered from its free form as it begins to interact with the solid system.

(2) As the photon field enters the solid system, it interacts with the current density, J, of the material evolving a linear coupling and scattering a particular electron, i, of momentum P_i. In the linear coupling form, the photon-material scattering potential assumes a symmetric form:

$$V = -\frac{e}{2mc}(\vec{A}\cdot\vec{P} + \vec{P}\cdot\vec{A}) \qquad (7)$$

where, as pointed out by Martin and Shirley[46] and Fadley,[47] if we consider the field of the vector potential only through the dipole approximation, then we need consider only the polarization part of $\vec{A}$, labeled here as $\vec{\epsilon}$. In this regard, Feynman[48] and others[49] have shown that to the level of the dipole approximation

$$\frac{\vec{P}}{m} \propto \upsilon\vec{r} \qquad (8)$$

When considering the radiation as a plane wave,

$$\vec{A}(\vec{r},t) = \left(\frac{8\pi\hbar c^2}{\upsilon}\right)^{1/2}\vec{\epsilon}\cos(\upsilon t - \vec{k}\cdot\vec{r}) \qquad (9)$$

where υ is the frequency of radiation spreading into the material with wave number $\vec{k}$ at $\vec{r}$. Then, in the dipole approximation

$$V \propto \vec{A}\cdot\vec{P} \qquad (10)$$

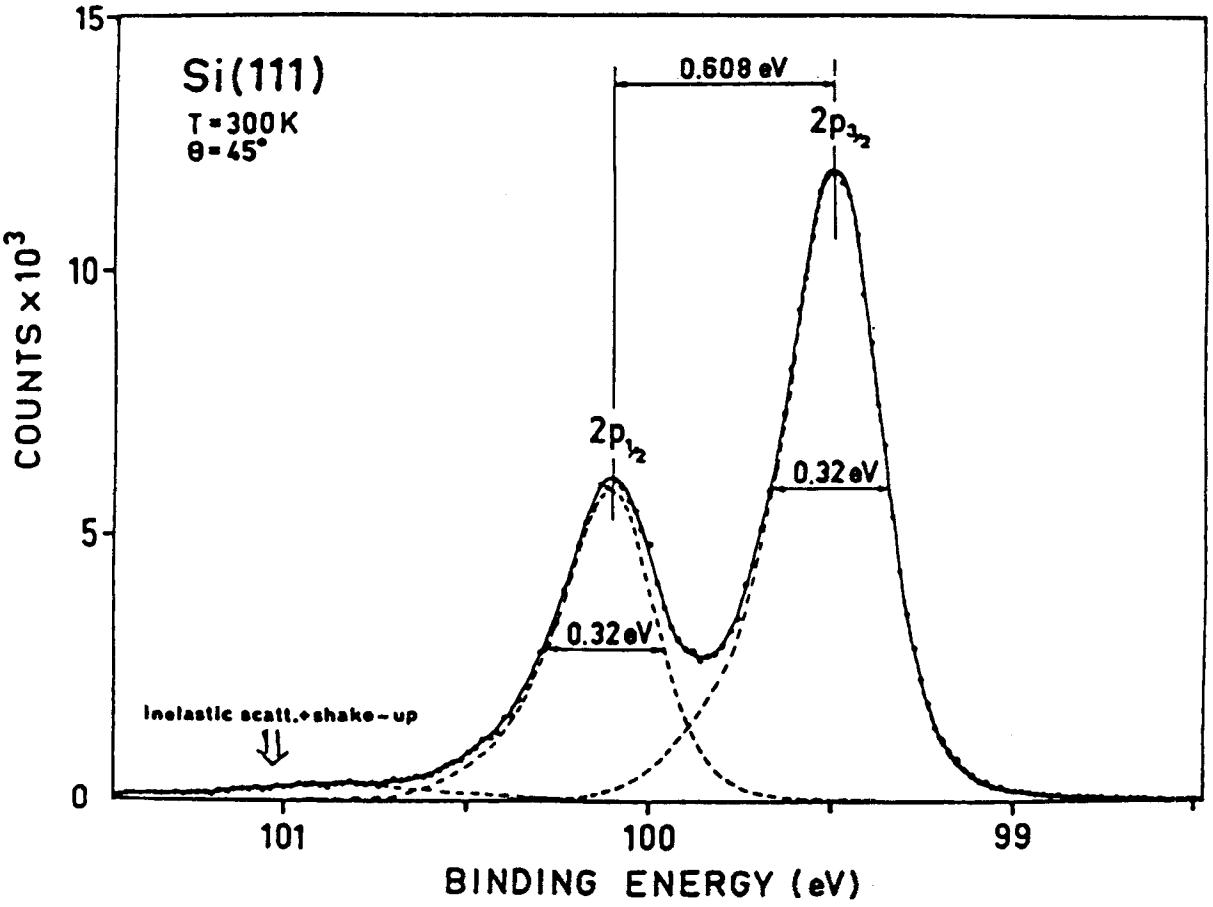

FIGURE 7. ESCA results from Scienta precursor demonstrating extreme resolution and sensitivity; SiO_2.

$$\text{and } \vec{A} \cdot \vec{P} \propto \vec{\epsilon} \cdot \vec{r} \qquad (11)$$

Thus, the quantum development can be represented at this point in terms of either a time-dependent or time-independent, many-body scattering relation. This has been described by Liebsch[50] and reiterated by Fadley,[47] i.e.,

$$|\Psi_F\rangle = \int d^3r_1 \cdots d^3r_N G(\vec{R}, \vec{r})(V)|\Psi_I\rangle \qquad (12)$$

where G is the exact many-body Green's function that motivates the "evolution" of $|\Psi_I\rangle$, the many-body initial state, to $|\Psi_F\rangle$, the corresponding many-body final state, as a result of the involvement of the potential V.

This problem is obviously beyond exact solution, but it may be substantially simplified by evoking the previously mentioned dipole approximation and the restriction mentioned in step 1 above to approximate the various exact $|\Psi\rangle$ by properly symmetrized products of one-body *orbitals*, realized, at most, up to the Hartree-Fock limit.

(3) With these restrictions the completion of the photoelectron process may be expressed as a V-perturbed one electron process evolving against a possible background of final-state interacting (excited) electron-hole pairs[45] (i.e., for the scattering cross section, σ_{dipole}),

$$\sigma_{dipole} \alpha \underbrace{\frac{1}{h\upsilon}|\langle\psi_f(\vec{r}, \vec{k})|\vec{\epsilon} \cdot \vec{r}|\phi_i(\vec{k})\rangle|^2}_{\text{I}} \cdot \underbrace{|\langle\Psi_F(N-1)|\Psi_I(N-1)\rangle|^2}_{\text{II}} \cdot \underbrace{\delta(\epsilon - \epsilon_{h\upsilon} - \epsilon_{fs})}_{\text{III}} \qquad (13)$$

where ϕ is a valid one-electron (perhaps H.F.) orbital from which the electron is to be scattered

(i.e., in this model ϕ_i is an orbital part of $\Psi_I(N)$, and $\psi_f(r,k)$ is the outgoing photoelectron state of the scattered electrons). The term I is, thus, the rendition of the photon-induced electron scattering into the photoelectron state, described to the level of the dipole approximation. The outgoing nature of this situation depends upon the appropriate choice of the one electron state, ψ_f. If the photoelectron proceeds to the detector without further interaction, it is reasonable to approximate ψ_f as a simple plane wave; however, if some form of intermediate (even elastic) scattering occurs between emission and detection, a more complex form may be necessary. Thus, as shown in detail by Fadley,[47] if one considers the (ready prospect) of the photoelectron emitted by atom 1 being diffracted by its neighbors, it may be necessary to consider ψ_f as, at least, a spherical wave. In addition, as we shall describe in the section on photoelectron diffraction, the question is still being considered as to whether this scattering may be adequately treated inside a single scattering, cluster (SSC) model,[47,51] or whether the arguments of multiple scattering are needed.[52]

Outside of these elastic events the most important secondary situations that can occur as part of stage 3 of the photoelectron process are the secondary inelastic scatterings resulting in relaxations and satellite formation. The prospects for these events are carried in the scalar product in part II of Equation 13, and their energetic development (or lack there of) will be reflected in the number of terms that appear in the delta function of part III of Equation 13.

B. Inelastic Scattering Processes

1. Relaxations

In this part of the process, we are trying to connect the *final (deep hole) state* (characterized by $E_F(N-1)$ in Equation 2) back to the *initial state* (characterized by $E_I(N)$ in Equation 2). In order to attack this problem, we must introduce some additional quantum mechanical consideration. As suggested, the appropriate many body states may be reasonably expressed in terms of properly symmetrized products of one-electron orbitals. In these cases it is constructive to consider the behavior of the N-1 balance of occupied orbitals during and after the photoelectron ejection. As noted earlier in Section II it may be reasonable to consider that these N-1 electron orbital states are unaffected by the photoelectron ejection. When the Ψ states are evolved to the Hartree-Fock level, this lack of change is referred to as the Frozen Orbit Approximation.[17] (Although more appropriate for molecular than for solid state systems, the loss arguments realized in the following discussions generally apply for either type of system.)

a. Frozen Orbit Approximation

We first consider the solution to the initial state, N electron Schrödinger equation:

$$H(N)\Psi_0^A(N) = E_0^A(N)\Psi_0^A(N) \qquad (14)$$

As an approximation we consider the following approximate Hamiltonian:

$$H^0(N) = \sum_{i=1}^{N} F_i \qquad (15)$$

where F_i is the ith Fock Hamiltonian, i.e.,

$$\langle\phi_m|F_i|\phi_m\rangle = \langle\phi_m|h_0(i)|\phi_m\rangle + \sum_p \{\langle\phi_m\phi_p|v_{ij}|\phi_m\phi_p\rangle - \frac{1}{2}\langle\phi_p\phi_m|v_{ij}|\phi_m\phi_p\rangle\} \qquad (16)$$

and where

$$h_0(i) = -\left(\frac{1}{2}\nabla_i^2 + \frac{Ze^2}{r_i}\right), \text{ and} \qquad (17)$$

$$v_{ij} = \frac{e^2}{r_{ij}} \qquad (18)$$

This implies (1) that a possible (approximate) wave function, Φ_0, for Equation 14 may be constructed from Slater determinants of the orbitals in a single particle (one electron, independent particle approximation) set $\{\phi_n\}$; and (2) that each of these ϕ_n's are the ground state, Hartree-Fock

(HF) orbitals for our A system of N electrons (i.e., that they are the "best" basis set of one electron orbitals in terms of their ability to describe [minimize] the energetics of the Ath system). Any improvement upon this Φ_0 solution for the A system would require the introduction of the previously mentioned correlation (i.e., the explicit introduction of electron-electron interaction), in place of the average self-consistent field generated in the HF approximation.[17] The restriction to the HF limit is thus one that is often imposed in ESCA to avoid these complications and, in turn, to retain the ability to say that an ejected photoelectron comes from a specific orbital (e.g., Cu[$2p_{3/2}$]).

Therefore, in this approximation,

$$\Psi_0 \rightarrow A\{\phi_1(1) \cdots \phi_n(N)\} \equiv \Phi_0 \quad (19)$$

(i.e., a single Slater determinant for a closed shell system), where ϕ is an HF (spin) orbital, and A is the appropriate (anti) symmetrizer and normalization function. Note that the subfix o assumes a ground state system.

Returning now to Equation 3, we see that we have described (up to the HF limit) a solution to the second energy term on the right side of the equation, i.e.,

$$E_{I_A}(N) = \sum_{i=1}^{N} \epsilon_i \quad (20)$$

where the ϵ_i's are obtained from

$$F_i\phi_i = \epsilon_i\phi_i \quad (21)$$

Thus, ϵ_i is the HF energy for the ith state described by the HF orbital ϕ_i. Working through the details of this *Independent Particle Approximation* one finds that when the N-body wave function is a properly symmetrized product of the N single-electron orbitals, the N-body energy, E_I, is a sum of these individual orbital energies (i.e., Equation 20).

If we further suppose that the only thing accomplished by the interjection of the (X-ray) photon is the removal of the electron from say the kth orbital (i.e., nothing else happens to the system A), then

$$H^0(N-1)\Phi_0^{-k}(N-1) = E_F^{-k}(N-1)\Phi_0^{-k}(N-1) \quad (22)$$

where, $\Phi_0{}^{-k}(N-1)$ differs from $\Psi_0(N)$ only through the "disappearance" of orbital k. Therefore, if this "restriction" is logical, then

$$\Psi_0^{-k}(N-1) = A\{\phi_1(1) \cdots \phi_{k-1}(k-1)\ \phi_{k+1}(k+1) \cdots \phi_N(N)\} \quad (23)$$

and

$$E_F^{KT}(N-1) = \sum_{i=1}^{N} \epsilon_i - \epsilon_k \quad (24)$$

and therefore from Equations 3 and 20 to this level of solution

$$E_A^m = -\epsilon_k \quad (25)$$

Thus, inside the bounds of this approximation, *the measured photoelectron energy is equatable directly to the original (pre-photoelectron experiment) orbital energy, and its (k'th electron) removal by the XPS experiment merely provides the means to measure that (initial state) property.* Note that this "approximation" presupposes that the remaining N-1 orbitals will (1) either not change at all during the XPS experiment or (2) that any change they do experience will be "well after the fact," and thus not "perceived by" the photoelectron. This supposition is often called the Frozen Orbital Approximation. It was originally derived (theoretically) by Koopmans and is known to theoreticians as Koopmans' theorem; thus, the superfix "KT" in Equation 24.[18]

If this approximation is reasonably valid, we may then consider a second molecular unit (B) that also contains the same element and easily describe the (Siegbahn) chemical shift, ΔE^M, as the difference in orbital energy for these two chemical states (Equation 5). Thus, inside this approximation the measured difference between binding energies for two (or more) units is a true chemical shift (i.e., inherently a measure of only

the [initial state] chemical change experienced by the atom in question between these two systems).

Unfortunately, the Koopmans' theorem or Frozen Orbital Approximation is just that—an approximation, and it only applies (reasonably) to a few systems. Generally, there are substantial differences between the results realized one the left side of Equations 3 and 5 and those calculated employing Koopmans' theorem. Also, there are numerous, often significant, secondary peaks or relaxations realized in the experimental spectra. None of these facts can be described inside the limits of Koopman's theorem. This necessitates the documentation of final state effects that may lead to relaxations and secondary peaks, and thus remove some of the "chemical" from the (Siegbahn) chemical shift. It has been noted that the relaxation effects to be described are those for a particular orbital of a particular atom in two different chemical states. Therefore, some have suggested that these relaxation effects may often cancel when one considers the chemical shift subtraction (Equation 4). In fact, sometimes substantial parts of this relaxation do cancel. However, as demonstrated by Davis and Shirley, the relaxation to be described has both an interatomic and extraatomic part.[53] The latter, which depends primarily upon the interaction of a particular atom with its neighbors, will often vary substantially when those neighbors are changed, making the relaxation effect quite different for states 1 and 2 in a $1 \rightarrow 2$ chemical change.

b. Modification of Koopman's Theorem for Slow Electrons

If the orbitals that remain in the N-1 electron system are "allowed" to relax following ejection of a photoelectron (from $\Phi_k[m]$), then they may all evolve in time into a new set, such that:

$$\Phi_F(N-1) = A\{\phi_1'(1)\cdots\phi_{k-1}'(k-1)\,\phi_{k+1}'(k+1)\cdots\phi_N'(N)\} \quad (26)$$

where the orbitals $\{\phi_i'\}$ differ from the initial state set $\{\phi_i\}$ in that the former have relaxed (following photoelectron ejection) in an attempt to compensate for the presence of the core hole. This problem may be attacked directly, by trying to solve $H_F(N-1)\,\Psi_F = E_F\Psi_F$. However, even SCF calculations are difficult for hole-ion systems, and, therefore, other forms of approximate treatments are often employed. One way to model this process[54] is by assuming a polarization of each (retained) ϕ_i', i.e.,

$$\phi_i' = \phi_i + \delta\chi \quad (27)$$

where χ is a polarization correction to ϕ as a result of the long time retention of a hole in the vicinity of state i, and δ is the appropriate weighting. Now it should also be noted that, since our SCF H (Σ F_i) contains the orbitals explicitly, the (eigen) Hamiltonian for the best, one-body solution to the final state also must be changed to recognize this alteration, i.e.,

$$H_F^0(N-1) \cong \sum_i^{N-1} F_i' \quad (28)$$

where

$$\langle\phi|F_i'|\phi\rangle = \langle\phi|h_0(i)|\phi\rangle_p + \sum_p \{\langle\phi\phi_p'|v_{ij}|\phi\phi_p\rangle - 1|2\langle\phi\phi_p|v_{ij}'|\phi_p\phi\rangle\} \quad (29)$$

and

$$F_i'\phi_i' = \epsilon_i'\phi_i' \quad (30)$$

This approximation is often referred to as "adiabatic,"[17,54] to designate that the N−1 electron balance of the system will, following photoelectron ejection, slowly (in a relative sense) drift into the previously defined relaxed states without any discontinuous change in the Hamiltonian. Thus, comparing any point in time j with its immediate predecessor j−1, we find that E(j) = E(j−1).

In this case it has been shown by Hedin and Johansson[54] that the new final states $\{\phi_i'\}$ will shift the actual measured binding energy of the outgoing photoelectron by an amount that often may be significantly different from that predicted by the frozen orbital approximation, i.e.,

$$E^{m}_{A(j)}(1) \cong + \epsilon^{KT}_{A(j)} + E^{R}_{A(j)} \qquad (31)$$

where $E^{R}_{A(j)}$ is defined as the relaxation energy experienced by the jth orbital of the Ath atomic system.

Imposing the predefined HF limitation, and further truncating the resulting solution at a convenient point, Hedin and Johansson[54] have shown that one may express E^{R} as

$$E^{R}_{A(j)} = \frac{1}{2}\langle\phi^{A}_{j}|V_{p}|\phi^{A}_{j}\rangle \qquad (32)$$

where ϕ^{A}_{j} is the (pre-photoelectron) HF solution for the jth orbital in the A system, and V_p is defined as a polarization potential, given by

$$V_{p} = \sum_{i}(J_{ij} - \frac{1}{2}K_{ij}) \qquad (33)$$

where J_{ij} is the coulombic term, i.e.,

$$J_{ij}\phi_{j}(t) = \int \frac{\phi'_{i}(s)\phi'_{i}(s)\phi_{j}(t)}{r_{ts}}\, d\tau_{s} \qquad (34)$$

and K_{ij} is the corresponding exchange integral, i.e.,

$$K_{ij}\phi_{j}(t) = \int \frac{\phi'_{i}(s)\phi_{j}(s)\phi'_{i}(t)}{r_{ts}}\, d\tau_{s} \qquad (35)$$

where t and s label any two electrons retained in the system.

As mentioned, this description provides a reasonably accurate rendition for the final state behavior of a system that suffers a (relatively) slow ejection of a photoelectron.[54] Many observed photoelectron peaks fall into this classification. They are generally seen as singular (principal only) discrete lines in the resulting spectrum. Thus, a reasonable theoretical description of their realized ^{m} may be achieved with Equations 31 and 32.

Unfortunately, however, many photoelectrons do not exit the material system in this slow fashion. Rather they often rapidly "jump" out to the detector (in a relative sense) before this adiabatic relaxation has a chance to occur. Thus, these "fast electrons" will experience a dramatic or sudden upheaval as they evolve into the quantum world of the N − 1 electron system. This type of phenomenon is best represented in the "Sudden Approximation."[17,55]

2. Satellites—The Loss Process

a. The Sudden Approximation

Any type of sudden (fast) electron ejection may cause a discontinuous change in the N − 1 electron Hamiltonian, i.e.,

$$H(N) \rightarrow (H_{F}(N-1) + h(1)) \qquad (36)$$

Note that, as required, the "total" N electron Hamiltonian is still continuous. However, the change expressed in the N − 1 part of the Hamiltonian (from $H_I(N-1)$ to $H_F(N-1)$) is discontinuous.[55] At the same time, of course, the wave function for the N − 1 electron set must experience a continuous change from the eigenspace of $H_I(N-1)$, $\{\Phi_I(N-1)\}$, to the eigenspace of $H_F(N-1)$ (i.e., $\{\Phi^{J}_{F}(N-1)\}^{\infty}_{j=0}$), where the infinity symbol indicates both discrete and continuous states, and where now not only does the J = 0 state contribute (as in the adiabatic transition), but the entire manifold of eigenstates of $H_F(N-1)$ contribute.[56] Therefore (assuming, for convenience, only discrete states), continuity of the wave function demands the transformation (photoelectron ejection) at t^{α}, with $\alpha \rightarrow 0$, such that

$$\Psi_{I}(N-1) = \sum_{j=0}^{\infty} C_{J}\Phi^{J}_{F}(N-1) \qquad (37)$$

where

$$H_{F}(N-1)\Phi^{J}_{F}(N-1) = E^{J}_{F}(N-1)\Phi^{J}_{F}(N-1) \qquad (38)$$

As noted, all of the N − 1 electron hole ion states contribute to Equations 37, 38, and

$$C_{J} = \langle\Psi_{I}(N-1)|\Phi^{J}_{F}(N-1)\rangle \qquad (39)$$

Thus, the system, beginning in state $\Psi_0(N)$,

before interaction with A, is extensively and rapidly disturbed by the "speedy" ejection of electron k (from orbital ϕ_k) in a manner that "shakes" the system[57] into the manifold of eigenstates of $H_F(N-1)$ as depicted in Figure 8.

Further manipulations lead to a version of the Manne-Aberg sum rules:[57]

$$E_{F_A}^{KT}(N-1) = \sum_{j=0}^{\infty} |C_J|^2 E_F^J(N-1) \quad (40)$$

and

$$\epsilon_{k_A}^{KT} = \sum_{J=0}^{\infty} |C_J|^2 \epsilon'_{J_A} \quad (41)$$

where C_j^2 is the probability weight for each of these "shake up" states, and ϵ_j' is the orbital energy in the relaxed, final state that "announces" the "transition" into the $N-1$ electron manifold[57] (i.e., for a hypothetical spectrum with loss lines as shown in Figure 8.)

Thus, this shake up type process produces a multiple (weighted) transition to the relaxed final states, the eigenstates of $H_F(N-1)$.[57] The weightings are such that the manifold sum realizes the singular unrelaxed initial state solution $E_{F_A}^{KT}(N-1)$. These transitions are *intrinsically (hole) induced*.[58] Spectroscopically we may prefer to describe all of this in terms of a properly weighted (hole ion) spectral function, $N_+(\omega)$, where ω is the transition frequency[59]

$$N_+(\omega) = \sum_{J=0}^{\infty} |\langle \Phi_o^I(N-1) | \Phi_J^F(N-1) \rangle|^2 \delta(\Delta E) \quad (42)$$

where

$$\delta(\Delta E) = \delta(E - E_J) \quad (43)$$

and the approximation $\Psi \rightarrow \Phi$ is recognized.

As mentioned above, two "extremes" of this physical problem have previously been examined in detail both theoretically and experimentally.[59]

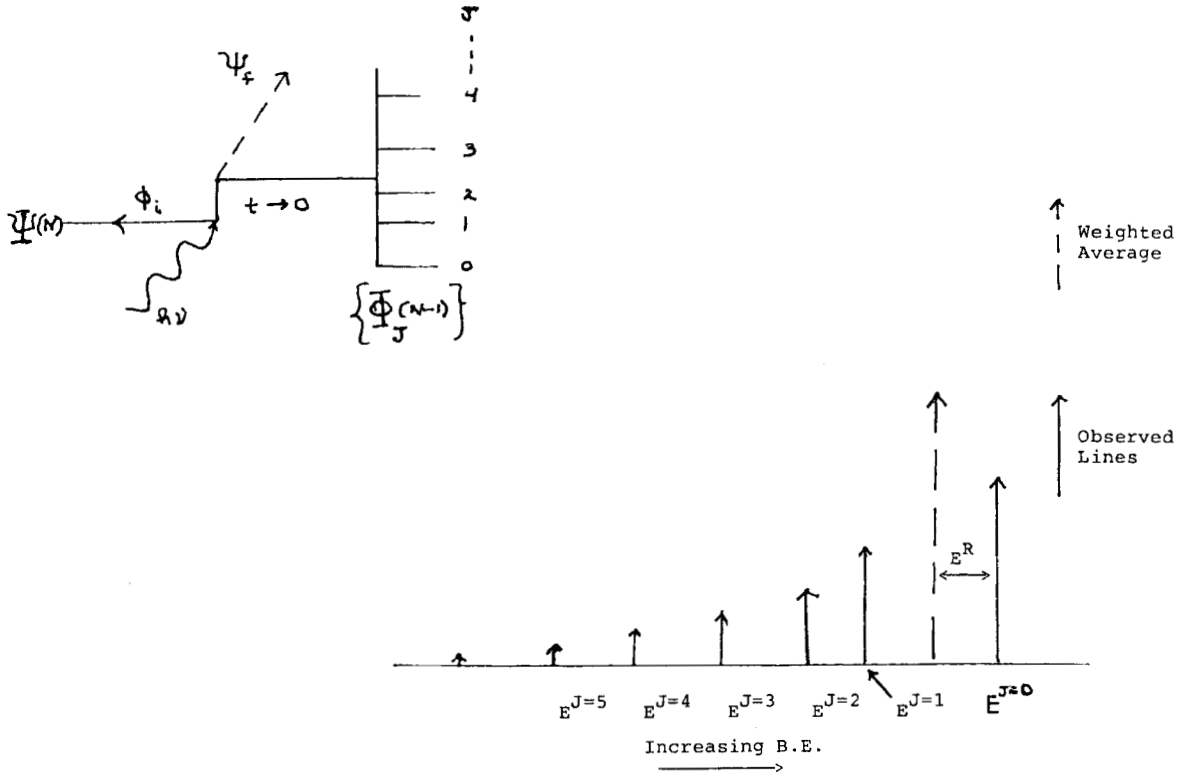

FIGURE 8. Schematic representation of the (intrinsic) shake up process.

b. The Two Extreme Cases

Molecular (Chemical) Solids—In these cases, the emphasis is on the word "molecular" with any solid state involvement considered to contain regions of interest describable by molecular (or atomic) orbitals. The emphasis is on local bond effects rather than delocalized symmetry and k space. These cases are thus characterized by well described orbital to orbital, or band to band, type transition. The resulting discrete peaks* are sometimes referred to as Manne-Aberg shake-up effects[59] to differentiate them from those described below. In some cases these transitions are of the charge transfer type, as apparently occurs for CuO,[60] (see, for example, Figure 9). We will expand upon select aspects of these arguments in Section VI on loss spectroscopy.

Metals, With Zero Band Gap—As also described above, if the sudden ejection of the photoelectron occurs for certain metals, ($E_g = 0$), it has been shown that a form of collective or plasmon-type excitation will dominate the satellite loss scene. The featured properties of this process will be a series of regularly spaced discrete peaks that fall off in intensity in an exponentially decreasing Poisson array. Aluminum produces an excellent example of this effect, as was first published by the Shirley group,[61] (see Figure 10). Because of the historical development of the explanations for these effects, Gadzuk[59] has referred to these collective phenomena as Mahan shake-up features.[62]

Some uncertainty still exists as to the degree of extrinsic (electron-induced) vs. intrinsic (hole-induced) character in these loss spectra, (see the following). Our principal concern, however, will be to consider what happens to these loss features when the ingredients for the Manne-Aberg and Mahan forms are mixed. This occurs for many semiconductors, and even some insulators. This feature is discussed in more detail in the section on loss spectroscopy.

V. ESTABLISHED ADVANCED ESCA PROCEDURES

A. Quantification

Quantification is one of the most important and, in many cases, *the* most important feature of ESCA. Surprisingly, although this capability was recognized in the pioneering work in Uppsala,[63] the development and explanation of the degree and methodology of quantification in ESCA is still a very active, necessary area of research.[64] Part of the reason for this is the evolution of the spectroscopy itself. Thus, as ESCA expands to encompass new and often more challenging techniques, the methods and scale of precision for its quantification need to be reexamined and often revised. Another evolving area of concern arises due to the somewhat uncertain nature of the materials being analyzed in ESCA. Thus, the fact that ESCA seems to detect photoelectrons over a shallow mean free path, λ, that in one sense is considered a surface analysis, and in another, a subsurface examination, makes the exact definition of its quantification very difficult. In particular, we must keep in mind that the predisposition of a factor labeled as an escape depth, η, can be a very beguiling fact. Thus, for example, if it is suggested that the average ESCA observation is rendered to a depth of 30 A, this generally tends to immediately produce the type of image presented in Figure 11a, where we have blocked out a cylindrical section of a material with an atomically flat surface with the predetermined diameter of the X-ray beam analysis area (in this case assumed to be circular and of a rather typical 1 to 2 mm diameter) and with a cylinder height of 30 A. Many casual practitioners are inclined to employ this image immaterial of the exact conditions imposed in the measurement. Unfortunately, this type of image is often far from accurate, and may not even be suggestive of anything with even qualitative merit. A

* Note that, in addition to the discrete (shake-up) peaks, a continuum of shake-off peaks may result (see Figure 8).

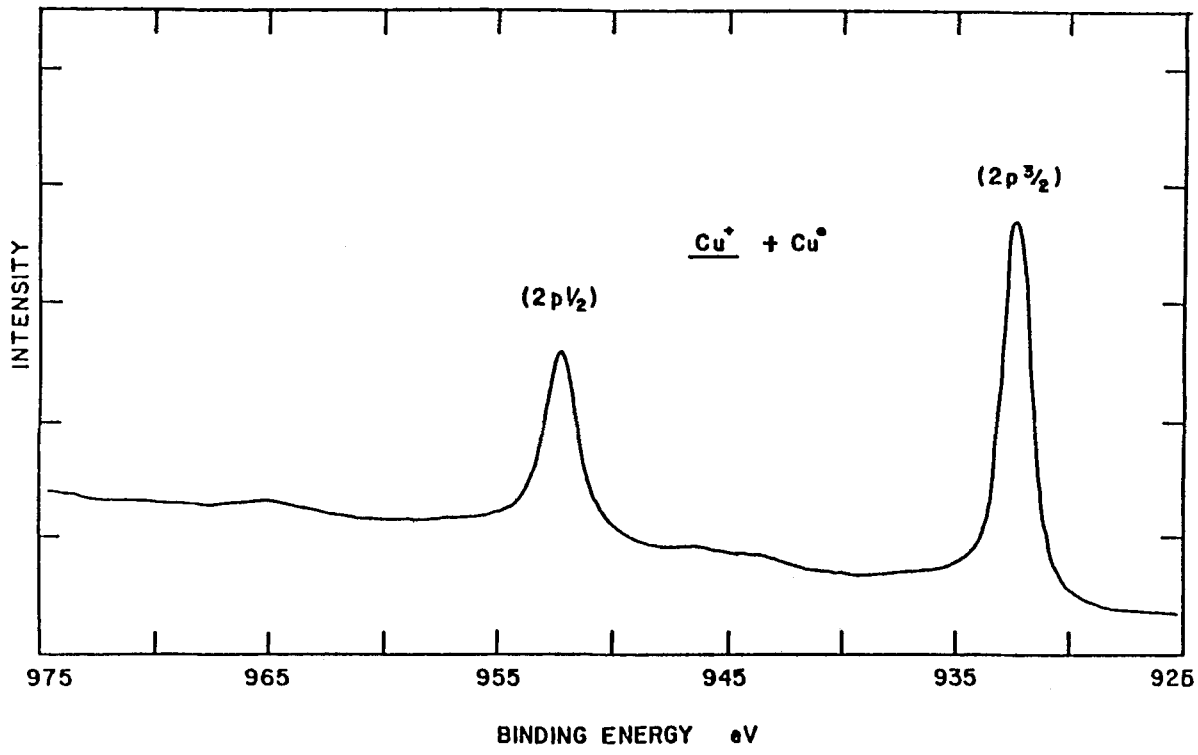

a

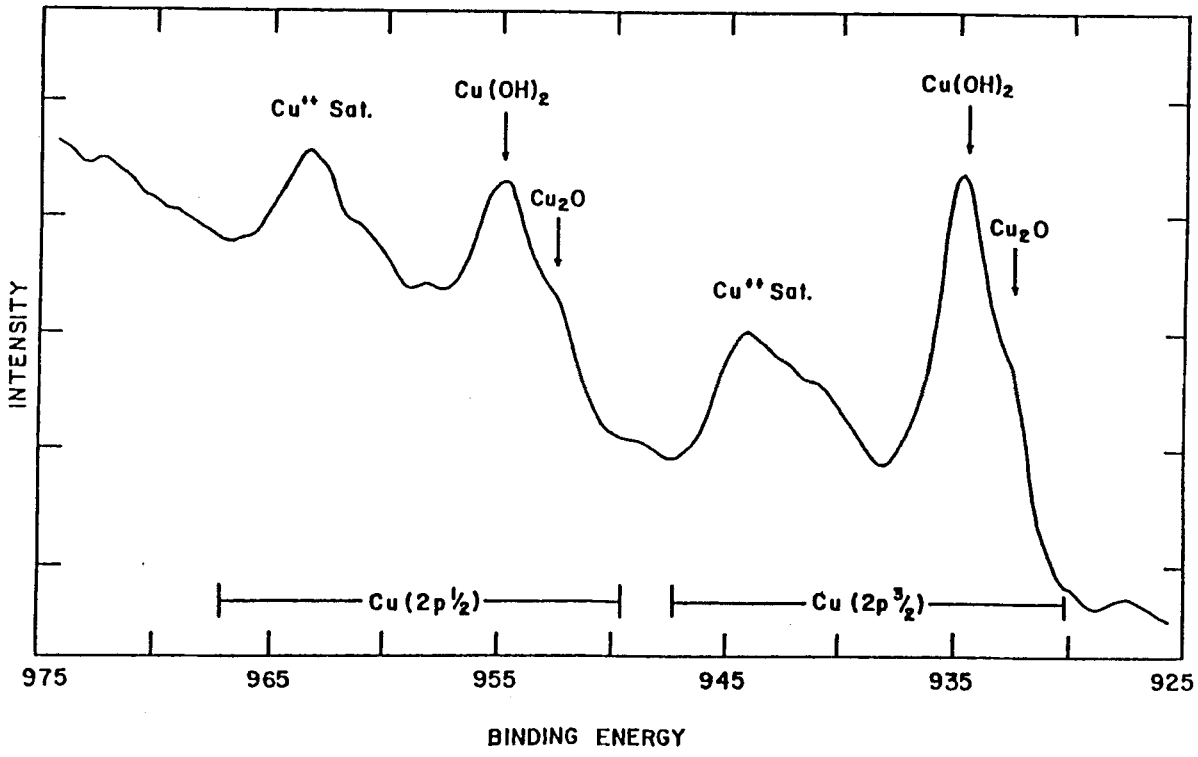

b

FIGURE 9. Representative (Manne-Aberg) shake up demonstrating its use in chemical analysis: Cu°, Cu(I) and Cu(II). Only Cu(II) produces distinct shake up.

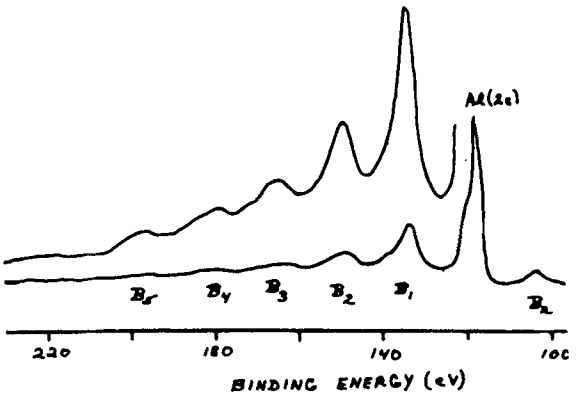

a

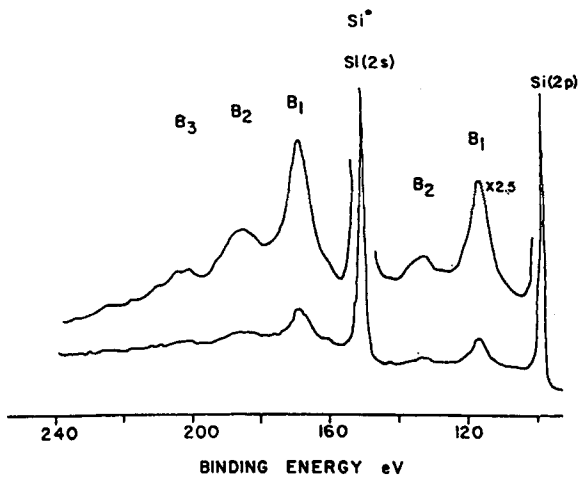

b

FIGURE 10. Representative (Mahan) plasmon dominated loss cases: (a) Al° and (b) Si°.

major problem is, of course, that the actual depth of detection, η, of an element, labeled as A, may be expressed as

$$\lambda_M(E_{AX}) \cos \theta$$

where M defines the particular matrix containing A, and the appropriate photoelectron is emitted from the X core level with energy E, at angle Θ with respect to the surface normal. Thus, as mentioned earlier, even for an ideal sample the actual escape depth will vary (sometimes substantially) with the energy of the source, the photoelectron binding energy, and the angle of emission. This means that the depth of photoelectron detection, for a given ESCA system, may vary dramatically from measurement to measurement, and even vary inside the same measurement.

The ready assumption of an "ideal" regularity for the materials in question, such as that depicted in Figure 11, may prove to be an even larger problem. Thus, although simple to model and often suggested by visual, even light microscope analysis, most materials are not nearly as surface regular as depicted in Figure 11a. In fact, many have cracks or other displacements, whereas others are prone to steps and kinks, and still other

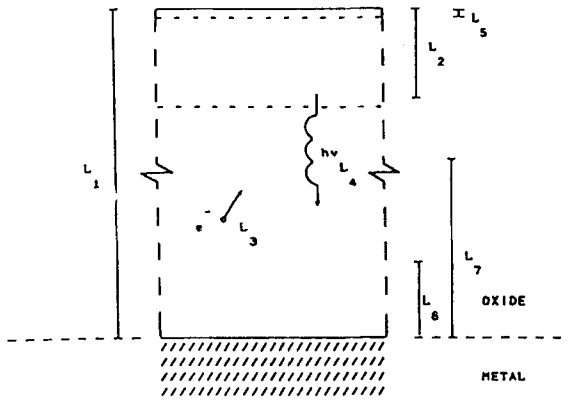

a

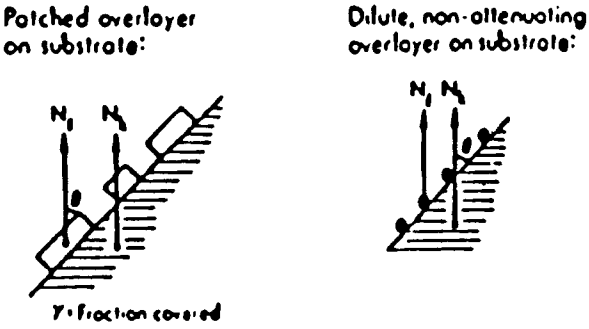

b c

FIGURE 11. (a) Representative renditions of surface situations expected during ESCA analysis: atomically flat surface (unrealistic) and representative penetration depths for fields realized in ESCA (L_1, oxide film thickness; L_2, escape depth of photoelectrons; L_3, migration distance of internally-created photoelectrons; L_4, effective depth of X-ray photons; L_5, penetration depth of flood gun electrons; L_6, space charge region of conductive electrons from metal substrate; L_7, total depth of influence of substrate electrons). (b) Surface with patch deposition or segregation. (c) Useful rendition of regular overlayers or substrate.

surfaces are in the form of microscopic boulders and indentures that may assume a variety of shapes, clusterings, and stackings. Some renditions of these types are displayed in Figure 11 (b and c). Obviously, the presence, or lack of presence, of these nonuniformities may have a dramatic effect on the ESCA detected quantification, since the previously mentioned escape depth often places the major extent of the ESCA analysis on the same scale as average size of many of these "deformities."

As suggested above, quantification in electron spectroscopy has been the active research area of a number of the best practitioners in the field. Originally, the efforts in ESCA were championed by Wagner[65] who, among other things, has contributed several painstakingly researched, empirically derived, atomic sensitivity factor scales.[66] Suggestions as to the proper usage and the extent of applicability of these tables also have been provided by Wagner[67] and others.[68] Subsequent developments in quantification have been led by two senior electron spectroscopists, Seah (primarily for Auger spectroscopy)[69] and Powell[70] (primarily for ESCA). Both are mentioned here because of the near total interchangeability of many of the results in these two fields. Because of the existence of several excellent, recent treatments of this subject by both of these authors[71] (and others[72]), we only outline the details herein, providing more than cursory comments only when there is a direct connection to our other highlighted areas.

The feature measured in an ESCA experiment and directly related to quantification is expressable, as expected, in terms of an electron current, or intensity factor, generally labeled herein as I_{AX}, where both A and X are defined as above, and[71-73]

$$I_{AX} = \sigma_{AX}(h\upsilon)D(E_{AX}) \int_{\gamma=0}^{\pi} \int_{\phi=0}^{2\pi} \times L_{AX}(\gamma) \int_{y=-\infty}^{\infty} \int_{w=-\infty}^{\infty} \times J_0(wy)T(wy\gamma\phi E_{AX}) \times \int_{z=0}^{\infty} N_{AX}(wyz) \times e^{-Z/\lambda_M(E_{AX})\cos\theta}\, dz\, dw\, dy\, d\phi\, d\gamma \quad (44)$$

where $\sigma_{AX}(h\upsilon)$ is the quantum mechanical photoelectron cross section for the emission of an electron from the X core level of atom A as a result of the "consumption" of a photon of energy $h\upsilon$, D is the detection efficiency of the photoelectrons, $L_{AX}(\gamma)$ is the atomic angular asymmetry of the photoelectron intensity, J defines the properties of the X-ray line in the detection plane, T is the transmission function for the analyzer of the spectrometer, N_A is the atomic density, z the detected distance into the sample in question, and λ is defined as before. As pointed out by Seah,[73] Equation 44 and/or its corresponding form for AES are far too complex to employ in their entirety. As unwieldy as Equation 44 may seem, however, it is still specifically constructed for the so-called, homogeneous, semi-infinite slab model and therefore must be extensively modified if the sample is nonuniform.

Calculations of absolute intensities employing Equation 44 are generally not attempted. Although many of the characteristics of the outgoing photoelectrons may (and generally should) be determined, it is also necessary to accurately and simultaneously gauge the properties of the incoming X-ray flux and the detection efficiency of the spectrometer in order to make these calculations. All of this generally is cumbersome, if not impossible. Shortcutting schemes are readily available, and these have often been employed with reasonable success, but it is in this area that the often used arbitrary gauge of precision of $\pm 10\%$ appears, and even this rather poor capability may be stretching the facts. Generally, however, absolute quantification is not needed. In almost all cases, particularly in practical analysis, the analyst is interested in *relative* knowledge. Thus, questions such as, "What is the silicon to aluminum ratio in that zeolite?" or "How much more potassium is there on the surface of thin film A than B?" are indicative of typical requests. Fortunately, in this form of analysis, one may generally simplify Equation 44, and the relative precision may be substantially improved. In fact, if one is careful in the selection of the materials and peaks involved, it may be possible to employ the following:

$$\frac{I_{AX}}{I_{BT}} \simeq \frac{\sigma_{AX}}{N_{AX}} \sigma_{BT} N_{BT} = \frac{\sigma_{AX}}{\sigma_{BT}} \cdot \frac{N_{AX}}{N_{BT}} \quad (45)$$

For this relationship to apply, it is necessary that the different photoelectrons AX and BT be emitted under nearly identical circumstances, i.e., from the same place in the same (or, at least, very similar) materials and with kinetic energies such that,

$$E_{AX} \sim E_{BT} \tag{46}$$

When these criteria are not observed, it may be necessary to include in Equation 45 all terms that are energy dependent, particuarly λ_M. An example that we feel demonstrates a reasonable use of Equation 45 was accomplished when we generated the Si/Al ratio for a series of zeolites employing the Si(2p) and Al(2p) peaks, as displayed in Table 2. Even in this case, however, a slight compensation was included for the fact that the more energetic Al(2p) are sampled at a slightly greater depth than the Si(2p).

It is possible, of course, to employ in Equation 44 the terms determined by Wagner,[66] and others,[67] labeled as Sensitivity Factors, K. Often the latter are determined from measurments of purportedly standard reference materials, perhaps coupled with the σ calculations of Schofield[74] and perhaps the $\lambda_M(E_A)$ values calculated by Penn.[75] The resulting values, which have been presented in a variety of sources,[73] have generally been pruned of many problems and may be considered a useful alternative for semiquantitative results. However, one must be very cautious, as various assumptions regarding homogeneity and depth of analysis are being arbitrarily employed.

In many cases, particularly in applied studies, the relative analysis is actually what we refer to as relative/relative. Thus, for example, the A/B ratio for sample 1 may be compared to the A/B for sample 2. Now, if all features are ideal,

$$\frac{(I_A / I_B)_1}{(I_A / I_B)_2} \simeq \frac{(N_A / N_B)_1}{N_A / N_B)_2} \tag{47}$$

Interestingly, the use of Equation 47 may actually relax the requirements of homogeneity and the concept of an infinite slab. If the samples are subject, for example, to inhomogeneities, then it is only important that they be equally so. Consider the results for several zeolites reported in Table 3. These results are for relatively smooth, similarly prepared wafers pressed from uniformly sized powders.

TABLE 2
ESCA Detected Relative Quantification For Select Zeolites: [Si/Al]

Material	Representative materials examined [Si/Al] Bulk (reputed)	Surface (determined)	%Na^+
Na A	1.0	1.1	100
Na Y	2.4	2.6	100
Ca X	1.25	1.3	<5
Ca Y	2.4	2.7	10
NH_4 Y	2.4	2.8	10
Kaolinite	1.0	1.1	0
Bentonite	2.0	2.2	0
α-SiO_2	—	—	0
Silica Gel	—	—	0
α-Al_2O_3	—	—	0
α-Al_2O_3	—	—	0

Note: Each example listed is one of several commercial systems examined. All are reputed to be of excellent purity. Our ESCA survey scans suggest that claim to be correct.

TABLE 3
ESCA Detected Relative/Relative Quantification for Zeolites: $[Si/Al]_A/[Si/Al]_B$

	[NaX]/[NaY] compositional formulae	[NaX]/[NaY] surface (XPS)[a]
Na	1.57	1.47
Si	0.77	0.77
Al	1.57	1.53
O	1.01	1.08

[a] Based upon several measurements of same and different systems, ± 0.5.

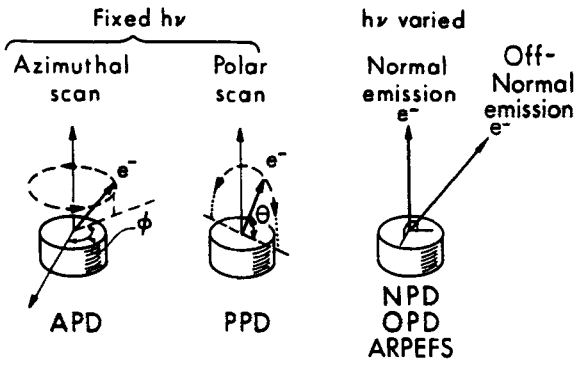

FIGURE 12. Operative rendition of variables that may be employed in angular resolution-XPS.

In general, however, lack of surface uniformity and various types of inhomogeneities have played a major role in the interpretation of surface analysis. In ESCA, researchers who are interested in catalysis, particularly dopant dispersion with its generally variable sized particulate formation, have extensively studied these questions and proposed a number of models.[76-78] Fung, in particular, has introduced specific factors to take into account the various shapes that may occur in any undispersed phase.[79] More recently, Fadley[80] has provided fairly detailed descriptions of the modifications expected for Equation 44 when overlayers, patches, noncontinuous overlayers, and variable concentration profiles result. Figure 11 displays some of these model systems. One must be cautious when applying these models, as they depend upon a certain regularity of variable morphology that may be difficult to produce or even verify. For the correct cases, however, the methods should be very valuable.

Angular resolution studies constitute one of the principal areas for quantification in ESCA. This has been a matter of concern for several research groups, with the work of Fadley et al.[80] standing out in particular. The basic angular resolution experiment, such as presented in Figure 12, seems to strongly suggest the detection of regular thin film overlayers. Cursory analysis indicates, however, that these experiments are readily susceptible to surface roughness, shading, and even the instrument response function. All of these features may play a major role in the detected N_A when plotted vs. $\lambda_M\cos(\Theta)$. We will expand further on this aspect of quantification in the following section on angular resolution ESCA.

B. Angular Resolution—Photoelectron Spectroscopy (AR-PES)

1. Background

It is certainly true that, depending upon one's point of reference, the limited depth generally detected in an ESCA experiment may be either a benefit or a hindrance. In reality there is no single standard depth that results from conventional ESCA analysis, although it is common for ESCA practitioners to refer to depth limits of ~40 ± ~ 15A. Even though this range of values is just a reference point, it is not hard to see why conventional ESCA may be viewed as *too* surface sensitive for some potential uses, whereas it is *not surface sensitive enough* for others.

The X-ray photons generally employed to eject the photoelectrons (typically $Al_{k\alpha}$ or $Mg_{k\alpha}$) are able to penetrate for thousands of angstroms into most of the solids to be analyzed. These photons will create photoelectrons at all accessible depths, but due to the relatively short mean free path of electrons (see Figure 12) only those electrons ejected at or near the surface are able to escape materials capture and make their way to the detector.

Close scrutiny of the mechanism of the ESCA process and Figure 12 indicates that photoelec-

trons (and other types of electrons) ejected at substantially different energies may be emanating from quite different depths. This is one reason why one should generally pick photoelectron peaks that are fairly close in binding energy for relative quantitative analysis (see the separate discussion on quantification in Section V). As an example, we chose to ratio the Ge(3d) and O(2s) peaks in a study of possible nonstoichiometries in germania systems, rather than the much more intense (but very widely split) Ge(2p) and O(1s) (see Table 4).[81]

TABLE 4
Select [O/Ge] Values Determined Employing O(2s) and Ge(3d) Peaks for Variously Treated Germanium Oxides

State	Process	[O/Ge]*
a	Fresh Thin Film Deposition	2.0
b	Following Ion Alteration	1.4
c	Air Exposure Partial Oxygen Reinjection	1.65
d	Thermal (Total) Oxygen Reinvestment	2.0

* ± 0.2

2. Angular Resolution Development and Procedure

As with so many aspects of ESCA, Angular Resolved Photoemission (AR-XPS) had its origins in the pioneering studies in the research group of Kai Siegbahn.[63,82] These studies were initiated not long after it was determined that ESCA was a tool that examines the surface and near surface regions of solids. Simple arguments in electron optics and knowledge of their escape depth suggested that by rotating the sample X-ray source and collection optics in order to obtain near grazing angles, one may achieve a substantially enhanced surface sensitivity. Although simple to argue, the actual experimental procedures needed to achieve this feature without substantial reduction in resolution and sensitivity require adroit manipulation.

A variety of scientists, in particular, Fadley,[80,83] rapidly examined and expanded the AR technique to include variable angle studies (both polar and azimuthal) at fixed energy and variable energy at fixed angle situations. The procedure proved to yield not only elemental qualitative and chemical analysis with depth, but also to provide reasonable quantification, surface geometry, and valence region information.[80,83] The general geometric description provided by Fadley, and reproduced herein (see Figure 12), is a useful feature to study. Although the variable energy approach suggests the use of a synchroton source, one may achieve some useful AR-XPS data with a conventional system employing two or more X-ray anodes, or even by monitoring photoelectron peaks with distinctly different E_b. All of these efforts have succeeded so well that all commercial manufacturers regularly provide AR options on their systems, operable even in the small spot mode.

The angular resolved procedure may, of course, also be exploited in the UPS mode, and numerous useful studies of the presence of alterations in band character, surface states, preferential surface orientations, etc., have been provided in AR-UPS.[84]

The extension of the procedure to exploit the channelling and diffraction of surface emitted photoelectrons from crystals (PED) has also developed into a separate procedure.[83] The latter is described later in some detail (see Section VIII).

3. The Use of Angular Resolution

Because of the extreme importance of surfaces and interfaces in the behavior of thin films and in cases of adsorption or surface segregation, the ESCA literature of the last decade is full of descriptions of the use of the conventional AR technique. As a rather basic example, consider Figure 13 in which Fadley describes the use of AR in the vicinity of the interface between SiO_2 and Si°.[80] In a somewhat more involved example, our own research group employed AR to examine the O(1s) and Pt(4P) and several of their satellites during the thermal induction of a modest oxygen adsorption and slight oxidation of platinum. Ex-

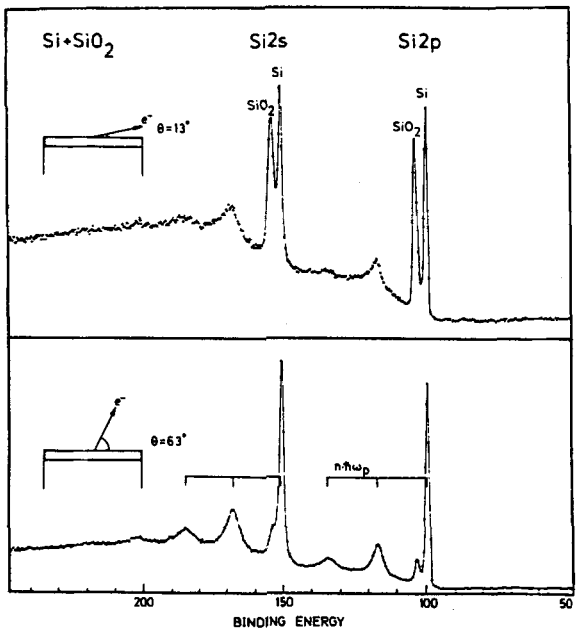

FIGURE 13. Typical angular resolution result: SiO_2 thin film on Si°.

amination of the changes in relative sizes of the peak structures in both Figures 14 a and b are readily indicative of the potential depth of field and sophistication of the angular resolution procedure. In Figure 14a, for example, we find a partial answer to one of the major questions in surface science. Most noble metals (e.g., Pt) do not readily form surface oxides when exposed to air, and yet following sputtering to remove any "superficial" oxide a Pt(111) surface still reveals a noticeable peak at -532 eV long attributed to dissolved (and presumably reacted) oxygen. Examination of the angular resolution spectrum for this material (Figure 14a) suggests that the persistent (most prominent) part of the peak structure around 532 eV is, in fact, the Pt° ($4P_{3/2}$) loss line (see Section 6), rather than that due to oxygen.

Examination in Figure 14b of the angular resolved peak structure between 540 and 565 eV for two stages in the sputter "cleaning" provides further evidence in this case. The resulting peaks all appear to be due to loss lines (Section VI). Grazing incidence (13°) of the outer surface demonstrates that those peaks around 555 to 560 eV are most prominent. These are due primarily to O(1s) losses from adsorbed oxygen and carbon. The possible peak near 550 eV may be Pt $4P_{3/2}$ losses due to the modest formation of PtO. The peak structure around 546, on the other hand, is relatively weak on the outer surface and much more prominent in the bulk of the sputtered

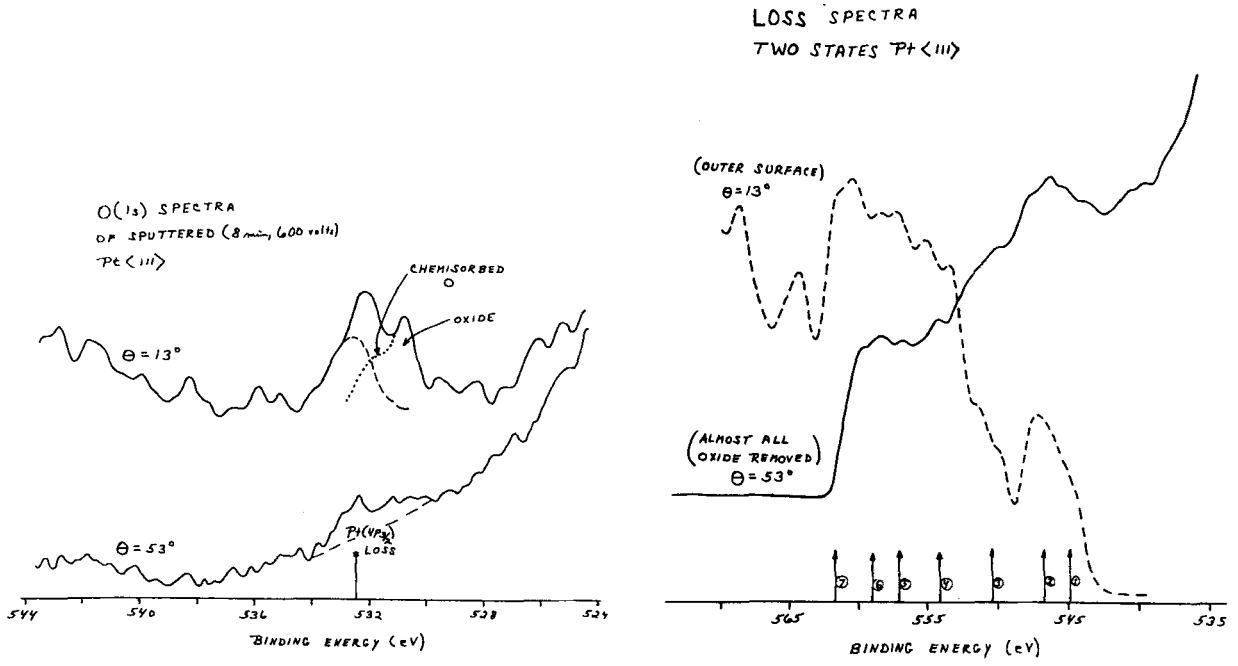

FIGURE 14. More involved angular resolution result: oxidation of Pt° (note satellite changes with depth). States (1) and (2) due to Pt° losses, states (4) through (7) due to chemisorbed oxide.

Pt(111). This suggests therefore the 2nd $4P_{3/2}$ plasmon loss line of Pt° (Section VI).

The AR method has been the pivotal feature in even more detailed analyses. Consider, for example, a film of high purity, catalytically prepared (but purportedly unreactive) polypropylene, subjected to a variety of oxidative treatments.[85,86] For our purposes, we examine herein the results following exposure to ambient air at standard temperature and pressure (STP) (labeled by our group as natural passivation or NP) and simulated sea water (3% NaCl). The systems to be studied were examined in the form of small coupons with angular-resolved XPS (AR-XPS). This procedure was employed rather than sputter etching to permit a detailed chemical analysis from the outermost surface layers to a depth of ~60 A. Sputter etching would permit analysis to an even deeper level, but we have discovered that even moderate energy Ar^+ will substantially sputter reduce the organic by-products generated in the treatments under consideration. The resulting lack of depth realized by AR-XPS did not turn out to be a major problem, however, because most of the critical changes induced by the various treatments are realized in the outer 60 A, and are thus discerned in detail by AR-XPS.

After exposure to STP air,[85,86] polypropylene (despite its visual indication of inertness) is subjected to modest oxidation, producing a variety of products. Instead of just an indiscernible mixture, high resolution analysis (employing the detailed XPS analyses achieved on pure organic systems with different functional groups by Clark[87] and others[88]) is able to demonstrate that the NP process produces a variety of discernable oxidized byproducts. Repeated angular resolution analyses suggest that these products are realized (produced and deposited) in repetitive layers.[86,87] The products formed and their semidiscrete interfaces are depicted in Figure 15. One should note that the resulting oxidized carbon products do not entirely cover the surface, but do seem to form a product distribution that is still present more than 35 to 40 A below the outer surface.

The general lack of oxidized products formed (during NP), and the fact that they always occur in mixtures, greatly complicates detailed analysis. Fortunately, the degree of oxidation is dramatically enhanced following exposure of the polymer to various simulated liquid environments, particularly the sea water. In all of these fluid exposure cases the large preponderance of retained C-H and C-C type carbons ensures that the C(1s) spectra will be dominated by these species making positive analysis of the C(1s)-oxygen species very difficult. Therefore, most of the identifications were rendered using AR versions of the resulting O(1s) spectra. Several typical examples[85,86] of these spectra are presented in Figure 16.

The most important feature detected in these results was the general nature of the oxidation chemistry formed in the semidiscrete layer structures during exposure to NP and various fluids, and, in particular, the obvious interrelationship that exists between the results obtained for this polymer[85,86] and similar results found for many metals and alloys.[85,89-91]

A comparative summary of the key results for exposure of the polymer to NP and simulated sea water has been generated.[85] Simulated sea water, for example, produces species on the polypropylene that resembled those found on α-brass.[92] Thus, in these cases, there is a substantial (near total) production of oxidized products that extend well below the 60 to 70 A cut off of AR-XPS visibility. Also, the interfaces of the product layers found following NP are effectively destroyed, and those species that are almost entirely subsurface following NP are now pulled out toward the outer surface.[86]

Despite the aforementioned interesting and perhaps even dramatic results, they are not as significant as those realized during natural passivation (NP) of the polypropylene. As mentioned above, STP air seems to oxidize only about one third of the polypropylene units.[85,86] (It should be noted that total oxidation should produce one carbon-oxygen unit for every three carbons [i.e., one for each propylene unit].) The AR discerned course of the NP of polypropylene (see Figure 16) suggests that there may be some type of relatively ionic unit formed near the interface between the polymer and its oxide products. The latter seem to occur ~35 A into the evolving layers of oxidized material. The species found outside these ions seem to form the thickest layer detected, and also one that exhibits fairly good

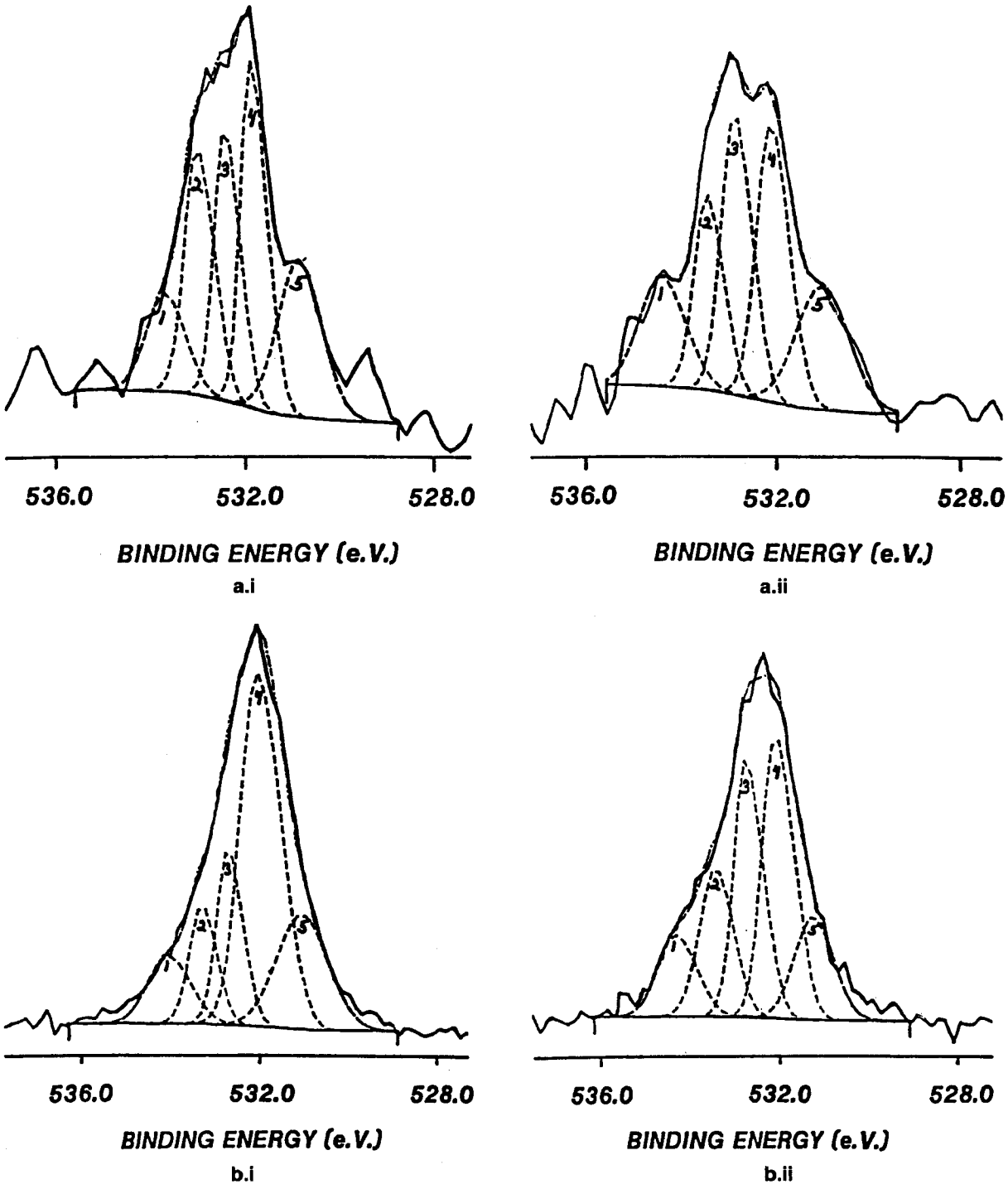

FIGURE 15. Select angular resolution ESCA study of O(1s) on polypropylene: (a) natural passivation (air oxidation) (i) 8°; (ii) 53°; (b) simulated sea water (i) 18° (ii) 38°.

integrity. This layer is primarily composed of single bonded (ether-type) species. As the layer extends outward it begins to exhibit C = O (carbonyl type) species. In these initial carbonyl layers the ether type species are still detected, suggesting an interfacial region with mixed ether-carbonyls. As the AR-XPS analyzes closer to the surface of the oxidized products, a region is detected which is apparently composed of primarily carbonyl-type species. Finally, a very thin layer composed primarily of hydroxide (i.e., alcohol-type, C-OH units) is found on the outermost sur-

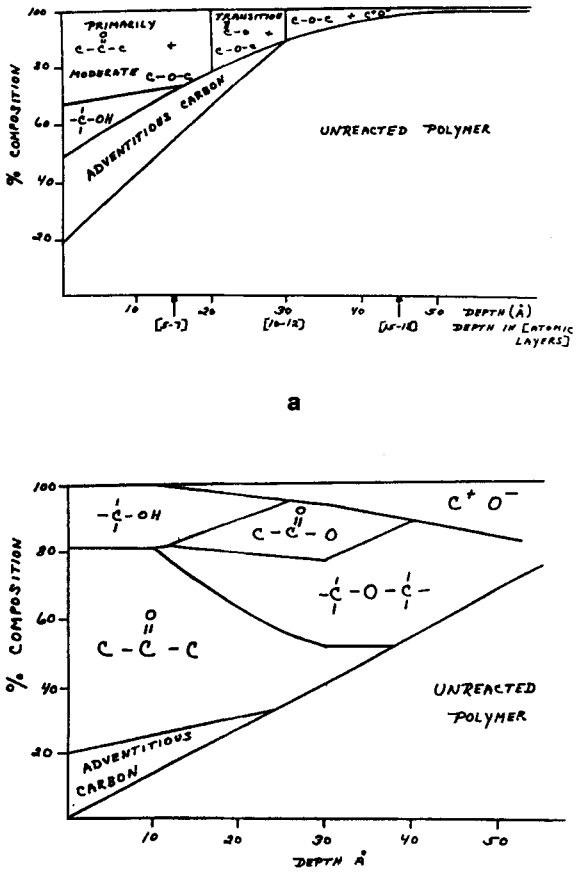

FIGURE 16. Qualitative rendition of oxide layer structure produced on polypropylene detected by AR-XPS: (a) natural passivation; (b) simulated sea water.

face. It should be noted that there is also a fairly extensive deposition in this region of the species dubbed (by surface analysts) as adventitious carbon (see Section VI).[85] The latter is deposited on the surface of all air exposed materials, and produces XPS spectra that so closely resemble those for the polypropylene that its initial presence complicated the analysis, particularly the semiquantitation.[85]

The interesting aspect of these results may be realized by noting that the carbonyl species are oxidized versions of the ethers (i.e., the carbon in our supposedly inert polymer is first oxidized in a relatively thick layer of species in its lowest common oxidation state, followed by a relatively thin, but contiguous, layer of carbon in its highest common oxidation state). The latter layer seems to be terminated by a layer of hydroxide. It should be *apparent that one may replace carbon in these arguments with any one of a variety of metals and argue the same general results for natural passivation.*[85,93] The latter analyses were also very dependent upon angular resolved XPS for their realization.

Many other cases of AR may be described. In the next part of this review we present a short description of substantially more involved techniques realized, starting with this basic technology.

VI. LOSS SPECTROSCOPY IN ESCA: ITS CAUSES AND UTILIZATION

A. Introduction

As noted previously, the XPS, or ESCA, process is made complicated, in part, because of the ready presence of a variety of secondary interactions that often shift the principal peak, and may, in some cases, also provide one or more discrete, satellite peaks. Although much of the inherent simplicity of the origin explanation of ESCA vanishes with these "loss" effects, a wealth of additional, often unique, analytical information is also realized. Certain aspects of this capability are now being employed on a regular basis by XPS scientists. These features, therefore, are only outlined herein. We do, however, describe in some detail an approach that emphasizes a realtively unexploited feature of the collective electron nature of some of these losses that seem to arise in many ESCA results.

The loss peaks that have been employed in the past by ESCA scientists generally fall under the heading of shake up phenomena.[94] In general, these may be considered to be the loss features that correspond directly to those that occur through rapid transitions, except that, in the case of the most frequently used shake up transitions, any delocalized behavior in the system may be ignored. More is said about this below.

The theoretical presentation to follow is designed to fill in some of the gaps that exist in XPS loss spectroscopy which we designate herein as ESCALOSS. In view of the numerous detailed

discussions in the literature for several of the select cases, this review only expands upon the rather diffuse, general outline presented above in the theoretical section in several key areas. For a more general treatment, we refer any interested reader to the most pertinent parts of the literature in this field. Particularly, if one is interested in the XPS loss spectra involving our predefined crystalline, conductive solid, we recommend the reports of Langreth[95] and Gadzuk.[96] On the other hand, if one is concerned with the materials we are classifying as molecular solids, then papers by Manne and Aberg,[97] Fadley,[98] and the Shirley group[99] should be very informative. In those cases of our principal concern (i.e., the extensive range of materials that are not described to be either of these extreme models) there are only a few considerations. Interestingly, the most detailed discussion of the effects that may occur when these two cases are mixed seems to have occurred in the often forgotten pioneering reports of Pines et al.[100] and of Nozières and Pines.[101] Thus, these authors not only established the existence of the plasmon as a fundamental quantum particle, but also considered in some detail what occurs with plasmons as the solid under consideration evolves from one adequately described by a free electron gas model (zero periodic potential, i.e., V[r] = 0), through the Bloch formulation (regularly varying V[r]), to cases that may only be approximated by our predefined, *molecular solid.* The missing feature in the Pines and Nozières studies (for those interested in ESCALOSS) is that they considered only the extrinsic (electron induced) loss spectra, produced in a system by outside electrons without the creation of deep holes.

Mahan,[62] Langreth,[95] Gadzuk,[59,96] Sunjic,[96,102] Doniach,[103] and others[104] have greatly expanded on these plasmon arguments for cases in which core holes are a necessary adjunct (e.g., during photoelectron and X-ray spectroscopies). Thus, these authors have tried to describe situations in which intrinsic (hole-caused) losses, and hole-induced couplings and shifts accompany the extrinsic effects in the loss spectra. Unfortunately, all of this had been done by the latter group without consideration of the possibility of collective (e.g., plasmon) vs. noncollective losses in a nonfree electron gas-type environment. This oversight has led some practitioners who are only slightly acquainted with the field to incorrectly assume that plasmons only occur in systems involving conductive materials.[105] Thus, one of our principal goals herein is to demonstrate (a la Pines)[100] that plasmon-like effects contribute to the loss spectra of semi conductors and (even) insulators. Unlike Pines et al.,[100,101] we will do this for ESCALOSS, with its accompanying hole induced effects.

1. Related Plasmon-Type Transactions

The bulk collective modes of interaction that are the principal concerns of this section of the review represent only a fraction of the possible types of collective effects. For example, it is quite possible for collective behavior to be restricted to particular regions of a material, such as, at its interfaces or surface. The results of the latter (labeled as surface plasmons) are generally produced by any relatively pure system that also yields reasonable bulk plasmons. This suggests that surface plasmons are often also achieved in cases where bulk plasmons exhibit free electron character. In these cases, the surface plasmons have a frequency

$$W_s \simeq \frac{W_p}{\sqrt{2}} \tag{48}$$

where W_p is the bulk plasmon frequency, as exemplified below in Equation 63. A representative example occurs for In° in Figure 17. Even in the case of very clean samples, at conventional XPS incidence, the intensity of the surface plasmons are generally substantially less than their equivalent bulk form (reflecting on the two-dimensional character of the former). If one resorts to grazing incidence in the manner described in Section V however, the ratio of I_s/I_p experiences the anticipated increase. These features have been exploited in a variety of forms of analyses.[106]

A number of other types of specialized plasmons have also been proposed. For instance, several groups have experimentally and theoretically described the special collective situations that result when adatoms are introduced into select matrices.[103] These situations are of special significance in cases related to catalysis and composite

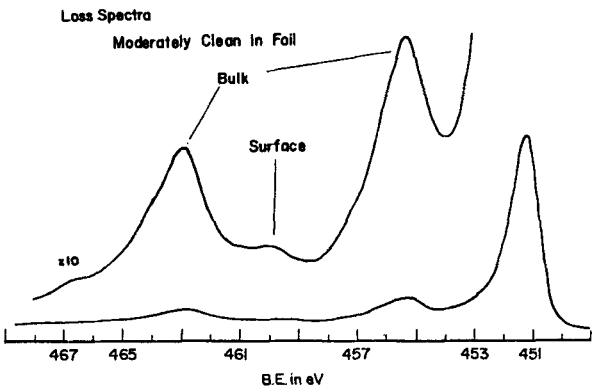

FIGURE 17. ESCALOSS for In° demonstrating E_L and moderate surface plasmon.

formation.[107] There are a number of interesting, unique features to the theory of these adatom plasmons that have only recently been totally described.[108] Experimentally, they often require superior resolution and sensitivity[107] to yield spectra of analytical quality.

Pines and Nozières[101] have also suggested that it should be possible to achieve low energy plasmon-type transitions due to collective behavior in modestly populated conduction bands. As Pines has shown, these states, with their relatively small N values, should produce discrete transitions in the infrared region.[102] The quantum mechanics of the latter processes represent another interesting set of select situations, but their use in analysis awaits improvements in measurement techniques.

2. The Early History of Loss Spectroscopy and Plasmons

It is, of course, important to realize that an entire science of plasmon oriented spectroscopy involving inelastic electron scattering predated its development as a part of ESCA and other forms of photoelectron spectroscopy. Pines[101] and Pines and Nozières[102] earlier described a variety of these studies in support of their theoretical arguments. Shortly thereafter, a number of scientists extended this extrinsic-only spectroscopy by introducing a UHV form. One of the most important of these early UHV studies was the work of Powell and Swan,[106] who described in some detail the loss spectra of readily oxidized metals, such as Al°. A number of other research groups have extended the latter studies to include nonmetallic systems, even nonconductive materials.[109]

Another form of UHV loss spectroscopy has been developed over the last two decades centered around the detection of the very low energy, inelastic, loss transitions induced by the various vibrational modes produced by surface and near surface bonds. This form of low energy, loss spectroscopy has become so popular, it is often the only type suggested by the designation Electron Energy Loss Spectroscopy, or EELS[110] The procedures, technology, and theory of EELS have been extensively developed, particularly by Ibach,[111,112] and although the method requires a very sensitive, stable spectrometer, its use may be worth the effort, as it is often the most informative tool for descriptions of the bonding in chemisorption and other surface studies.[110-112]

B. Utilization of XPS-Induced Loss Spectroscopy (ESCALOSS): Advantages and Disadvantages

It should be obvious that one of the principal reasons that some ESCALOSS results have appeared in the literature is the natural tendency of scientists in a particular area (including electron spectroscopists) to try to exploit every unique feature related to a particular technique, immaterial of its true utility. Therefore, since this is a review of the *analytical potential* of the methods described, we should in fact, ask the following question: What is there about the ESCALOSS method that would recommend it as a *unique, useful,* supplemental procedure to the nonexpert user of electron spectroscopy? In order to properly explore this question we need to examine some of the possible shortcomings of "conventional" ESCA, and ask whether ESCALOSS provides valuable information in these areas.

As described previously, the principal purpose of ESCA seems to be the definition of the chemistry, and to some extent structure, (both fixed and evolving) of a materials system in its surface and near surface region. In order to accomplish this with "conventional" ESCA, it is

necessary to be able to resolve the principal core level peaks with their proper sizes and shapes, and have them fixed in their *proper* binding energy positions. It is, of course, also important that these positions exhibit discernible shifts from one position to another as the chemistry evolves. Although, in principal, "conventional" ESCA can often achieve all of these features, there are frequently cases in which shortcomings arise, and unfortunately, many of these cases seem to be exacerbated during studies of more practical systems. These shortcomings would seem to include

1. **Charging and Fermi-Edge Decoupling:** We have previously described the charging problem, noting how it may be removed in many of the examinations of applied materials.[19] As we have shown, however, if the goal is chemical analysis, then, due to the inherent difficulties in establishing the Fermi edge, distinct problems may still arise in accurately (and universally) determining the binding energy scale, even if charging can be removed. It would be advantageous, therefore, to have access to an ESCA-based procedure that produces peaks and shifts that are not adversely affected by charging, and particularly by the floating Fermi edge problem.[19] As we describe below, ESCALOSS, because of its reliance on energy differences, exhibits this attribute.
2. **Large, Relatively Easy to Discern Shifts, With Changes in Chemistry:** As mentioned above in a number of important cases, the conventional (Siegbahn) chemical shifts in ESCA are often very small. This occurs for a variety of reasons, some of which we have described elsewhere in more detail. Often these small shifts can not be detected with commercial ESCA systems [e.g., In° → InSb using the In(3d)]. In many of these cases it turns out that there are corresponding, much larger shifts in the ESCALOSS splittings that may be easily detected. Some examples of this attribute are presented below (see Table 5). The reasons behind these attributes for ESCALOSS are presented later in this review.
3. **Nonchemical Basis for Chemical Shifts:** As described elsewhere in some detail, the positions of the binding energy peaks in ESCA result not only from initial state features, such as differences in chemistry, but also from final state effects, such as the previously described relaxations induced into the photoelectron peak position by the contraction of the valence shell inward (toward the nucleus) *as* the photoelectron is ejected.[54] Thus the peak position of a photoelectron line has a multifaceted origin. Unfortunately, the relaxation contribution to a principal core line for a particular element in one chemical state (e.g., Al°) may differ significantly from the relaxation contribution for the same element in another chemical environment (e.g., Al_2O_3). This means that one can not attribute the total detected shift, ΔE^M, in binding energy (for example, for Al° → Al_2O_3) to initial state chemical changes, and thus the separation of chemical from non chemical causes may be difficult.[54] This tends, in some instances, also to be injurious to efforts to relate ESCA shifts to other parametric features that are purported to describe changes in chemistry.[54] *As we describe below, the shifts detected with ESCALOSS, on the other hand, are generally either devoid (or nearly de-*

TABLE 5
Representative ESCALOSS, ΔE_L, Relative to Common Chemical Shifts, ΔE_S (S ≡ Siegbahn) for Select Compounds in eV ± 0.3 eV

From — to	Element and state	Principal (Siegbahn) shift	XPS loss shift
Si° - SiO_2	Si(2p)	3.4	5.2
Al° - Al_2O_3	Al(2p)	2.2	8.6
In° - InSb	$In(3d_{5/2})$	0.2	1.8
In° - InN	$In(3d_{5/2})$	0.4	4.0
In - In_2O_3	$In(3d_{5/2})$	1.0	7.0
GaSb - GaAs	$Ga(2p_{3/2})$	0.4	0.9
GaSb - Ga_2O_3	$Ga(2p_{3/2})$	1.0	1.9
Ga_2O_3 - $Ga(OH)_3$	$Ga(2p_{3/2})$	0.3	4.0
Sb° - InSb	$Sb(3d_{5/2})$	−0.2	−2.7
Sb° - GaSb	$Sb(3d_{5/2})$	−0.1	−0.7
Sb° - Sb_2O_5	$Sb(3d_{5/2})$	2.5	2.6
Sn° - SnO	$Sn(3d_{5/2})$	1.2	6.0

void) of relaxation and other noninitial state effects.

C. The Plasmon Domination Argument

As mentioned earlier, the process of electron loss spectroscopy involving plasmons was first described in some detail by Pines, Bohm, and Gross[100,113] and later by Pines and other co-workers,[100] particularly Nozières.[101] These descriptions involved situations in which the excitation particle (always an electron) employed to excite the plasmons is issued and detected outside of the materials involved (e.g., in a manner of the inelastic electron scattering that may be produced in electron microscopy). Thus, the peculiar additional fields and problems induced by the presence of the hole(s) which occur during X-ray and photoelectron spectroscopy were ignored. Also considered in the treatment by Pines et al.[100,101] were situations in which forms of excitation, other than plasmons, are excited by the excitation source. In particular, Pines et al.[100,101] considered cases in which the valence and/or the conduction band electrons in a solid may act individually, rather than collectively (i.e., plasmon-like), and thus experience band-to-band type transitions. Pines et al.[100,101] demonstrated in some detail that the apparent "competition" between these band-to-band transitions and the plasmon transitions depends both on the nature of the solid material involved, and/or the conditions of the experiments.

The previous discussions of the loss spectroscopy that occurs during a photoelectron experiment, on the other hand, were considered almost exclusively from two entirely separate points of view; plasmons, for free electron metals,[95,96] and shake-up-type transitions for molecular solids.[94,95,97,98] Possible dispersions of the plasmons were considered as small perturbations of the plasmon field, but *still in the context of the free electron model.* Thus, the latter become slight displacements of the solutions for a quantum harmonic oscillator (the plasmons) in which the free electron gas was also shown to suffer an infrared catastrophe.[95,114,115] The latter can be solved *exactly* in the long time limit (for a free electron gas) producing a term that merely "disperses" the resulting plasmon dominated peaks up field by small amounts referred to as Nozières-de Dominicis shifts,[115] as shown in Figure 18.

The problem with these two extremes is that neither one addresses the many systems of interest between these cases (e.g., semiconductors, many alloys, composites, and even certain oxides and polymers). Our analysis, on the other hand, suggests that even the latter systems exhibit loss transitions that seem to be strongly influenced, perhaps even dominated, by plasmon-type (collective) effects, but transitions that are also, significantly perturbed by the individual electron (or molecular) behavior of the system. The latter property is obviously not completely explicable in terms of the Nozières-de Dominicis effect. In fact, it is readily apparent that these systems can not be properly modeled by the simple free electron model.[95] The presence of plasmon dominated loss peaks in cases of semiconductor, and even insulating, materials was described in some detail by Pines[100] and Pines and Nozières[101] in their pioneering studies of plasmons, and used by our group for cases of photoemission losses.[116-122] Because this "mixed" case has never adequately been described for situations involving both electron and hole-loss excitations, we present here at least the rudiments of that argument.

D. General Quantum Mechanical Basis for ESCALOSS

1. The Pines and Nozières Arguments (Extrinsic Only)

There are a number of essentially equivalent ways of representing the electronic system of a standard solid about to be subjected to photoelectron ejection (with the accompaniment of any subsequent loss phenomena). One of the most expressive ways is to employ a perturbative partition of the system Hamiltonian, using the advantages of creation and annihilation operators in either position or wave vector space; i.e., as before, we begin with the Schrodinger equation,

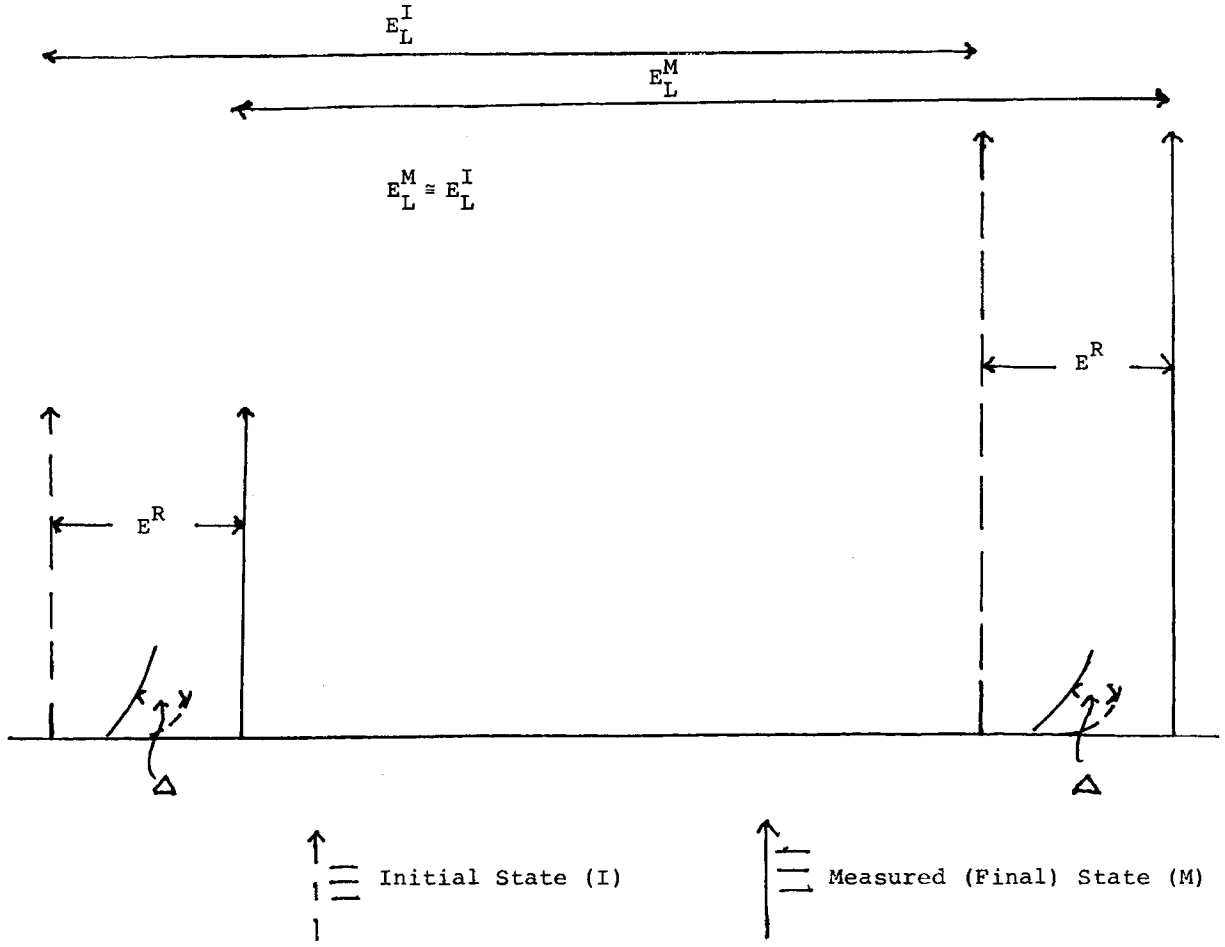

FIGURE 18. ESCALOSS results with moderate dispersion of both ΔE^R and Δ (where Δ corresponds to Nozieres-de Dominicis shift).

$$H\Psi(N) = E\Psi(N) \qquad (49)$$

where now we assume that,

$$H(N) = H^0 + \lambda H^1 \qquad (50)$$

where N defines the number of system electrons being considered, and, as in Section IV.

$H^\circ \equiv$ an appropriate, approximate sum of independent, one electron problems,

and

$H^1 \equiv$ any resulting electron—electron interaction terms over all 3m individual electron terms, and all $3(N-m)$ collective coordinates (see the following). In this manner, as shown by Pines et al.[100,101]

$$\Psi(3N) \rightarrow \int \Phi(3m)\chi(3(N-m)) \qquad (51)$$

where $\int$ represents an appropriately symmetrized, product partitioning of the coordinate space of the system designed to reflect the possible presence of both a space of individually functioning electrons and "regions" where these electrons only "evolve" *collectively*.

a. H°—The Various Models

Depending upon the nature of the systems involved, any one of several possible H° may be chosen, and constructed in terms of the previously mentioned creation and annihilation operators. These include

Valence Electrons Only:

[1] The free electron model

$$\sum_k \frac{k^2}{2m} C_k^+ C_k \qquad (52)$$

where C_k^+ is the appropriate electron creation operator in k space, and C_k is the corresponding annihilation operator.

Three cases, with two extremes: (i) No collective (plasmon) terms (i.e., H^1 above will lead only to Nozières and de Dominicis).[115] (ii) All valence electron interactions are collective (plasmon-type) (i.e., H^1 as in Lundquist,[104] Mahan,[62] and Langreth[95] models). (iii) Plasmon *dominated* interactions, dispersed by electron-electron interactions, Langreth[95] and Gadzuk[96] models.

[2] The Pines Model.[100]

$$\sum_i \left[\frac{p_i^2}{2m} + V(\vec{r}_i)\right] C_i^+ C_i \qquad (53)$$

where C_i^+ is the appropriate electron creation operator in position coordinates, etc. H° includes lattice periodicity, $V(\vec{r})$. Φ° now contains Bloch-type functions.

[3] The Fock Hamiltonian, as earlier in Equation 16.

$$\sum_i F_i \qquad (54)$$

This is our previously defined "Molecular Solid," or Gadzuk's, Manne-Aberg Shakeup[96] case.

Inclusion in H° of Certain Core Electron Effects:

1. Inherently as a part of [2]

2. These may also be added simply as polarization corrections to [2], or to [1]. Thus, the core inclusion can be shown to modify the plasmon dispersion (see below) from:

$$1 = \frac{4\pi e^2}{m} \sum_k \frac{f_k}{w_p^2 - w_k^2}$$

to also include

$$\frac{4\pi e^2}{m} \sum_i \frac{f_i}{w_p^2 - w_i^2} \qquad (55)$$

where f_k and f_i are respectively representative valence and core electron induced, oscillator strengths, and w_p, w_k, and w_i are the appropriate frequencies for the free plasmon, intra [1] or inter [2] band, individual valence electron transitions, and appropriate core level transitions, respectively. All of this may in some instances be made more tenable by noting that

$$\epsilon_c = 1 + \frac{4\pi e^2}{m} \sum_i \frac{f_i}{w_i^2} \qquad (56)$$

and therefore, as we shall argue, the approximation

$$w^2 \cong \frac{w_p^2}{\epsilon_c} \qquad (57)$$

may be employed, where ϵ_C is a reasonable rendition for a static, core, dielectric constant.[100] One can employ certain empirical arguments for the latter in order to avoid quantum mechanical calculations.

3. The inclusion of core electrons in case [3] above is generally a much more difficult proposition that may substantially enhance the scale of the Hartree-Fock calculations.

Explicit Inclusion in H° of Electron-Electron Correlation:

It is also possible, of course, to expand on the initial treatment of the system, and explicitly include some degree of the electron-electron correlation in our H° for either cases [1], [2], or [3]. As shown by Nozières and Pines,[101] such alterations will still permit a detailed perturbative treatment of the plasmon problem as part of H^1, but will naturally substantially increase the complications.

b. H^1—The Various Types of Electron Interactions:

Having described various possible H° cases,

we can continue to follow Pines,[100] and Nozières and Pines,[101] and describe the *extrinsic-only* H^1:

$$H^1 = \underset{(i)}{H_{SR.}} + \underset{(ii)}{H_{Coll.}} + \underset{(iii)}{H_{int.}} \qquad (58)$$

where

(i) H_{SR} - Short range - electron pair (e.e) interactions. (Part of these would move into H° for the inclusion case mentioned above.) According to Pines,[100] these interactions may be expressed as

$$H_{SR} = \sum_{k>k_c} \frac{2\pi e^2}{k^2} (\rho_k^+ \rho_k - N) \qquad (59)$$

where ρ_k^+ and ρ_k are the appropriate, respective, electron *pair* creation and annihilation operators, for example,

$$\rho_k = \sum_i e^{i\vec{k}\cdot\vec{r}_i} C_i^+ C_i \qquad (60)$$

In this case, k_c defines the range in k space over which the electrons behave as a collective, (plasma-like) entity. Thus, above k_c the plasmon is no longer a valid particle, and one must consider all electrons as exhibiting only individual behavior. (Note that the phrase "short range" occurs because position space is the reciprocal of k space!) In general, it is crucial to the present argument that k_c be relatively large for most of the conductors under considerations; i.e., that the short range (e.e) effects enter a plasmon dominated free electron situation as reasonable, relatively small, perturbations. (This type of phenomenon was adroitly argued for the photoelectron case by Langreth[95] and later by Gadzuk.[96])

(ii) H_{coll} - Long Range (H_{LR}) Collective (plasmon) fields

$$\text{(ii) } H_{Coll} = \sum_{k<k_c} \left[\frac{P_k P_k^*}{2} + \frac{w_p^2 Q_k^* Q_k}{2} \right] \qquad (61)$$

where P_k and Q_k are the appropriate momentum and coordinate operators, respectively, for the plasmons. For some purposes it is more convenient to rewrite this expression in terms of appropriate (boson) creation and annihilation operators:

$$H_{LR} = \sum_{k<k_c} w_k a_k^+ a_k \qquad (62)$$

where, without dispersion for case [1] above

$$w_k \rightarrow w_p = \left(\frac{4\pi N e^2}{m} \right)^{1/2} \qquad (63)$$

where N is the total valence electron density, and the effective mass $m^* = m$ for cases of maximum k_c; i.e., where there is no valence or core dispersion. As we shall see, reduction in k_c (introduction of dispersion) can be approximated as a deviation of m^* from m, and also by a reduction of the collective coordinate space from N to N′, where

$$N' = k_c^3/6\pi^2 \qquad (64)$$

and, where the difference $3(N - N') = 3m$ is that part of the general coordinate space that "retains" its individual electron character.[100] Note the previous discussion of the wave function in Equation 51.

(iii) $H_{int} \equiv$ Dispersions of the Collective Field

Dispersions that result from interactions between collective and individual valence electrons: As Pines has shown,[100] these effects are dominated by linear interaction terms

$$H_{int}^L = \sum_{k<k_c} V_k Q_k \qquad (65)$$

where V_k is our rendition of a general interaction operator. There are also related nonlinear interaction terms that mix several plasmons with a particular electron. As we shall show later, the short range, individual electron (e.g., band to band) transitions also play a direct role in this dispersion.

Dispersions that result from core interactions (see Equations 55 and 57): It should be

noted that all such interactive effects depend crucially on two factors: (1) the relative size of the interactive oscillatory strength, f_j, (specifically the strength of the interaction between a particular (jth) electron state and the appropriate plasmon); and (2) the relative similarity of the energy of any individual electron transitions, hw_i, (e.g., valence-to-conduction band or near core state-to-conduction band) to the appropriate plasmon transition, hw_p. As we describe below, these features may be best expressed in the form of the development of a standard perturbation theory.[119]

2. Loss Spectral Development Following Photoelectron Ejection (Inclusion of Intrinsic Processes)

As we mentioned earlier, the problem of relating the developments of Pines et al.[100] to a photoelectron experiment is that the latter evolves in a hole ion environment, which was not considered by Pines.

In view of the results to be described, it is important to consider the character of the temporal development with the photoelectron ejection involved. A detailed study of this problem has been made by Meldner and Perez[123] and Müller-Hartmann et al.[124] In this regard, they noted that there is a substantial difference between the behavior of a photoelectron ejected from a deep core state (e.g., In (3d) in In°) compared to one from a substantially delocalized (e.g., valence band) state (e.g., In (5P) in In°). The former may be considered to be recoilless,[124] and thus to retain its suddenly evolving character[123] throughout the photoelectron process (initiation to detection); i.e., the presence of the hole may be expressed as

$$H_{DH} = \epsilon b^+ b \qquad (66)$$

where DH designates a typical, deep hole of constant (ϵ) energy that has been suddenly created by the Fermion operator, b^+.[124] In view of the persistence of this field during a photoelectron experiment (as well as the photoelectron itself), a much more complex Hamiltonian arises that (compared to equation 58) includes interacts with two "excitation" particles: (1) the photoelectron (extrinsic processes), and (2) the deep hole (intrinsic processes). This Hamiltonian, H_T, may be expressed as[95]

$$H_T = \epsilon b^+ b + H^0 + H^1 + H^2_{int} \qquad (67)$$

where H° and H^1 have been previously defined, and

$$H^2_{int} = \sum_{k,k'} V_{kk'} D^+_k D_{k'} b b^+ \qquad (68)$$

The latter is a generalized relation depicting the interaction of the deep hole with the two types of electron fields (whose creations are symbolized by D^+) previously attributed to the solid system; i.e., interactions with the individual electrons:

$$H^{S.R.(2)}_{int} = \sum_{k,k'>k_c} V'_{k,k'} C^+_{k'} C_k b b^+ \qquad (69)$$

and the collective (plasmon) type field:

$$H^{L.R.(2)}_{int} = \sum_{k,k'<k_c} v''_{kk'} Q_k \overset{Q_k}{\nearrow} Q^+_k \; b b + \qquad (70)$$

It should be noted that these last two interactions are, in fact, the solid state physics equivalent of those parts of the final state, hole ion Hamiltonian that provide for the sudden evolution into the eigenstate, $\Psi^f(N-1)$, of that system. All of this was outlined above in Section IV where the present case corresponds to the case referred to by Gadzuk as "Mahan shake-up."

As Langreth was the first to demonstrate,[95] and Gadzuk has clarified,[96] the shifts and states that result from H_T may be solved for exactly, if one assumes that the system is adequately described by a free electron solution with no, or only modest, dispersions (i.e., starting with the H° in [1]). In this regard, one obtains a photoelectron probability that contains several terms, including an electron (extrinsic) induced term

$$P(n,z) = e^{-z/\lambda}(z/\lambda)^n/n! \qquad (71)$$

where z is the distance within the solid where the photoelectron originates and creates n plas-

mons, and λ is the mean free path of those plasmons. In the total, sudden manifold, *where plasmons predominate for a free electron system,* the term in Equation 71 must be convoluted with a contribution due to the sudden creation of the deep hole (intrinsic) effects; i.e.:

$$P(w) = \sum_{n=0}^{\infty} |\langle 0|n\rangle|^2 \delta(hw - \epsilon^0 + \Delta\epsilon^R - nw_p) \quad (72)$$

where we are considering the so-called principal, no loss peak (n = 0), and only losses due to collective (plasmon-type) transitions (n = 1, 2, etc.).[96,97,127]

As mentioned earlier, it is possible to obtain an exact solution for the term $\Delta\epsilon^R$ (the relaxation correction), if the system is assumed to behave only as a manifold of slightly perturbed, free electrons.[95] In this case, $\Delta\epsilon^R$ may be divided into two distinct effects: (1) Long Range:

$$\Delta\epsilon^R_{LR} \rightarrow -iaw_p = \sum_{k<k_c} \frac{g_k^2}{w_k^2} w_p \quad (73)$$

where, due to the nature of the problem, *a* is a constant shift; and (2) Short Range:

$$\Delta\epsilon^R_{SR} \rightarrow i\Delta t + \text{additional smaller corrections} \quad (74)$$

where Δ is also a constant rendition of the previously mentioned, catastrophically induced, long wavelength (infrared) manifold of transitions. The latter were originally realized by Nozières and de Dominicis,[115] and, where finite, should shift the centroid of each peak (both nonloss and loss) upfield (to higher binding energy). As demonstrated by Anderson,[114] this "infrared catastrophe" results from the fact that the resulting hole-particle situations are, in fact, bosons. An excellent discussion of the nature of these shifts, with figurative renditions, was provided by Langreth.[95]

It should be noted that Müller-Hartmann et al.[124] have demonstrated that, if the aforementioned hole is not sufficiently deep (e.g., for a valence band photoemission), then the previously described relaxation shifts should be muted. The intrinsic transitions, however, may still occur.[124]

3. Further Arguments on the Nature of the Electron-Induced Dispersions in Loss Spectroscopy

In the case where the free electron model still applies (i.e., where E_g [the band gap] < 1.2 eV), following Pines,[100] it is easy to see that dispersions of plasmons may be described in terms of those features often referred to in solid state physics as the k · P approximation.[125] In this method (sometimes also labeled as the near free electron model),[126] the electron traversing the lattice is assumed to experience small, constant, perturbative accelerations that reflect the lattice periodicity. In this regard, terms occur related to

$$\Delta E^{(s)}_{Dis} \propto \sum_r \sum_i \frac{|\vec{k} \cdot \vec{p}_i|^2_{sr}}{m^2(\Delta E^0_{sr})} + \text{additional, higher order corrections} \quad (75)$$

where i labels the particular valence electrons involved, and the ΔE^S_{Dis} modulates the effects of the free electrons in state s by introducing the modest "impact" of the lattice, represented by all other states [r]. ΔE^0_{sr} is the energy separation of states s and r at k = 0. This impact seems to act to produce a nonlinearity in k space in that the free electron behavior, originally expressed by Equation 52, no longer applies. In fact, energetic changes occur as if the electron is forced to accelerate (or alternatively, deaccelerate) by the factor ΔE_{Dis} as it (effectively) crosses the lattice. As mentioned above, it is common to express this acceleration as if the rest mass of the electron's involved in plasmon formation have been altered from their "free" value, m, to an effective value, m*.[125] In this case, the dispersion of the free electron, plasmon frequency may be reasonably expressed as in Equation 55.

In addition to this effect, when $E_g > 1.2$ eV we note that dispersion implies that the short range interactions of the electrons also must be finite, and we find higher order correction terms that should be proportional to k^2. If the system is described by the H° given in Equation 53 and H^1 in Equations 58 and 61, then we must further allow for the effect of band-to-band transitions (from say state 0 to all n possible states) on this

process. As Pines has shown,[100,101] this leads to the relationship:

$$\left[\frac{\alpha^2\rho_k}{\alpha t^2} + w_p^2\rho_k\right]_{no} = -w_{no}^2(\rho_k)_{no} + \sum_{k'\neq k}\frac{4\pi e^2}{m(k')^2}\vec{k}\cdot\vec{k}'(\rho_k'\rho_k)_{no} \quad (76)$$

where the first term on the right is the linear electron-plasmon ($k \cdot P$) correction (as described previously), and the second is a corresponding nonlinear electron(k)-plasmon(P)-electron(k′) correction.

In this case, we may then write

$$w_{no}(\rho_k)_{no} = \left|\sum_i \left(\frac{(\vec{k}\cdot\vec{p}_i)}{m} - \frac{\hbar k^2}{2m}\right)e^{i\vec{k}\cdot\vec{x}_i}\right|_{no} \quad (77)$$

and, following Pines,[100,101] we therefore can expand these "corrections" in the form of a perturbative expansion where

$$w^2 = w_p^2 + \frac{4\pi e^2}{\hbar k^2}\sum_n \frac{2|w_{no}(\rho_k)_{no}|^2}{w^2 - w_{no}^2 w} + \text{higher order corrections} \quad (78)$$

Dispersion terms, such as those on the right in Equation 76, may be generally expressed in the form of Equation 65. It is important to note that all of the terms in this relationship may be obtained from independent measurements of the spectroscopic properties of the particular electronic system under consideration.

Perhaps it is useful at this point to stop and quickly review those features of the ESCA process that have been described so far in this section.

We have noted that

1. Many materials with zero, or relatively narrow, band gaps have collective loss features, described as plasmons, that often provide a significant presence in the ESCA spectrum.
2. *All* of the peaks detected in the ESCA spectrum exhibited by materials of this type are shifted by relaxation effects that can be reasonably modeled by Equations 73 and 74.
3. In addition, we have noted that only the "most pristine" plasmon sources will produce loss lines split from the no-loss peak by the hw_p of Equation 63; i.e., most systems will experience some additional dispersion (perturbation) shift, and a reasonable approximation for many of these shifts is provided by Equation 78.

Viewed from another perspective, the completely undressed, free electron plasmon expressed in the intrinsic relation of Equation 72 must generally be modified to include hw in place of hw_p, where w reflects the dressing (dispersions) expressed in Equation 78. (It should be noted that this modification of the frequency of the collective effect also influences the extent of the relaxation, as for example, in Equation 73.)

All of these possible effects are hypothetically rendered in Figure 18.

4. On the Separation of Hole- and Electron-Induced Losses

We have thus suggested that loss spectra may be created by both the influence of the photoelectron itself (Equation 71) and what we have described as *the hole spectral function* (Equation 72). These terms are presented in the manner of Gadzuk,[59,96] as two separable functions. This has been shown to be a reasonable concept when the photoelectron escape velocity is sufficiently fast to warrant the application of the sudden approximation (i.e., photoelectrons of several hundred eV, or more). As the photoelectron slows, and remains for a longer period in the vicinity of the hole, an interference term also results, indicative of an adiabatically induced, interaction of both excitation sources (see Section IV). This leads to modifications of the extent of relaxation; e.g., the *a* factor in Equation 73 is damped to

$$\left(a' = a - \left(\frac{e^2}{hv}\right)F\right) \qquad (79)$$

where v is the velocity of the electron and F is a function that is proportional to the charge and velocity and inversely proportional to the plasmon frequency. The term a′ thus modifies the plasmon relaxation, and the Δt factor[95,96] is also damped. These interference terms are generally considered to be inherent parts of the intrinsic (hole-induced) excitation.[102]

As pointed out by several researchers,[95,96,102] the photoelectron experiment often does not yield situations that permit ready separation of the extrinsic and intrinsic contributions. This occurs, in part, because all photoelectron ejections must correspondingly create a hole, and thus the intrinsic excitations must always be present. However, as we have described above, the determining factor in reducing the relative contribution of intrinsic effect depends upon the energetic location of that hole.[20,118,123,124] In this regard, it is important to note that whereas a localized deep hole may maximize the intrinsic contribution inside a particular layer, an experiment can be constructed in which the photoelectron created in one layer *may* be forced to pass through another, chemically detached layer, before being detected. This *"displaced" photoelectron may produce loss transitions in the latter layer that are only of extrinsic origin.*[20,118,127] Examples that suggest the possible registration of this situation are described later in this section.

5. ESCALOSS

E_L and ΔE_L for Materials with Nonzero E_g. It is useful now to consider the expressions that we feel will most appropriately describe the loss splittings, $E_L^A(1)$, for atom A in chemical state (1) (as defined in Figure 19), and the change that results in these loss splittings when the state is changed from 1 to 2, $\Delta E_L^A(1 \rightarrow 2)$. It should be noted that Tables 6 through 8 contain comparisons of the experimental, and select theoretical values of these types of terms, for a variety of materials systems. In all cases the approximate dispersions and values are listed based upon ranges of band gaps, E_g. As we shall describe below this correlation is fairly general, but not universal.

Because of the relative ease in detecting and reproducing those often distinctive features, we have labeled the registration of E_L and ΔE_L for analytical purposes as ESCALOSS.

Relaxations and Loss Peaks Inside the Free Electron Model. If one scrutinizes Equation 72, one will notice that the plasmon states defined by the quantum numbers n = 0, 1, 2, etc., form a series of poles as first displayed by Langreth.[95] In the latter description, each of these plasmons states form poles that are displaced by the ΔE_{LR}^R in Equation 72 from the positions established before considering hole induced relaxations, but it should be noted that as expressed, these ΔE_{LR}^R values are constants, aw_p, for each state, 1, of each element, A. In addition, if one considers the short range relaxations, ΔE_{SR}^R, the resulting, weak, downfield shifts (generally in the infrared range) are also constant.[95] Thus, as demonstrated in Figure 19, even though the principal (no loss) peak and all of the plasmon dominated loss peaks suffer significant relaxation effects, *for dispersions out of the free electron model, the amount of the resulting peak shift is a constant for each peak; therefore $E_L^A(1)$, the loss splitting for material A in state 1, and $\Delta E_L^A(1 \rightarrow 2)$, the change in loss splitting going from state 1 to 2, are independent of this particular relaxation.*[116,117,119,120]

Summary of Photoelectron Loss Splittings for Different Models

(1) $E_g \leq 1.2$ eV:

In this case, if we start with no dispersion we obtain:

$$E_L^A(1) = h\left(\frac{4\pi Ne^2}{m}\right)^{1/2} = K\sqrt{n^A}(1) \qquad (80)$$

where K is employed to symbolize all constant terms, and

$$\Delta E_L^A(1 \rightarrow 2) = K[\sqrt{n_2} - \sqrt{n_1}] \qquad (81)$$

When we take into consideration the modest dispersion that may be realized through Equation 75 above, we find that we can express the results as

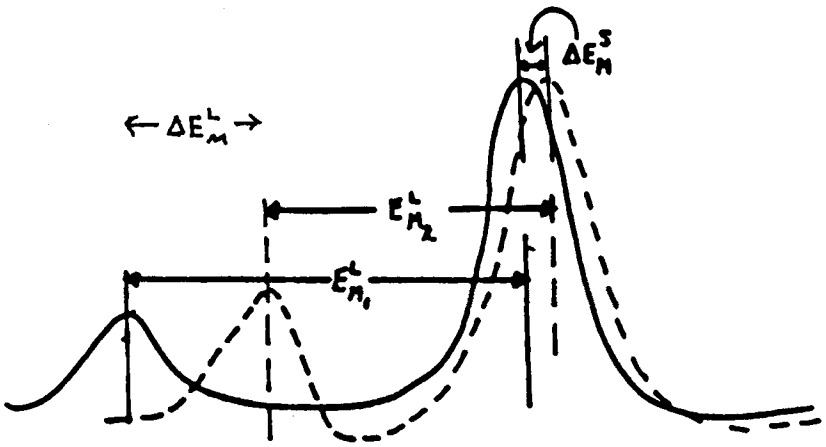

_____ (Chemical) State 1

_____ (Chemical) State 2

ΔE_M^S = "Measured" Core Level (Seigbahn) Shift

ΔE_M^L = "Measured" Shift Loss Splitting

FIGURE 19. ESCALOSS showing figurative E_L and ΔE_L values.

TABLE 6
Elemental, E_L Values Compared to Other Experimental ESCALOSS, Non-ESCALOSS, E_L Values and Calculated E_P
All results in eV[e]

	Band[d] gap	hWp free electron	Barr XPS	Pollack[99b] loss	Pines[100b] optical	P & E (HEELS)[c]
In	0	12.5	11.5	11.8	12	
Sn	0.08	14.1	14.0	14.2	12	
Sb	0.11	15.1	N.A.	16.0	15	
Al	0	15.8	15.8	15.6	15	
Cd	0	10.5	9.4	9.3	20	
Si	1.17	16.6	17.8		17	16.9
Ge	0.74	15.6	16.5		17	16.4
C	5.2[a]	31.1	21.6[b]		22	

[a] Diamond.
[b] Adsorbed hydrocarbon.
[c] P&E ≡ Philipp, H. R. and Ehrenreich, H., *Phys. Rev.*, 129, 1550, 1963.
[d] Intrinsic.
[e] Loss results from this lab ± 0.2 eV. Consult original references for other precisions.

$$E_L^A(1)' = K\sqrt{n_i} + \frac{\hbar k^2}{2m}\left(\frac{m}{m^*}\right) + HOT \quad (82)$$

where HOT designates higher order terms. A shorter approximation to these corrections may be expressed by substituting $m^*_{1(A)}$ for m in Equation 63.

TABLE 7
Molecular E_L Values

	B.G.	hWp	Barr XPS loss	This lab HEELS	
GaAs	1.5	16.3	16.2		
InSb	0.25	13.9	13.5	14.0	
GaSb	0.8	14.8	15.3		
InN	1.7	19.0	15.5	16.0	
				Pines[100b]	P & S[c]
In_2O_3	3.6	22.5	18.5	19	
Al_2O_3	7.2[a]	N.A.	24.4[b]	23	22.2
SiO_2	9.0[a]	N.A.	23.0[b]	25	

[a] Indirect.
[b] Average 2p - Variable.
[c] P&S ≡ Powell, C. J. and Swan, J. B., *Phys. Rev.*, 118, 640, 1960.

TABLE 8
In° and In Compound ESCALOSS Results.

	Direct band gap	XPS this lab ± 0.2	XPS other lab ± 0.2	Optical ± 0.5	Heels this lab ± 0.5	Heels other labs ± 0.5	hWp free electron calculation
In°	0.0	11.5	11.8[c]	12.0	—	—	11.0[a] 11.5[b]
InSb	0.25	13.3	—	—	13.5	13.0[d]	13.5
InN	1.7	15.5	—	—	16.0	—	19.0
In_2O_3	3.6	18.5	—	—	19.0	—	22.5

[a] Taken from Reference 100b.
[b] This Lab.
[c] Taken from Reference 61 and Reference 99.
[d] From Powell, C. J. and Swan, J. B., *Phys. Rev.* 118, 640, 1960. With permission.

This leads to

$$\Delta E_L^{A'}(1 \rightarrow 2) = K'\left[\sqrt{\frac{n_j}{m_2^*(A)}} - \sqrt{\frac{n_i}{m_1^*(A)}}\right] \quad (83)$$

Effective mass values, m*, may be found in the literature for some of the appropriate systems. Based on Equation 83, therefore, the differences recorded in Table 4 between E_L and E_P for such systems may be reflected by these m* values. These results should, at least, suggest whether m* is larger or smaller than m. One should be careful at this point, however, since, as we have outlined above in Equation 51, the processes previously described as short range may also produce a corresponding, effective reduction in the number of electrons experiencing collective effects from N to N′; as we shall show below, this effect should be factored into Equation 83.

(2) $1.2 < E_g \leq 3.5$ eV:

By including the electron-plasmon dispersion arguments[100,101] suggested in Equations 76 and 78, we find that we may argue that

$$\Delta E_L^A(1 \rightarrow 2) = K[\sqrt{n_i} - \sqrt{n_j}] - K'' \sum_{k<k_c} \left[\frac{1}{n_i}[A]_1 - \frac{1}{n_j}[A]_2\right] \quad (84)$$

where, for example,

$$[A]_1 = \sum_n^{(1)} f_{on}^1(k) \frac{w_{no}^1 w_p - (w_{no}^1)^2}{(w_k^2 - (w_{no}^1)^2} \quad (85)$$

where $f_{on}^1(k)$ is the previously defined oscillatory strength for a 0 to n transition.

In this case, therefore, we are assuming that the dispersion experienced by the free plasmon is primarily due to short range effects conveniently expressed as quasi perturbation corrections induced by noncollective band-to-band transitions, from state 0 to n.

At this point we should reconsider a key feature expressed above in both Equations 83 and 84. In view of the fact that our plasmons (and for that matter our individual electrons) are now (of necessity) "dressed" with dispersions, we must reexamine whether E_L and ΔE_L may still be considered free from relaxation effects. This feature is considered in Section VI.

(3) $E_g > 3.5$:

It should be noted that we have not proven that the loss spectra for materials with band gaps greater than ~1.5 eV are dominated by collective (plasmon) effects. In fact, it seems apparent that the relative importance of plasmons should generally decrease as the band gaps of the involved materials grow. Despite this, *it is our contention that the principal loss lines detected for most materials, even those with comparatively broad band gaps (including, for example, Al_2O_3[120] and even SiO_2[117] are still primarily of plasmon type.* In this sense, we are following the lead of Pines[100] and Pines and Nozières,[101] and arguing against the implied thrust of the theoretical work of the 1970s. It should be obvious, however, that the following points must be considered as valid, whichever source one accepts as the principal cause for the loss transitions in question:

1. The size and influence of the plasmon contribution to any loss peak structure is directly proportional to the electron density at, or very near, the Fermi edge. Thus, as the valence band density of states shrinks, and/or the leading edge pulls back away from the Fermi edge, (as happens, for example, for the sequence of materials In° → InSb → InN → In_2O_3[116]), then the relative sizes of the loss peaks decrease, and the exclusive nature of any plasmon contribution must decrease.
2. Band-to-band and/or near core level-to-conduction band discrete loss transitions may alternate in intensity with the corresponding plasmon transitions. Thus, as the "effects" of the latter weaken, the relative contributions of the former generally grow.[100,116,118]
3. As various types of transitions of the right symmetry (e.g., plasmon and band-to-band) approach one another in size and energy (see Equation 78), *these transitions will mix and create combined features.*[119] Thus, as we have argued, no matter what effect one accepts as the dominant influence of the resulting loss transitions, the experimental E_L is generally subject to extensive quantum mixing with any near degenerate transitions.[119]

The principal reasons for *our* supposition of plasmon domination for most E_L are the following:

(a) The arrangement and position of the loss peaks—In numerous cases, even those with E_g not 0, multiple loss peaks have been detected (e.g., SiO_2,[117] InSb,[116] GaAS,[119] etc.), and in all cases most of these multiple features follow the Poisson distribution pattern required for harmonic oscillator-driven plasmons, rather than band-to-band type transitions.

(b) The lack of energetically appropriate band-to-band transitions—Based upon the ESCA determination of the positions of the valence band density, and any realized near core states, there are *often* no ready choices for

possible band-to-band or near core-to-band candidates to explain many observed loss transitions.

(c) Improper sequencing of loss transitions with chemical changes—It should be noted that the sequences observed in the loss splittings for select elements, ΔE_L (such as that reported in Table 8 for indium in going from $In^\circ \rightarrow InSb \rightarrow InN \rightarrow In_2O_3$), cannot be explained by invoking band-to-band arguments using the corresponding energy differences between the In(4d) and the valence and conduction bands.[116,119]

(d) Further aspects of inappropriate band-to-band features—In the case of Al_2O_3[118] and SiO_2[117] (and many related oxides),[119] if one argues that the E_L are due to band-to-band transitions, then one must explain why, with a substantial difference in the corresponding valence band features and gaps, there is so little difference in the E_L values for these oxides, and also why the small E_L differences detected seem to change in the wrong direction.

It may appear to the reader that the author is being somewhat equivocal at this point in referring to the types of material systems whose loss transitions may be described as "of plasmon origin." This equivocation is purposeful, as there is really no adequate, simple model that encompasses all experimental cases.

As indicated, we have found that the size of the band gap is one useful signpost of the degree of plasmon character, but a far from inclusive one. Thus, while there are certain periodic sequences of material which as the band gap, E_g, shrinks, their loss spectra become more and more plasmon dominated, there are other groups of elemental or compound species that exhibit this type of loss behavior long before E_g reaches zero, while still other materials with zero E_g may produce little or no significant plasmon dominated losses.

Thus, an alternative method of designation is obviously needed. Although, still incomplete, the following composite statements are proposed:

(1) If a material has a zero band gap that results from the Fermi edge coupling (electron occupancy) of only s or s + p bands that are conductively configured (delocalized) at E_F, then readily discernible, plasmon dominated, loss transitions will result.

(2) If the sole presence of delocalized s or s + p states at E_F is substantially mitigated by the ready, near E_F, presence of highly directed, localized orbitals (e.g., those of d and/or f type), then materials with this type of electron distribution will generally exhibit significant Nozières-deDominicis (up field) peak distortions, at the cost of plasmon losses. Many of the elemental transition metals are ready examples of this type of system.

(3) If there are no near valent, d or f states, then a system may still produce plasmon dominated losses, even if its s + p states are "organized" and pulled back from E_F into a semiconductor format (e.g., Si°).

(4) If the materials in question are wide band gapped semiconductors or insulators, but do not have any near valent d or f states then the loss peaks of these materials are substantially dispersed, but are still most accurately described as "of plasmon origin" (e.g., Al_2O_3 and SiO_2).

(5) If, on the other hand, the material, in question, is endowed with a modest E_g, and its valence band states are substantially populated by partially filled, (or conversely partially unfilled) localized, directed d or f states, then arguments that initiate with band theory are generally not adequate to describe its loss spectra. These materials are some of the previously mentioned "molecular solid" systems, and their quantum character is best described using orbital models that lead to Manne-Aberg-type loss transitions (see Section IV). Examples of these materials include CuO, CeO_2, NiO, etc.

6. The Influence of Dispersions on Relaxation Effects in E_L

A feature that was not considered in any previous discussion of the plasmon effect, is that for

semiconductors and insulators the relaxation shifts of both the principal (no-loss) line and the corresponding plasmon dominated loss peaks should not be considered as a coupling of a (deep) hole state with a free electron plasmon (as in Equation 72), but rather as a coupling between that hole and a fully dressed (dispersed) plasmon,[100] such as that described in Equation 78. If these effects are properly considered, then one will find expressions such as

$$\overline{\Delta E}^{r}_{LR} = a'(q)w_q \qquad (86)$$

where $a'(q)$ will be needed to replace the simpler a relation in Equations 73 and 79. The complications represented in Equation 86 are severalfold. First, one must begin by recognizing the electron-plasmon, dispersion shifted frequency, w_q, in place of w_p. Second, it must be acknowledged that the collective-hole coupling term, $a'(q)$, is now affected through this dispersed collective, rather than the free electron plasmon. This means that a' in Equation 86 may differ substantially in size from the a in Equation 73. Further, a' is now a complex function that will, to higher orders in perturbation theory, include the dispersive forces acting on the plasmon, and thus introduce Fermion terms that will, in turn, couple with the Fermion hole. The result will not be exactly soluble into a constant term (such as a), and higher order terms may depend upon the final state index, n, which will sum on the mixed collective-individual states (i.e., states that no longer index just the plasmons). If the latter is true, terms similar to the following will occur in the energetic delta function in Equation 72[101]

$$\delta(\Delta E) = \delta(hw - \epsilon + a'(q)w_q + \Delta t - n(w_q - a''(q))) \qquad (87)$$

where the factor $a''(q)$ is employed to represent any higher order effects in the dispersion that affect each of the n states differently. *These effects will therefore make the loss splitting E_L (and correspondingly ΔE_L) relaxation dependent.* Based upon the nature of this argument, however, it is felt that any effect of this type will generally be quite small; therefore, it should be reasonable to ignore relaxation shifts in applying Equation 72 to most semiconductor (and even some insulator) loss shifts.

7. Final Argument for Effects of Dispersion

In view of the previous arguments, if one wishes to determine the nature of the loss spectra in photoemission (and perhaps use it in analysis), one needs to estimate the relative contributions of the collective and noncollective behavior. In some cases we will find the latter to be similar in size to the former; however, as we have argued above, generally *for solids of major interest,* the collective (plasmon) features dominate. (Recall that despite the previous discussion there is no absolute proof for this statement other than the fact that it seems to support the resulting data.) On the other hand, Pines has demonstrated,[100,101] and we have pointed out,[116-122] that, for most nonconductive materials, the noncollective effects should be large enough to influence the plasmon feature, and therefore, cannot be ignored. Generally, however, despite the large size that might be predicted for some of these noncollective effects, one can generally construct reasonable arguments for their inclusion, in terms analogous to conventional perturbation theory.[119] For example (as we have seen), we may assume that a reasonable solution may be achieved through second order; then,

$$E_L(i) \simeq E^0_0(i) + E^1_0(i) + E^2_0(i) \qquad (88)$$

where, by analogy, $E^0_o(i) = E_P(i)$, the free electron, plasmon value, and i is employed in this section to collectively index both the element (A) and its state (1). Now, based upon previous arguments:

$$E^1_0(i) = 0 \qquad (89)$$

and

$$E^{2o}(i) \cong \sum_{j=1} \frac{|\langle \phi_j | H_{int} | \phi_0 \rangle|^2}{(E^0_0 - E^0_j)} \qquad (90)$$

where $E_o^2(i)$ is thus the approximate change in the loss splitting ($E_L(i)$), created by the dispersion of the collective motion by the individual electron behavior. Thus, using Equation 78, it is reasonable to consider the energies E_j^0 to be appropriate band-to-band, or near core-to-conduction band transition energies, and the numerator of Equation 90 corresponds to the interactive matrix elements in Equations 77 and 78. The latter tend to grow as the band gap broadens. In this regard, we may obtain a qualitative feel for the relative size and direction of the shift provided by $E_o^2(i)$ by noting that

$$E_0^2 \text{ increases in size as } |E_0^0 - E_j^0| \rightarrow 0 \quad (91)$$

That is, as the appropriate individual electron transitions to the conduction band become similar in size to that for free electron plasmon, and more specifically when

$$(E_p(i) - E_j^0) > 0, \text{ then } E_L > E_p \quad (92)$$

and when

$$(E_p(i) - E_j^0) < 0, \text{ then } E_L < E_p \quad (93)$$

A further concept, that should be obvious, is that when relationship 91 does not hold (i.e., when there is no band-to-band or core-to-conduction band transition of energy close to E_p), then $E_L \sim E_p$. Although these arguments are worthy of consideration, they should not be oversubscribed to. One should note in the tables in this review and also the papers of Pines[100,101] that there are numerous exceptions.

It also should be noted that a lack of dispersion does not necessarily signify that the loss peak will be large in relative intensity.[99] Nor does it necessarily indicate that systems containing a particular element in a particular state (i) with large dispersions will produce loss peaks with less intensity than those systems containing (i) with modest dispersion.

E. Examples of the Use of ESCALOSS in Chemical Analysis

1. Elemental Systems

The relative size of the previously described loss peaks seems to depend upon several factors—the primary one being the number and character of the density of states at or near the Fermi edge of the system.[100] Close study of loss size and type suggests that the best source of a system with a primarily, plasmon-only loss spectrum of relatively large size, is a spherically symmetric (i.e., s or p state) valence density at or near the Fermi edge that is relatively free from localized, directed, valence density coming from the low binding energy parts of the valence region.[99] Therefore, *most* transition metals with large near-Fermi edge, directed, d-state densities should exhibit poor loss intensities, with little or no plasmon character.[99,119] Thus, for example, Al° ($3s^23p$) forms a well recognized loss pattern, Figure 20, that is dominated by strong, plasmon peaks with little or no dispersions,[99,119,127] whereas Cu° ($4s^13d^{10}$), on the other hand, exhibits only a weak loss spectrum which may not contain any plasmon character.[128] As expected, In° also exhibits a strong, plasmon dominated, loss pattern, similar to Al°.[116,119] Interestingly, Cd°, which has a near valent d band, still produces a significant plasmon dominated loss spectrum,[99] apparently because its d band is pushed to relatively high binding energy, separating it from the symmetric, plasmon producing, s band state.

One of the most interesting expressions of these features for the Group B metals is exhibited by Ag°, which apparently has a d band density sufficiently separated from its s state (the edge of the former is at ~3.5 eV), compared to Cu°, such that Ag° exhibits significant, plasmon dominated losses.[99] Finally, moving further down the same column of the periodic table to Au we find the d band returned to a position close to the Fermi edge (~1.7 eV), and the loss spectrum (and its corresponding plasmon character) dissipated. More is said about these features in a recent publication.[129]

In all of these cases, it should be noted that the loss splittings, E_L, realized by the aforementioned elemental systems in photoelectron spectroscopy, are essentially the same as those produced by (extrinsic only) losses during "conventional" electron scattering loss spectroscopy (see Tables 6 and 8). This demonstrates the lack of relaxation influences in ESCALOSS, at least to this level of dispersion.

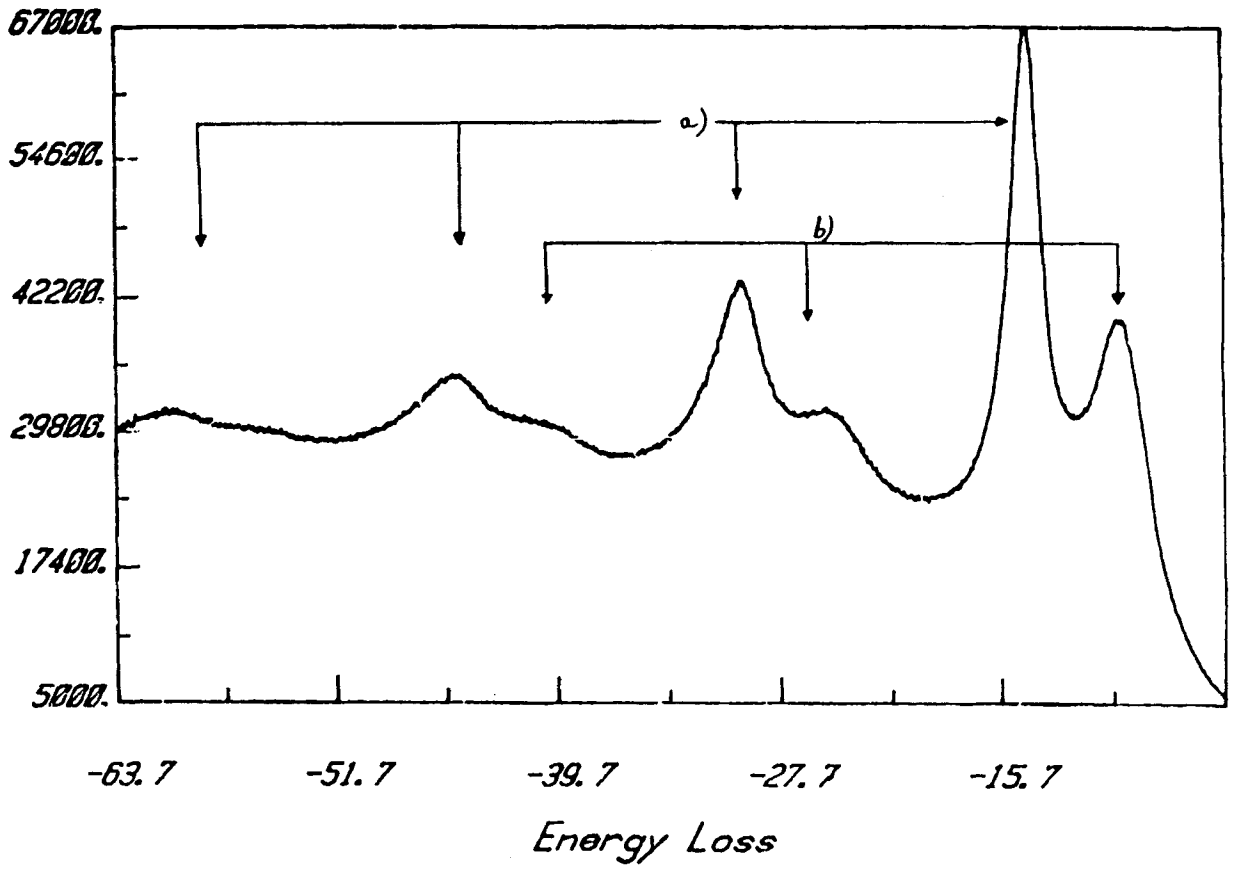

FIGURE 20. Loss pattern for Al° demonstrating Poisson distribution typical of free electron induced plasmons. (From Reference 131.)

2. Indium Compounds

The use of ESCALOSS as a tool in chemical analysis requires, of course, that it be directly expressive of changes in chemistry. One of the first detailed demonstrations of this capability was provided in a detailed study of loss spectra produced by a variety of solid indium systems, including In°, InSb, InN and In_2O_3, in both bulk and thin film form.[116] The critical aspects of the results are given in Table 8 and Figure 21, showing that the use of conventional, principal peak ESCA chemical shifts to differentiate between these systems is not feasible for all these compounds, due to the vanishingly small size of the shifts.[116,130] In addition, the InN, and particularly the In_2O_3, are nonconductive systems that exhibit noticeable charging shifts, making the registration of conventional binding energies difficult. The loss splittings, E_L, of all these materials, however, as mentioned earlier, are independent of charging. The large size of these loss splittings and their progressive shifts make them intriguing chemical signposts.[116] It should be noted, however, that the size of the change in ΔE_L and the position of their E_L values are more involved than just a registration of the differences in valence state electron density per unit cell, N_i (i.e., the differences in their free electron plasmon shifts). The size of the difference between E_L and E_p (i.e., the dispersion), is found to increase with the band gap (Table 8), and thus also influence ΔE_L. In all cases, in the manner provided for in Equation 90, the transition between the intense, near core, In (4d) and the conduction band produces a perturbative "push" on the ϵ_p for In systems.[119] However, this push should be relatively modest for In° and InSb, (due to Equation 82), and be countered by a push to higher binding energy by the valence band to conduction band

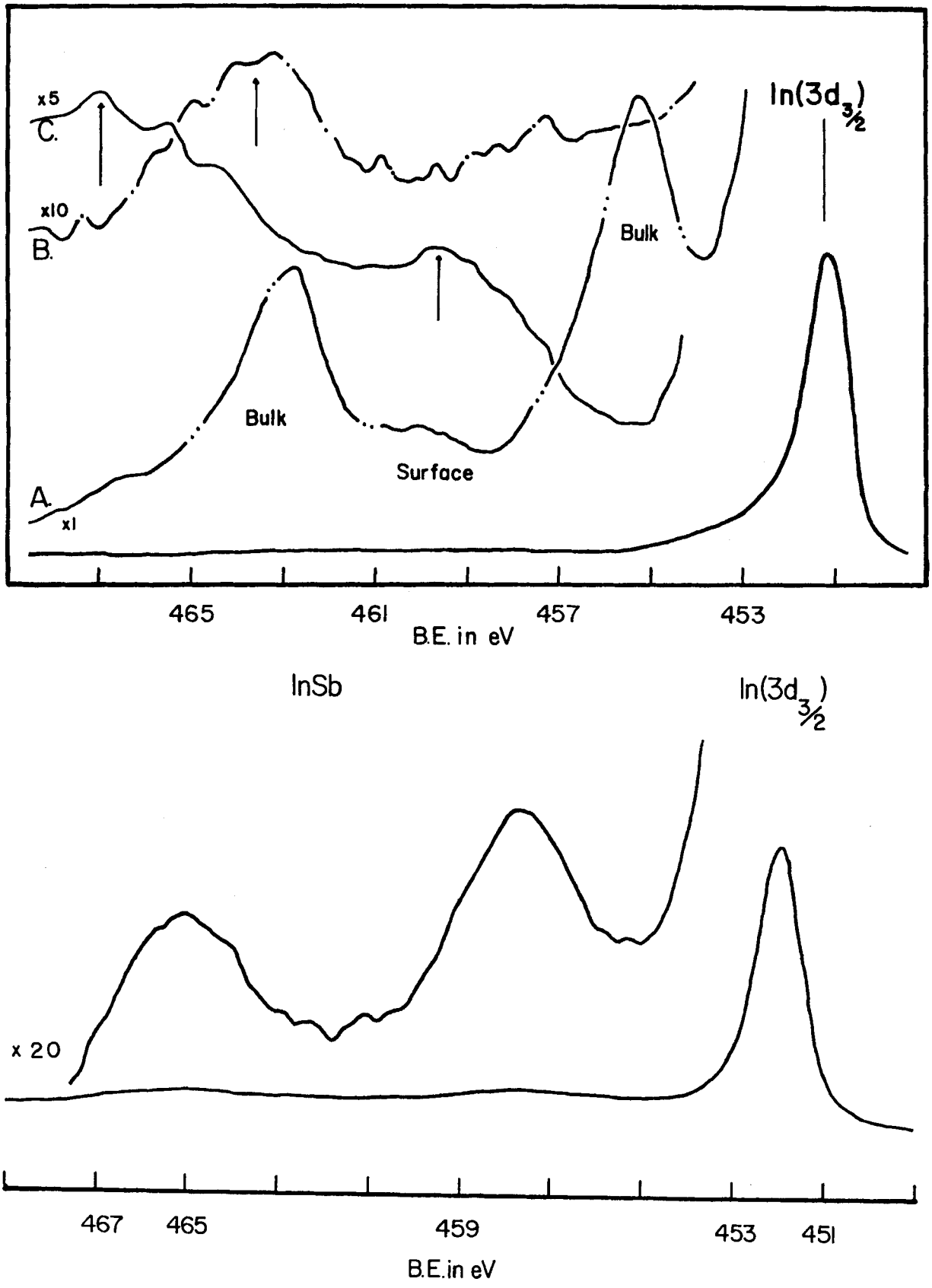

FIGURE 21. In(3d) loss lines for various Indium compounds: A(In°), B(In_3O_3), C(InN), D(InSb).

transition.[119] In the case of InN, and particularly In_2O_3, the down field push of In (4d) → conduction band transition is relatively large (due to the similarity of ϵ_p and those particular E_i), and the resulting dispersion is ~3.5 (InN) and 4.0 (In_2O_3) eV, respectively.[119]

3. SiO_2-Si° and Al_2O_3-Al° Systems

In the case of oxide systems, it is tempting to suggest that any dispersions may be induced by the near core transition from O(2s) to the conduction band. This transition is approximately 27 to 30 eV for SiO_2 and Al_2O_3 based upon the respective positions of the two states involved. Based upon Equations 55 and 90, and the corresponding values for ϵ_p, this should provide the ingredient for a significant perturbation. This, however, seems to be countered by the relatively weak density provided by the O(2s), and one does not anticipate significant dispersion from this source.[117]

Thus, in the case of oxides with significant covalent bonding (e.g., SiO_2 and Al_2O_3), one is more inclined to attribute any dispersions (always reductions) of the plasmon dominated losses to the reduction in "free" electron density in the valence band that results from their inherent covalency.[100,119] Thus, one should employ an electron density of N′ in place of N in the plasmon calculation (Equation 51), where $m = N - N'$ is indicative of the covalently "tied-up" valency electrons. Evidence in support of this contention is given in the loss spectra of the oxides (in Table 7), showing that the E_L is generally significantly less than E_p. SiO_2 may be an interesting exception as it exhibits little variation (perhaps due to a counter-variant, "push-up" dispersion provided by the valence band to conduction band transitions that, due to the extreme width of the SiO_2 bands, range from ~10 eV to ~22 eV).[117]

The character of the loss spectra for Si°(2p) shows that it is dominated by plasmon influences, despite the band gap of ~1.1 eV. The ΔE_L for SiO_2-Si° was utilized in a study of a SiO_2/Si° layered system, with particular applicability at the interface (Figures 22 and 23).[117]

In a related study of the ESCA loss spectra provided by Al(2s) and Al(2p) during the oxygen-induced growth of the oxide on the surface of pure Al metal,[118,131] the substantial ΔE_L (=8.2 eV) was used to follow the growth characteristics. However, as the oxide formed, the Al° subsurface was still detectible because of the (~40 A deep) depth of field of the ESCA. Thus, a variety of mixed loss lines resulted[118,131] (see Figure 24). Examination of these lines indicated a predominance of 15.8 eV E_L for Al° and 24.0 eV E_L for Al_2O_3. Further loss peaks shifted upfield from the Al(2p) of the metal by ~24 eV were detected suggesting the possible detection of extrinsic-only losses produced by Al°(2p) photoelectrons during their passage through the outer layer of Al_2O_3.[20,118] (The extrinsic-only character results from the localization of the hole of the Al° photoelectron in the metal matrix.) Additional details were also observed, but such studies are still too poorly controlled for any definitive judgments.

4. General Features

It is interesting to try to catalog the rationales for the different dispersions suggested for ESCA loss spectra of various compound systems. Some of these speculations are summarized in Table 9. Table 10 demonstrates another feature about the general nature of the loss spectra of these compounds. If these losses have primarily a plasmon origin (based on Equation 88), then it is apparent that their E_L values should be directly proportional to the electron density in the valence band. This suggests that systems which are isoelectronic, *and not affected by other factors,* should yield essentially the same E_L values. In Table 10 we see that this is the case for most of the Ge° isoelectronic series, with the exception of KBr. The same argument, however, does not hold for the Sn° series. It is suspected that the exceptions noted are due to significant, selective dispersive forces that increase with the increased band gaps as one radiates out and down in these Group IV isoelectronic series.[119]

Perhaps one of the most interesting (and potentially the most useful) examples of the status of plasmon-only vs. dispersed plasmon losses oc-

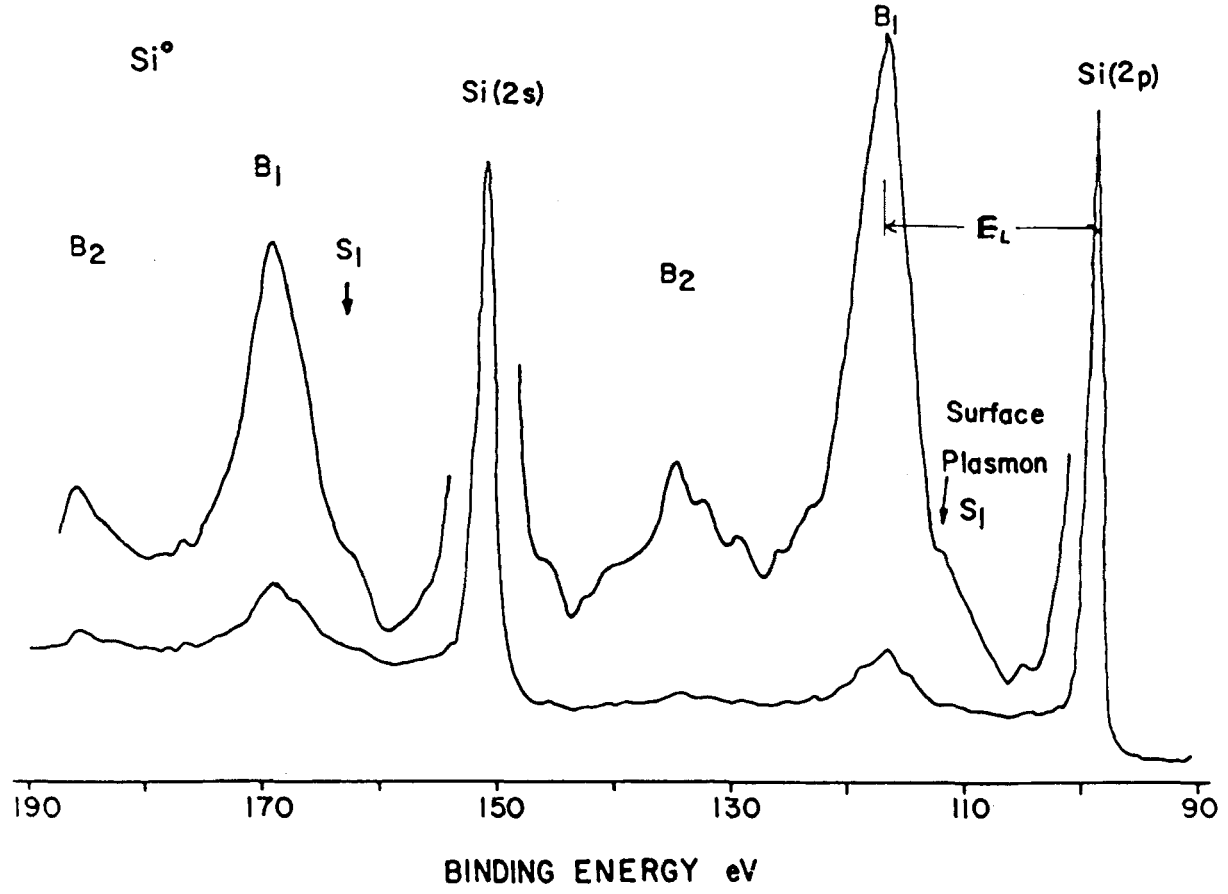

FIGURE 22. Loss spectra for Si(2s) and Si(2p) of Si° (note the E_L values and their Poisson repetition despite the $E_g \sim 1.1$ eV).

curs for carbon based systems. A preliminary analysis of a carbon system is presented below.

F. An Additional Important ESCALOSS Spectroscopy Example—The Carbon Problem

1. Introduction

One of the most discouraging problems in traditional ESCA analysis is the lack of uniqueness found in the positions of the principal C(1s) lines for many different carbon based systems (i.e., those with –C–C–, –C=C–, –C≡C–, and –C–H bonds).[121,132] Thus, whereas the (apparent) binding energy of the principal C(1s) peak may be employed to identify the presence of certain different organic functional groups (e.g., –C–O–, –C=O, –C–OH; as exemplified above in the AR-XPS study of polypropylene oxidation),[85,86] it cannot be readily employed to differentiate between, for example, polypropylene, polystyrene, and graphite. In fact, if asked to identify the bonding nature of the ubiquitous carbonaceous deposition that always occurs on air exposed surfaces (referred to in the surface analysis literature as *adventitious carbon*),[121,133] many researchers have classified it as a graphite-like substance, whereas others have suggested an adsorbed hydrocarbon polymer, with generally no evidence provided for either claim. There can be little doubt that this constantly present shortcoming is one of the more frustrating features of applied ESCA.

The principal reasons for this chemical shift problem would appear to be twofold and related. First, most of the systems in question are, at minimum, modest insulators and, therefore, due to charging produce somewhat uncertain C(1s)

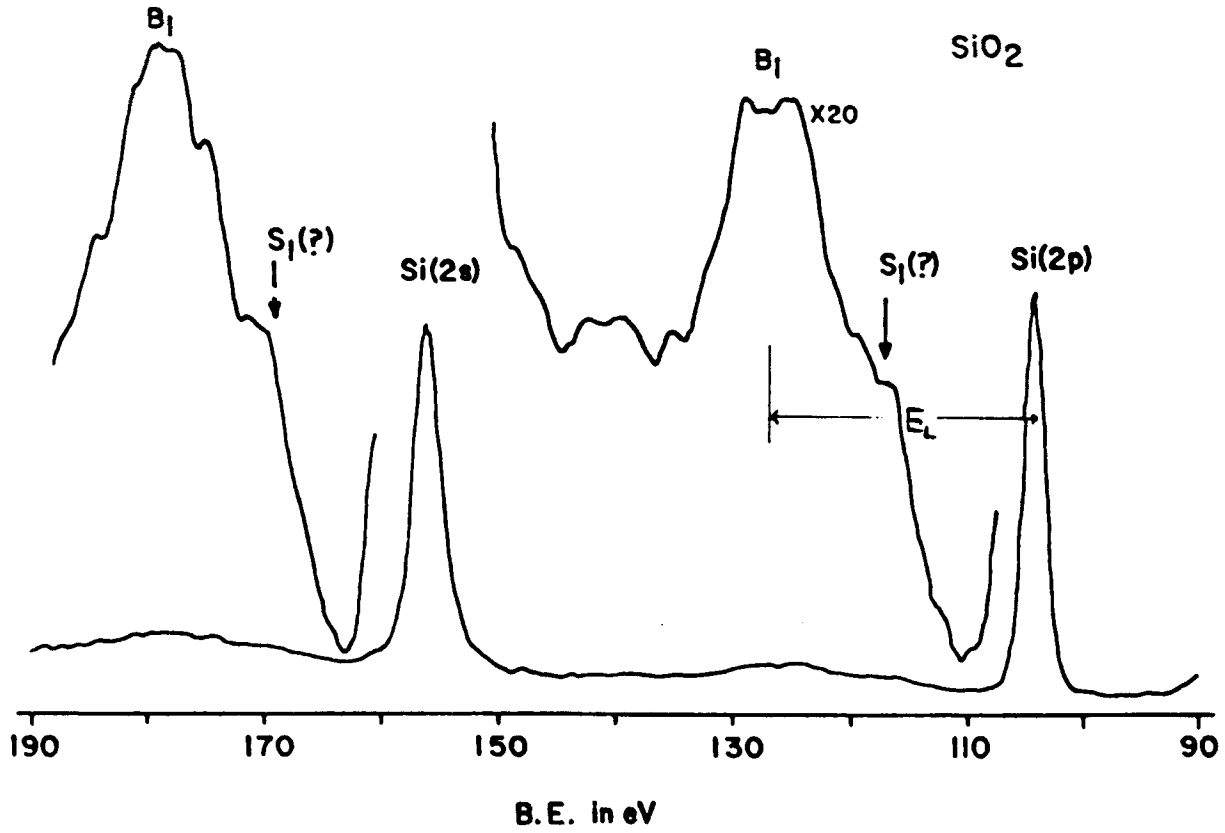

FIGURE 23. Loss spectra for Si(2s) and Si(2p) of SiO_2 (note the substantial increase in E_L over that for Si°, but significant reduction in loss peak intensity and lack of Poisson character).

binding energy positions. Even if charging is curbed, however, most researchers have suggested that the chemical shift (if any) for C(1s) between, for example, graphite and an adsorbed hydrocarbon is very small, perhaps too small to register. Hence, while some have suggested a C(1s) binding energy for graphite systems of 284.2 eV and that for a hydrocarbon polymer at ≃284.8 eV, it has now become common to shift all carbon-carbon and carbon-hydrogen C(1s) binding energies to a single value, recently adjusted to 284.6 ± 0.4 eV.[20,85,86,133] This lack of distinction, of course, makes ESCA a less than adequate tool for investigations in the rapidly growing fields of organic composites and films. It is the purpose of the present discussion to show how ESCALOSS may be employed to provide at least a partial answer to some of these questions.

Based upon the methodology outlined previously a series of ESCA spectra were recorded for a variety of hydrocarbon and carbon only systems, with particular emphasis on their core loss peaks. These results were produced using several different ESCA spectrometers (including the Hewlett-Packard 5950A at the UOP Research Labs [Des Plaines, IL], several types of PHI systems at the University of Minnesota, and the PHI Laboratories in Minneapolis, the SSI system at the University of Western Ontario, and the new VG ESCALAB at the University of Wisconsin [Milwaukee]). It is significant to note that reasonably reproducible loss results were achieved with all of these systems. Hence, the results described below are not unique to particular ESCA instruments. We have personally observed, however, that the ease with which these results are generated and the ability to differentiate certain subtleties in intricate use situations seem to be aided by use of a monochromator based ESCA unit. Total analysis also usually requires the generation of a good survey scan (to examine for ubiquitous impurities, such as O, N, Na, Cl, etc.) and a good high resolution scan of the C(1s) peak. The latter should be run with the use of an elec-

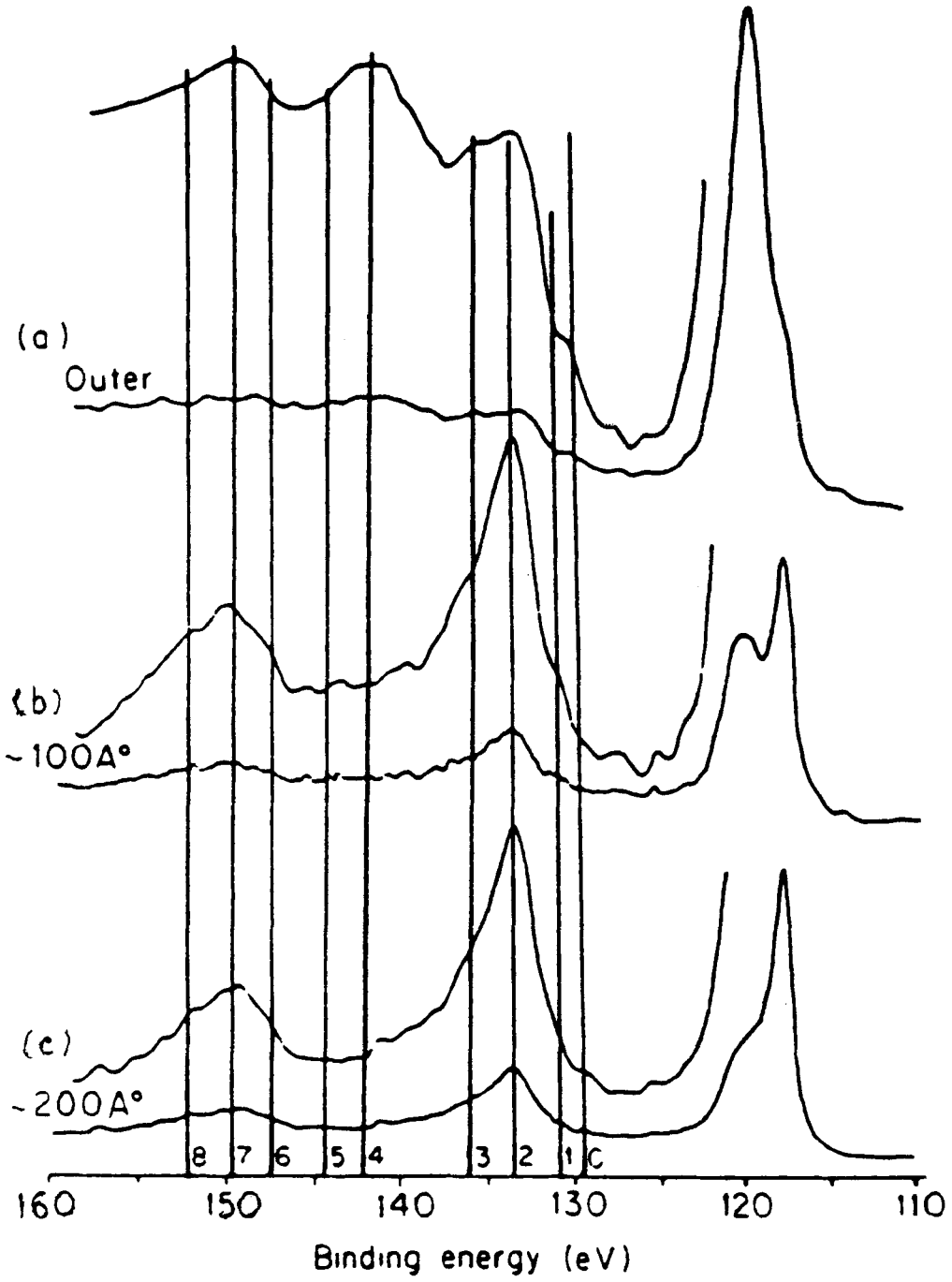

FIGURE 24. Loss results realized during growth of alumina on Al°.

tron flood gun to remove charging shifts. This method, however, is not absolutely necessary in the case of the loss spectral analysis due to the independence of the loss splitting, E_L, from charging.[19,20,121]

In addition, we found that valence band spectra scanned from about 0 to 30 eV may provide some delineation of the chemical character of carbon systems.[99,133] A recent use of this type of study has been provided by Madden and Allred.[134] Often, however, this valence band method may be even more difficult to register and control than the loss peaks. Fortunately, only one of these methods is generally necessary to achieve analytical results. (One version of appropriate valence band data for certain carbon-based systems

IDENTIFICATION OF PROBABLE LOSS LINES IN Al_2O_3/Al^0 SYSTEM

	SOURCE OF PHOTOELECTRON	SITE OF LOSS TRANSITION	TYPE OF LOSS TRANSITION	SEPARATION FROM Al LINES IN Al_2O_3	SEPARATION FROM Al LINES IN Al^0
P_1	Al_{2P}	—	—	0.0 (75.5)	0.0 (72.9)
P_2	Al_{2S}	—	—	0.0(120.4)	0.0(118.0)
0	Al^0	Al^0 SURFACE	S	9.1	11.5
1	Al_2O_3	Al^0 SURFACE	S	11.1	13.5
2	Al^0	Al^0	B	13.5	15.9
3	Al_2O_3	Al^0	B	16.0	18.4
4	Al^0	Al_2O_3	B	21.9	14.3
5	Al_2O_3	Al_2O_3	B	24.2	26.5
6	Al_2O_3/Al^0	Al^0/INTERFACE	BxS/SxS	27.1	29.5
7	Al^0	Al^0	2xB	29.5	31.9
8	Al_2O_3	Al^0	2xB	31.9	34.3

S ≡ SURFACE EMISSION

B ≡ BULK EMISSION

(ALL MAINLY CAUSED BY PLASMONS?)

1 — $\frac{}{Al^0}$

	BULK	SURFACE*
Al^0	15.8	11.3
Al_2O_3	24.4	17.4

*$W_S = \frac{W_B}{\sqrt{2}}$

is described in the second part of this review.)

A variety of C(1s) loss lines also have been examined, each with their own particular merit. Since the analysis to be described pivots on the determination of the loss splitting, E_L defined as the difference between the principal no-loss C(1s) line and the peak of the (rather broad) first, major, (perhaps) plasmon-dominated, loss line, it is useful to include a spectral run of both of these features in the same spectrum. In addition, we have often recorded spectra that run up field to 350 eV or more in order to determine the presence of any secondary loss lines. Such lines were included because plasmon-dominated losses are found to arise in evenly spaced (harmonic oscillator imposed) intervals, which fall off exponentially in intensity (i.e., with what is referred to above as a Poisson character.[99,100] (see Figure 20). Hence, spectra of this type were recorded for a variety of carbon only and/or C-H only compounds to examine for plasmon character in their loss spectra.

Initial detection of some of the characteristic XPS loss peaks described herein (for graphite and related compounds) were reported earlier by several of the pioneering ESCA groups (e.g., that of Kai Siegbahn[135] and David Shirley).[136] In the latter case, they have suggested two separate prominances in the broad, primary loss peak of graphite that surrounds the 30 eV, E_L point. We have not been able, however, to totally distinguish these weak peaks, therefore, we have suggested a singular transition of $E_L \sim 30$ eV.

Non-XPS generated losses for graphite and related material have also been considered by others. These have included studies in X-ray generated appearance potential spectroscopy by Park et al.[137] and high energy EELS investigations by Weissmantel et al.[138] and Liang and Cundy.[139] The carbon losses realized in Auger analyses of

TABLE 9
Loss Splittings Assuming Plasmon Character with Dispersion

System	ΔE_G	f_i[b]	Cal. ϵ_p	Exp. E_L	Comment
Group IV systems					
$C_{(CxHy)}$	5.2[a]	—	31.1	22.0[c]	LoCo ↓
Si	1.2	—	16.6	17.8	VB→
Ge	0.7	—	15.6	16.5	VB ↑
Sn	0.1	—	14.1	14.0	M(–)
Pb	0.0	—	13.5	13.5	M(–)
Select III-V Systems					
GaAs	1.4	0.32	16.3	16.2	Ga(3d)→C.B. ↓ VB ↑
GaSb	0.8	0.27	15.3	14.8	Ga(3d)→C.B. ↓ V.B. ↑
InN	1.7	0.5	19.0	15.5	In(4d)→C.B. ↓ Ion ↓
InSb	0.2	0.33	13.9	13.4	In(4d)→C.B. ↓ VB ↑
Select II-VI Systems					
ZnSe	2.8	0.62	15.6	16.0	Zn(4d)→C.B. ↑ VB ↑
ZnTe	1.2	0.60	14.5	15.5	Zn(4d)→C.B. ↑ V.B. ↑
CdS	2.5	0.68	N.A.	18.5	Cd(4d)→C.B. ↑ ↑
CdSe	1.8	0.68	14.7	17.0	Cd(4d)→C.B. ↑ ↑
CdTe	1.4	0.68	13.6	16.5	Cd(4d)→C.B. ↑ ↑
Selected Oxides					
BeO		0.62	29	29	None
ZnO	3.3	0.65	NA	—	—
Al_2O_3	7.5	0.80	27.0	24.0<	O(2s)→C.B. ↓ Ion ↓
Ga_2O_3	—	—	—	21.2	O(2s)→C.B. ↑ Ion ↓
In_2O_3	3.6	—	22.5	18.5	In(4d)→C.B. ↑ O(2s)→C.B. ↓ Ion ↓
SiO_2	9.0	0.57	23.0	23.0	O(2s)→C.B.
GeO_2	6.0	0.73	NA	—	Ion ↓
SnO_2	3.8	0.78	26.0	20.0	O(2s)→C.B. ↓ Ion ↓

Note: LoCo = Localized Covalent Bonding; Ion = Localized Ionic Bonding; M = Metal; V.B. = Valence Band; C.B. = Conduction Band; f_i = ionicity; ↑ = effect increases E_L.

[a] Diamond.
[b] From Levine, B. F., *J. Chem. Phys.*, 59, 1463, 1973.
[c] Approximate value for polymeric hydrocarbon.

select systems were also considered by Luries and Wilson.[140] All of these features have been recently surveyed by Tsai and Bogy.[141]

2. Graphite

As part of this analysis, several pressed wafers of chemically pure graphite were examined in various ESCA systems. Unpressed, pure, graphite powder also was examined. The state of graphite purity was gauged both by bulk specification and surface analyses (in the latter case, by employing the chemical detection of ESCA). In all instances, if air exposed, these materials were found to suffer very moderate surface ox-

TABLE 10
Loss Splitting (E_L) in eV ± 1.0 for Isoelectronic Series Based on Ge_2, and Sn_2.

	E_p	E_L
Ge	15.6	16.5
GaAs	16.3	16.2
ZnSe	15.6	16.0
KBr	11.1	13.7[a]
Sn	14.1	14.0
InSb	13.9	13.4
CdTe	13.6	16.5[a]
RbI	10.9	N.A.[a]

[a] Plasmons, for these cases, may be too weak to be primary producers of these peaks.

idation (see the survey scan in Figure 25). It should be emphasized that to varying degrees this is the case for *all* air exposed solids![85,90] Examination of systems cleaned of this slight oxide (and also of graphite more extensively oxidized) suggests that this level of oxidation does not play a significant role in the subsequent general analysis.

The characteristics of the C(1s) ESCA loss spectra for graphite are illustrated in Figure 26 and Table 11. The experimental patterns produced closely replicate that suggested for a carbon based material that is a near total producer of plasmon-type loss excitation. Further, based upon the loss results obtained on various other polycrystalline and/or powdered materials, we do not expect the previously mentioned lack of total, macroscopic structural integrity to influence the position of the loss peaks. Thus, we find an $E_L \simeq \epsilon_p$ of ~30.0 ± 1.0 eV. (The large uncertainty results from the broad nature of the loss peak, see Figure 26). It is suspected that a very pure, structurally sound, single crystal of graphite, oriented to permit maximum ESCA analysis perpendicular to its basal plane, should produce a substantial enhancement in resolution. This feature is under investigation.

The present samples of moderately clean

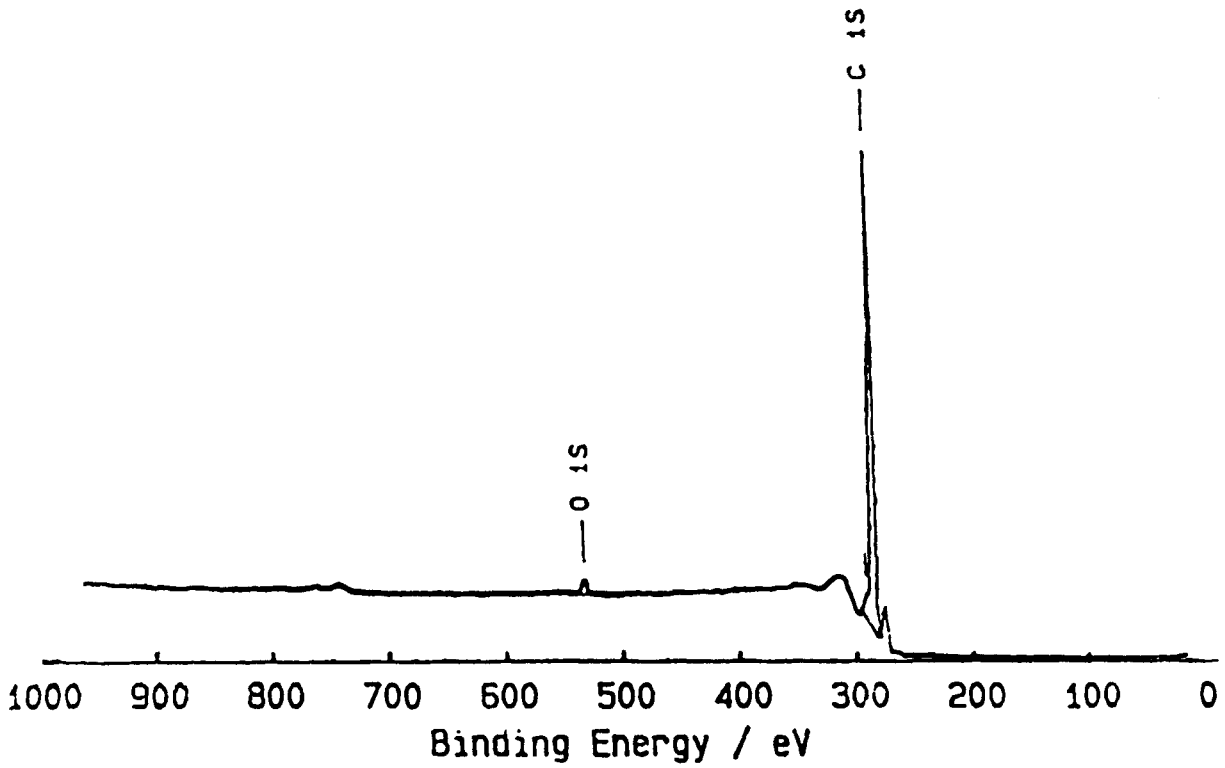

FIGURE 25. Survey scan for wafer of clean (but air-exposed) graphite.

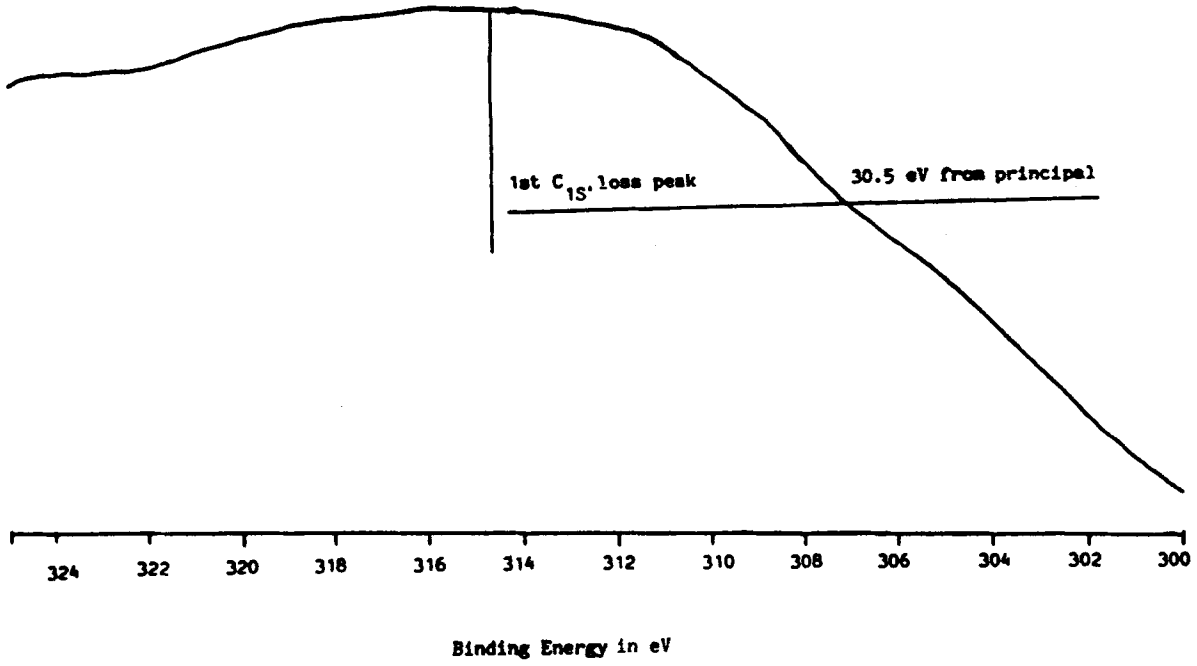

FIGURE 26. C(1s) loss splitting, E_L, for relatively clean graphite.

TABLE 11
Characteristic Loss Splitting for Carbon Containing Systems. Note Correlation Between Graphite and E_P for Carbon.

Carbon species	Loss splitting E_L	$\Delta E_L^{i \to j}$ [b]
Graphite	30.0 ± 1.0 eV	0
Polypropylene	21.0 ± 1.0 eV	9.0 ± 1.0 eV
Adventitious carbon	22.0 ± 1.0 eV	8.0 ± 1.0 eV
Diamond[a]	32.8 (23.0) ± 1.0 eV	−2.8 ± 1.0 eV

[a] Based upon results from Reference 136. All other results from our experiments.
[b] Take graphite as i, other species as j.

graphite also exhibit relatively intense, reasonably well resolved, second loss peaks at ~345 eV in Figure 27 (i.e., split from the first loss peak by ~30 eV). All of these results suggest that the aromatic π structure of graphite, with its density located primarily at or near the Fermi edge, is experiencing a near total collective (plasmon-like) loss behavior. The general lack of intensity in the resulting loss lines would further suggest that the sp^2 covalent part of the graphite system only provides weak "support" to this collective loss behavior.[121]

3. Carbon-Based Systems Devoid of Aromatic Structure—Polypropylene

The loss spectra of a variety of carbon based materials that do not feature any aromatic π character were also examined with several of the previously mentioned ESCA systems. One of the most detailed of these studies was that for very pure, catalytically produced films of polypropylene[86,90,133] (see the section on angular resolution). This system produced ESCA loss results that seem to be representative of those for

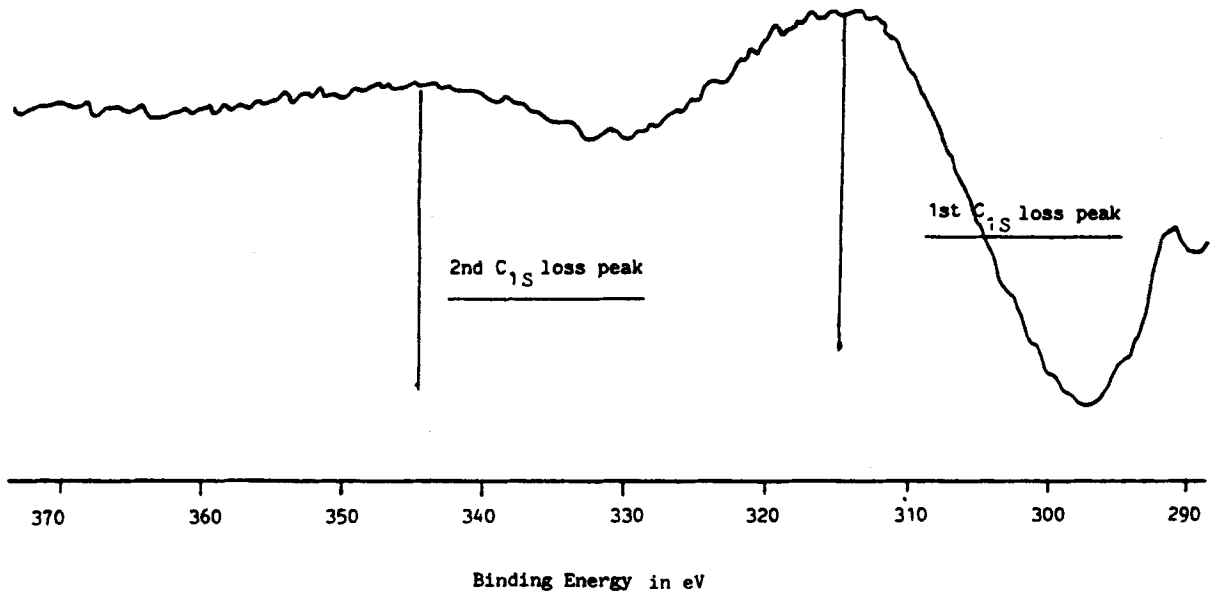

FIGURE 27. Poisson character of ESCA loss splitting for graphite.

many carbon based materials without the interjection of interlaced π networks. In this case, the valence band region displays the expected "pull back" of density from the Fermi edge, as the Π electron region of the graphite hybridizes into the balance of the covalent system. This results when the π bond in the propylene monomer is converted to form the sp^3 bonds of the hydrocarbon polymer (see Figure 28). As the carbon $3p_\pi$ density pulls away from the Fermi edge, and "rolls back" into the density region occupied by the covalent balance of the carbon valence band density, several additional features evolve. First, the charging shift (which was very muted or entirely absent for graphite) begins to emerge for the nonconductive, hydrocarbon polymer. Second (and more to the point of our present discussion), there is a substantial change in character and shift in the C(1s) loss spectra.

Hence, the C(1s) loss peaks for polypropylene are significantly attenuated in size compared to graphite and shifted in energy to an average E_L of 21.2 $\pm$ 1.0 eV. These features are summarized in Table 11 and Figure 28, including the $\Delta E_L^A(1 \rightarrow 2)$ case, where A indicates carbon, and 1 and 2 stand for graphite and polypropylene, respectively. In this case, the ΔE_L is 8.8 $\pm$ 1.0 eV. The C(1s) loss spectra of several other hydrocarbon dominated polymers, films, coatings and powders have been examined by ESCA; in all cases these materials were found to produce loss spectra with ΔE_L of ~9.0 eV with respect to graphite.[121]

A variety of other carbon-based materials with varying degrees of conjugated, π, character between polypropylene and graphite have also been examined with ESCA, and their C(1s) loss spectra reveal E_L values between 31 and 22 eV. Often several peaks have been produced, and there is a suggestion that the 9 eV, ΔE_L, may shift in a progressive fashion as the degree of conjugation is enhanced. Proof of the latter, however, awaits future evidence.

We also suggest here that the ~9.0 eV reduction in ΔE_L is not the only shift that can be experienced by carbon as it loses the (essentially) infinte π character of graphite. Diamond is the most covalent of all carbon systems, but its electronic system is quite different from that of the aforementioned hydrocarbons. Thus, whereas polymeric hydrocarbons represent a series of sp^3 bonds that repeatedly terminate at the hydrogens, diamond is an "interlaced," carbon-only sp^3 system with some delocalization of electrons throughout the lattice. This delocalization is not as "total" as that in the two dimensional, π lattice of graphite, but the diamond interlace extends over a complete three dimensional network.

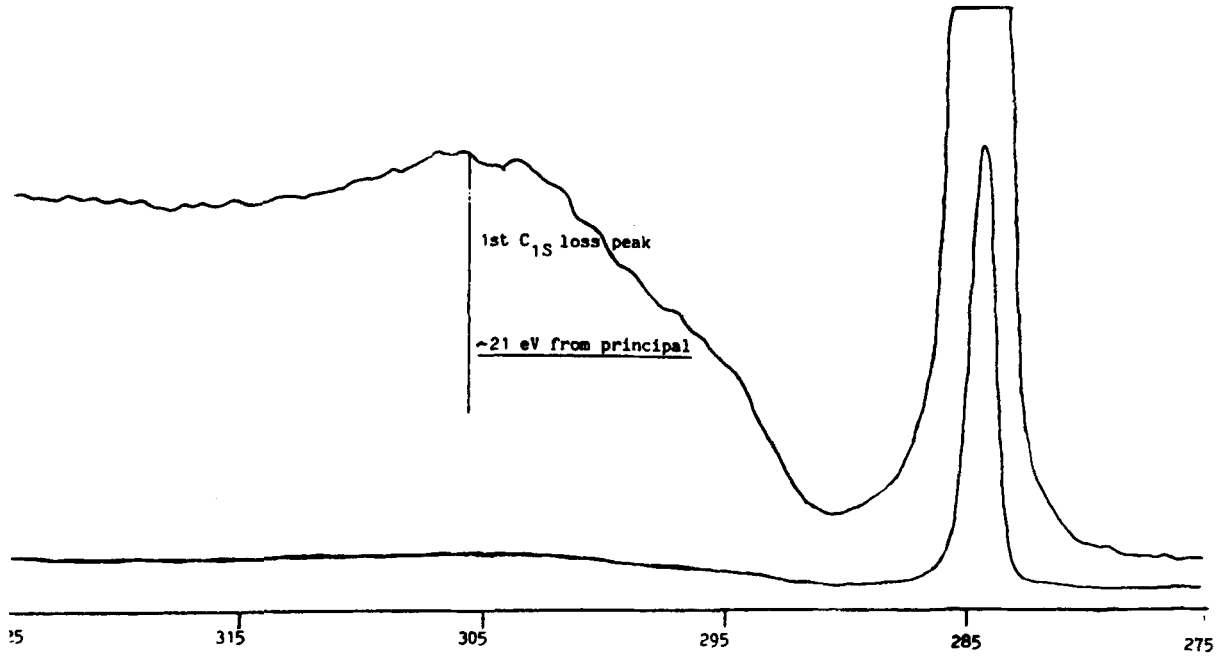

FIGURE 28. C(1s) loss splitting for clear film of polypropylene.

As a result, diamond seems to produce two distinct loss peaks when measured by XPS (see McFeeley et al.[137]). One peak, (1), produces an E_L of ~23 eV, while the other, (2), is at 32.8 eV. An interpretation of these results suggests that (1) may be due to localized electron effects, while (2) results from the aforementioned delocalized character. The shift in the latter from E_p may be due to a band to band perturbation of the free electron plasmon.

4. Adventitious Carbon

One of the least desired, but most persistent, parts of nearly every surface study (no matter what the problem) is the ubiquitous presence of carbon deposits which are difficult to remove and even more difficult to keep off. These deposits form on surfaces when they are not properly maintained in extreme UHV. These carbonaceous species were originally attributed to the vacuum pump oil, but it is now known that they arise from numerous sources, and are significantly deposited on all air exposed surfaces. Because of the persistent nature of these species, they have been generally labeled as *Adventitious Carbon*, (AC).[28]

Generally, the ESCA spectra produced by these deposits form a rather consistent pattern that demonstrates that 75 to 90% of the deposited species are either C–H or C–C containing compounds; the balance are various oxidized systems, usually carbonyls. The designation AC is often reserved for the former, and its binding energy is generally fixed by some means at 284.6 ± 0.4 eV. This value is frequently employed to establish a general (if somewhat precarious) binding energy scale (see Section II).[90] Because of the uncertain origins of these materials, and the lack of differentiation of the principal C(1s) peak, designation of the exact type of species involved in AC, as mentioned above, is uncertain.

We have employed ESCALOSS to examine a large number of adventitious carbon systems deposited on a variety of materials with diverse histories. In *all* cases, the loss spectrum produced was found to closely replicate that of polypropylene (see Figure 29). Thus, the characteristic E_L for most adventitious carbon seems to be 22.0 ± 1.0 eV. *This strongly suggests that the C–C and C–H parts of AC are hydrocarbon based species, with little or no graphitic materials present.*[121]

The insidious nature of many of these AC carbon deposits has been examined and docu-

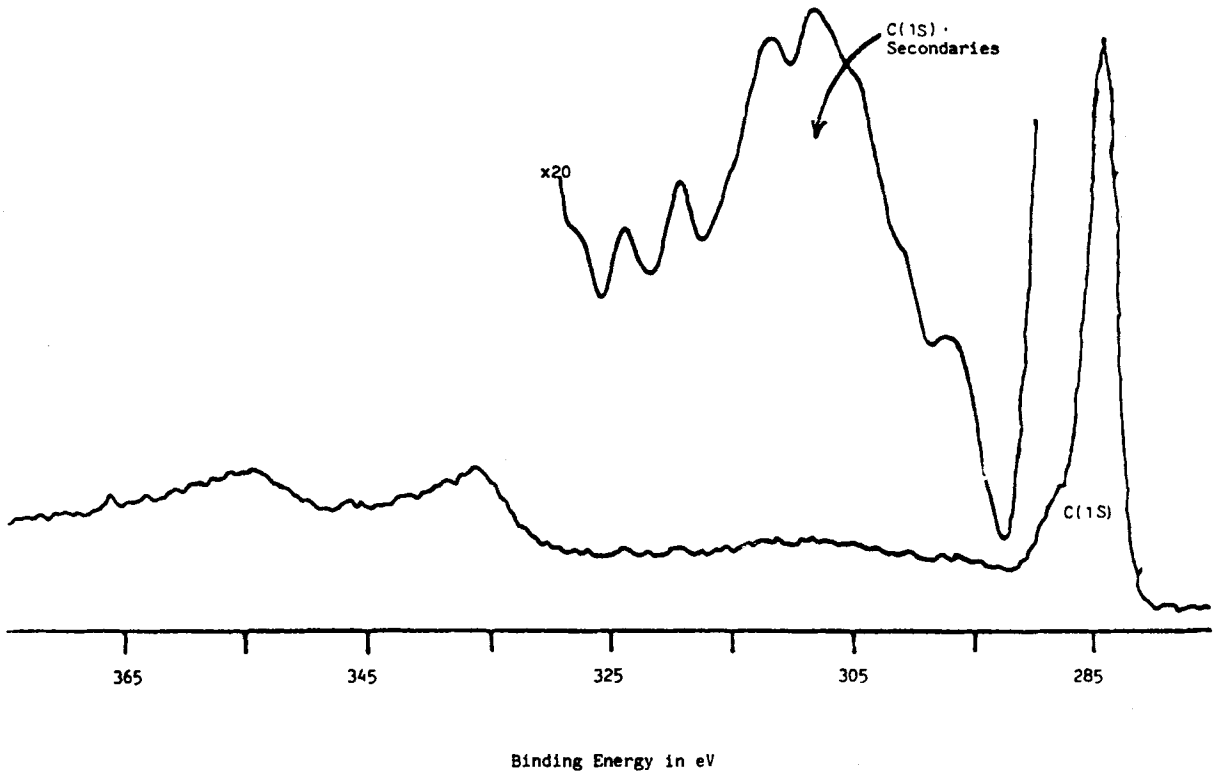

FIGURE 29. C(1s) loss pattern for typical systems coated with adventitious carbon (a pressed wafer of a catalyst, physically resembling the graphite in Figure 27).

mented by Barr in a companion study of various surfaces.[86,90] It should be noted that these carbon systems seem to form continuously, but are generally lacking in sufficient chemical bonding strength to prevent displacement by other, more voracious bonding species. Thus, assuming that over relatively long periods of time most of the growth of species on a surface is vertical then the AC products are continuously being pushed toward the outer, evolving surface by any chemically attached film of "growing" species, such as an oxide.[90] *It is also interesting to note that adventitious carbon species are even found on the outer surface of carbon films.* To illustrate air-exposed graphite, if examined by angular resolution, exhibits, in addition to a small amount of carbon oxides, an outermost surface that has a very thin deposition of adventitious carbon. The latter is detected, at grazing incidence, as an appearance of a small ~305.5 loss peak, and a shift of the main loss peak down field from 314.5 eV. This also may explain why our E_L for graphite at standard incidence is somewhat smaller than E_p.

In addition one should realize that loss splittings in the region of ~22 eV for noncarbon containing materials with "dirty" surfaces may be reflecting (extrinsic) losses in the adventitious carbon overlayer, rather than transitions of the material itself.

5. Utility

The ultimate proof of the analytical potential of the C(1s) loss spectra method rests, naturally, on its utility in research and applied situations. Several research groups in an association with that of the author (TLB) are presently exploiting this method in a number of areas, two of which are outlined here:

1. Certain potential forms of fuel cells may be prepared by using carbon based supports onto which metal catalysts, such as platinum, are implanted. Particular examples of this type of system have been prepared and tested in the laboratories of Professor Gior-

dano (U. Messina), and surface analyzed with ESCA by the research group of Barr.[122] The base for these systems was a pure, graphitic, carbon paper. The evolving materials were then examined with ESCA at select stages during their involved production. The ESCA, C(1s) loss analysis for the carbon paper base (Figure 30) revealed a pattern strongly suggesting graphite, with only slight alterations. During an early stage in the production of the fuel cell, this graphite material was coated with a fluorinate hydrocarbon polymer and subjected to lengthy heat treatment. The resulting, relatively thick, polymeric film was apparently rather spotty, with substantial uncovered regions. Thus, whereas the C–C–, C–H part of the principal C(1s) line suggested no change, the C(1s) loss spectra for this system (Figure 31) supported these suggestions of splotchy coverage by revealing peaks that suggest the simultaneous presence of both graphitic and hydrocarbon polymer materials. It should be noted (Figure 31) that, as expected, these peaks are shifted somewhat from exact correspondence with the pure precursors, and there is also the apparent presence of several ad-

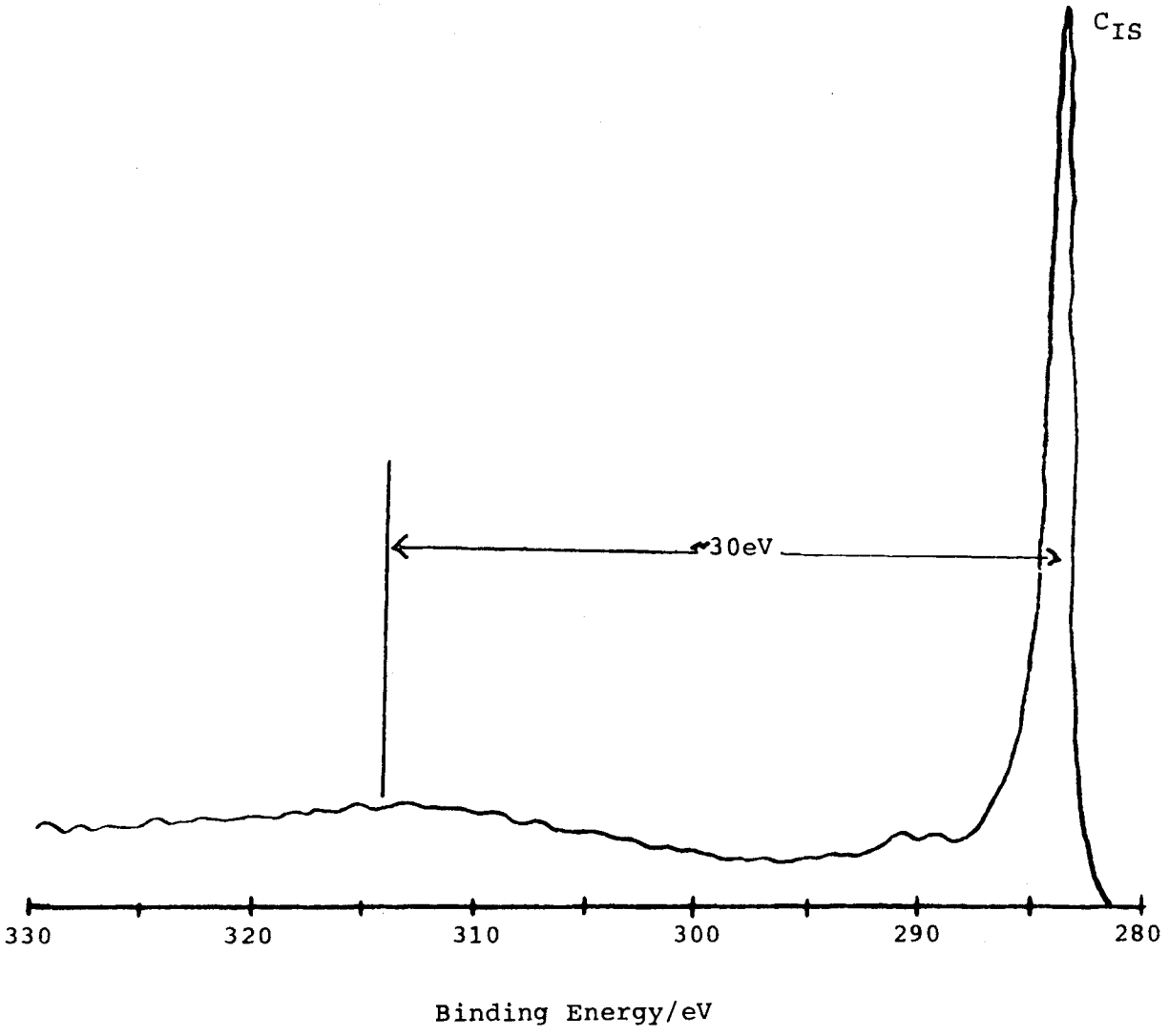

FIGURE 30. Carbon (1s) loss spectrum for pretreated carbon paper before surface alteration to form fuel cell (note 30 eV graphite-like E_L).

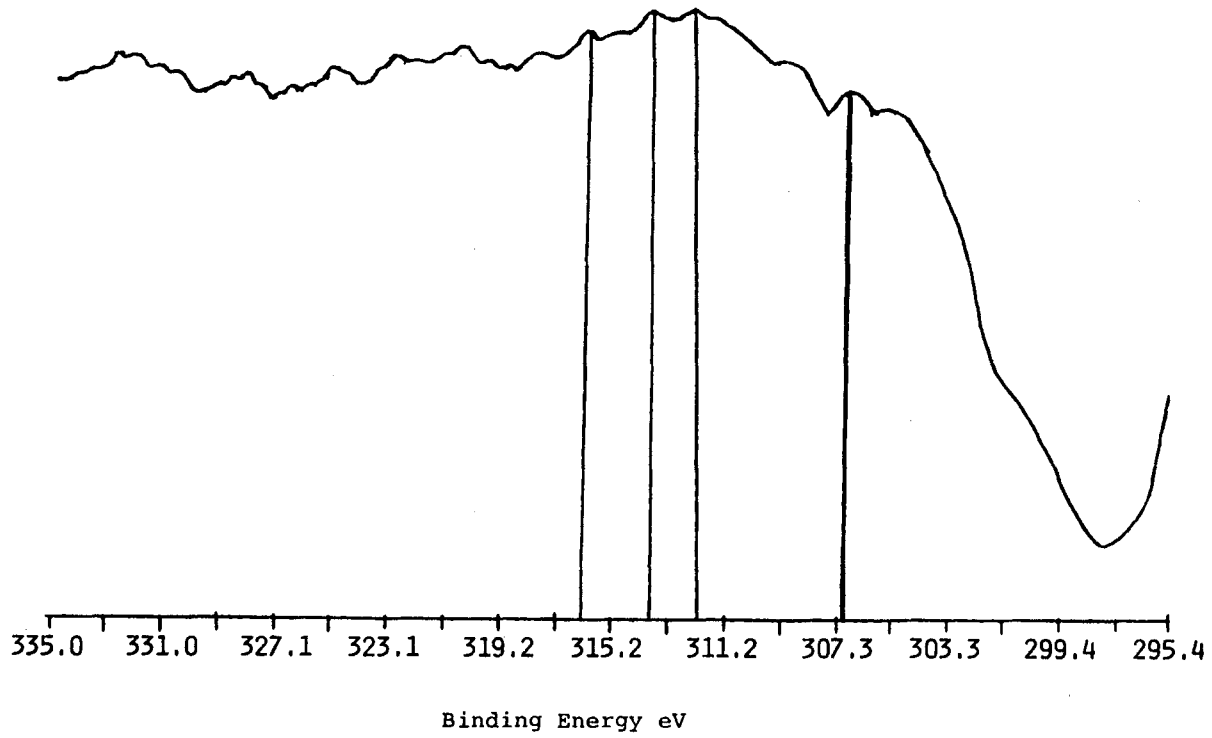

FIGURE 31. C(1s) loss spectrum realized following FEP polymer coating and physical alteration (note introduction of 21.8 eV E_L characteristic of hydrocarbon polymer plus retention of graphite loss due to spotty coverage).

ditional, "intermediate" peaks in the general manifold. The latter effects are perhaps indicative of the alterations in chemistry and interfacial properties resulting from the coating and subsequent treatment. Further treatments of these materials produce equally revealing scenarios, with ESCA analysis assisting in detecting changes in the fluorine and platinum chemistry, as well as the coverage.[122] The utility of the C(1s) loss spectra proved to be a key point in the total analysis.

2. A second, practical use of the C(1s) loss analysis has occurred during studies of aluminum alloy composites, doped with various amounts of graphitic or nongraphitic carbon, in order to provide instructive variations in the tribological properties of these systems. These materials are being prepared in the laboratories of Rohatgi of UWM[142] with ESCA analysis conducted in the laboratory of Barr.[143] Once, again, ESCA C(1s) loss spectra are playing a crucial role. Hence, the loss spectra were employed to examine the character of the carbonaceous species that were found deposited on, or segregating to, the surface of these composite systems. For example, C(1s) loss spectra were employed to differentiate between segregated graphitic deposits and the presence of nongraphitic carbons, including the ubiquitous, AC that also is generally present.[90,143] Most important, however, the spectra were used to determine when wear treatment begins to degrade graphite and destroy its lubricating properties.[143]

6. Rationale

In all of these analyses, use is made of the nature of the loss spectra for carbon-containing systems. In this regard, we have noted that if the potential Π density in the carbon system is maximized (graphite), it becomes an interlaced collective network of electrons that form a near perfect, free electron plasmon with $E_L \simeq E_p \simeq$ 31 eV. As the interlaced Π network is reduced and pulled back from the Fermi edge, the electron

density N in Equation 51 is reduced by this covalent formation. The degree of π network reduction in polypropylene is apparently ~ 30%, and that for diamond is suggested to be even larger. Possible perturbative involvement of the largest part of the valence band (located at ~ 17.5 eV) in band to band transitions of the type described in Equation 90 must also be included in the creation of E_L values in the 22 to 19 eV range.[90,99,121]

REFERENCES

1. **Hertz, H.,** Uber einen Einfluss des Utravioletten Lichtes auf die Electrische Entladung, *Wiedemannsche Annalen der Physik,* 31, 982, 1887.
2. **Jammer, M.,** *The Conceptual Development of Quantum Mechanics,* McGraw-Hill, New York, 1966, 28.
3. **Hoffmann, B.,** *Albert Einstein, Creator and Rebel,* The Viking Press, New York, 1972, chap. 4.
4. **Einstein, A.,** Uber einen die Erzeugung and Verwandlung des Lichtes Betreffenden Heuristischen Gesichtspunkt, *Annalen der Physik,* 17, 132, 1905.
5. **Planck, M.,** Uber eine Verbesserung der Wienschen Spektralgleichung, *Verhandlungen der Deutschen Physikalischen Gesellschaft,* 2, 202, 1900.
6. **Lewis, G. N.,** The Conservation of Photons, *Nature,* 118, 874, 1926.
7. **Millikan, R. A.,** A direct Photoelectric Determination of Planck's 'h', *Phys. Rev.,* 7, 355, 1916.
8. **Robinson, H.,** *Phil. Mag.,* 50, 241, 1925.
9. **Siegbahn, K.,** Photoelectron Spectroscopy: retrospects and prospects, *Royal Soc. London,* 1985.
10. **Siegbahn, K., Nordling, C., et al.,** *ESCA Applied to Free Molecules,* North-Holland, Amsterdam, 1969.
11. **Siegbahn, K., Nordling, C., et al.,** ESCA: atomic, molecular and solid structure studied by means of electron spectroscopy, *Nova Acta Regiae Soc. Sci.,* Sweden, 4, 20, 1967.
12. The acronym "ESCA" was coined by Professor Siegbahn fairly early in the development of the spectroscopy. References 10 and 11 marked its general acceptance.
13. **Turner, D. W., Baker, C., Baker, A. K., and Brundle, C. R.,** *Molecular Photoelectron Spectroscopy,* Wiley-Interscience, London, 1970.
14. **Price, W. C. and Turner, D. W.,** *Philos. Trans. Soc. London,* A268, 1970.
15. **Barr, T. L., and Davidson, E. R.,** Nature of the Configuration-Interaction Method in Ab-Initio Calculations, *Phys. Rev. A,* 1, 644, 1970.
16. **Martin, R. L. and Shirley, D. A.,** *J. Chem. Phys.,* 64, 3685, 1976.
17. **Szabo, A., and Ostland, N. S.,** *Modern Quantum Chemistry, Introduction to Advanced Electronic Structure Theory,* MacMillan, New York, 1982, chap. 3.
18. **Koopmans, T. A.,** Uber die Zuordnüng von Welten Funktionen and Eigenwerten zu den einzelnen Elektronen eines Atoms, *Physica,* 1, 104, 1933.
19. **Barr, T. L.,** Studies in Differential Charging, *J. Vac. Sci. Technol.,* A7, 1677, 1989.
20. **Barr, T. L.,** Applications of Electron Spectroscopy to Heterogeneous Catalysis, in *Practical Surface Analysis,* 2nd ed., Briggs, D. and Seah, M. P., Eds., John Wiley & Sons, Chichester, England, 1990, chap. 8.
21. **Lewis, R. T. and Kelly, M. A.,** *J. Electron Spectrosc. Relat. Phenom.,* 20, 105, 1980.
22. **Barr, T. L.,** Applications of ESCA in Industrial Research, *Amer. Lab.,* 10, 40, 65, 1978.
23. **Stephenson, D. A. and Binkowski, H. J.,** *J. NonCryst. Solids,* 22, 399, 1976.
24. **Wagner, C. D.,** *J. Electron Spectrosc. Relat. Phenom.,* 18, 345, 1980.
25. **Hicks, R. F.,** Characterization of Supported Metal Catalysts by X-ray Photoelectron Spectroscopy, in *Characterization and Catalyst Development: an Interactive Approach,* Bradley, S. A., Gattuso, M. J., and Bertolacini, R. J., Eds., ACS Symp. Series 411, Am. Chem. Soc., Washington, D.C., 1989, chap. 20.
26. **Barr, T. L.,** XPS As a Method for Monitoring Segregation in Alloys: Cu-Be, *Chem. Phys. Lett.,* 43, 89, 1976.
27. **Barr, T. L. and Yin, M. P.,** Studies of Pt-Metal Catalysis by High Resolution ESCA, in *Characterization and Catalyst Developments: An Interactive Approach,* Ed. Bradley, S. A., Gattuso, M. J., and Bertolucini, R. J., *ACS Symp. Ser.,* 411, Am. Chem. Soc., Washington, D.C., 1989, chap. 19.
28. **Briggs, D. and Seah, M. P., Eds.,** *Practical Surface Analysis,* 2nd ed., John Wiley & Sons, Chichester, England, 1990.
29. **Gelius, U., and Siegbahn, K.,** *Faraday Discuss. Chem. Soc.,* 54, 257, 1972.
30. **Frost, D. C., Ishitani, A., and McDowell, C. A.** *Mol. Phys.,* 24, 861, 1972.
31. **Wheeler, D. R. and Pepper, S. V.,** *J. Vac. Sci. Technol.,* 20, 226, 1982; **Chaney, R., and Barth, G.,** *Fresenius Z. Anal. Chem.,* 329, 143, 1987.
32. **Gelius, U., Basilier, E., Svensson, S., Bergmark, T., and Siegbahn, K.,** *J. Electron Spectrosc. Relat. Phenom.,* 2, 405, 1974.
33. **Kelly, M. A., and Tyler, C. E.,** Hewlett-Packard J., 24, 2, 1972.
34. **Kelly, M. A.,** More-Powerful ESCA Makes Solving Surface Problems A Lot Easier, *Ind. Res. Dev.,* 26, 80, 1984.
35. **Tonner, B.,** private communication.
36. **Barr, T. L., and Lishka, M. A.,** *J. Am. Chem. Soc.,* 108, 3178, 1986.
37. **Gelius, U., Asplund, L., Basilier, E., Hedman,**

S., Helenelund, K., and Siegbahn, K., *Nucl. Instrum. Methods in Phys. Res.*, B1, 85, 1984.
38. **Gelius, U. et al.,** *J. Electron Spectros. Relat. Phenom.*, 52, 747, 1990.
39. **Feibelman, P. J., and Eastman, D. E.,** *Phys. Rev.*, B10, 4932, 1974.
40. **Cederbaum, L. S.,** Non-Single-Particle Excitations in Finite Fermi Systems, *J. Chem. Phys.*, 62, 2160, 1975.
41. **Mahan, G. D.,** Theory of Photoemission in Simple Metals, *Phys. Rev. B*, 2, 4334, 1970.
42. **Pendry, J. B.,** Theory of Photoemission, *Surf. Sci.*, 57, 679, 1976.
43. **Sunjic, M. and Sokcevic, D.,** Inelastic Effects in X-ray Photoelectron Spectroscopy, *J. Electron Spectrosc. Relat. Phenom.*, 5, 963, 1974; **Gadzuk, J. W. and Sunjic, M.,** Excitation Energy Dependence of Core-Level X-ray Photoemission Spectra Line Shapes in Metals, *Phys. Rev. B*, 12, 524, 1975.
44. **Berglund, C. N. and Spicer, W. E.,** *Phys. Rev.*, 136, A1040, 1964.
45. **Sunjic, M.,** Theoretical Problems in Solid State Photoemission, *Stud. Surf. Sci. Catal.*, 9, 112, 1982.
46. **Martin, R. L. and Shirley, D. A.,** *Phys. Rev. A*, 13, 1476, 1976.
47. **Saguiron, M., Bullock, E. L., and Fadley, C. S.,** The Analysis of Photoelectron Diffraction Data Obtained with Fixed Geometry and Scanned Photon Energy, *Surf. Sci.*, 182, 287, 1987.
48. **Feynman, R. P.,** *Quantum Electrodynamics*, W. A. Benjamin Inc., New York, 1961, chap. 1.
49. **Bjorken, J. D. and Drell, S. D.,** *Relativistic Quantum Mechanics*, McGraw-Hill, New York, 1964, chap. 7.
50. **Liebsch, A.,** *Phys. Rev. Lett.*, 32, 1203, 1974; *Phys. Rev. B*, 13, 544, 1976.
51. **Fadley, C. S.,** The Study of Surface Structures by Photoelectron Diffraction and Auger Electron Diffraction, in *Synchrotron Radiation Research: Advances in Surface and Interface Science*, Bachrach, R. Z., Ed., Plenum Press, New York, 1990, in press.
52. **Poon, H. C. and Tong, S. Y.,** *Phys. Rev. B*, 30, 6211, 1984; **Tong, S. Y., Poon, H. C., and Snider, D. R.,** *Phys. Rev.* B, 32, 2096, 1985.
53. **Davis, D. W. and Shirley, D. A.,** *J. Electron Spectrosc. Relat. Phenom.*, 3, 137, 1974.
54. **Hedin, L. and Johansson, A.,** Polarization Corrections to Core Levels, *J. Phys. B*, 2, 1336, 1969. For examples of more direct calculations of the relaxed states realized in Equation 38 and their necessity, one should consult, **Basch, H. and Snyder, L. C.,** *Chem. Phys. Lett.*, 3, 333, 1969; **Bagus, P. S.,** *Phys. Rev. A*, 139, 619, 1965, **Schwartz, M. E.,** Direct Calculation of Binding Energies of Inner-Shell Electrons in Molecules, *Chem. Phys. Lett.*, 5, 50, 1970; **Schwartz, M. E., Coulson, C. A., and Allen, L. C.,** Dipole Moments, Atomic Charges and Carbon Inner-shell Binding Energies of the Fluorinated Molecules, *J. Am. Chem. Soc.*, 92, 447, 1970; Brundle, C. R., Robin, M., and Basch, H., *J. Chem. Phys.*, 53, 2196, 1970.
55. **Schiff, L. I.,** *Quantum Mechanics*, 2nd ed., McGraw-Hill, New York, 1955, chap. 31.
56. **Aberg, T.,** *Phys. Rev.*, 156, 35, 1967.
57. **Manne, R. and Aberg, T.,** Koopmans Theorem for Inner-Shell Ionization, *Chem. Phys. Lett.*, 7, 282, 1970.
58. **Fadley, C. S.,** Peak Intensities and Photoelectric Cross Sections, *Chem. Phys. Lett.*, 25, 225, 1974.
59. **Gadzuk, J. W.,** Many-Body Effects in Photoemission, in *Photoemission and the Electronic Properties of Surfaces*, Feuerbacher, B., Filton, B., and Willis, R., Eds., J. Wiley & Sons, New York, 1978, chap. 5.
60. **Kim, K. S. and Davis, R. E.,** *J. Electron Spectrosc. Relat. Phenom.*, 1, 251, 1972; **Kim, K. S. and Winograd, N.,** Charge Transfer Shakeup Satellites in X-ray Photoelectron Spectra of Cations and Anion of $SrTiO_3$, TiO_2 and Sc_2O_3, *Chem. Phys. Lett.*, 31, 312, 1975.
61. **Kowalczyk, S. P., Ley, L., McFeeley, F. R., Pollack, R. A., and Shirley, D. A.,** *Phys. Rev. B*, 8, 3583, 1973; **Pollack, R. A., Ley, L., McFeeley, F. R., Kowalczyk, S. P., and Shirley, D. A.,** *J. Electron Spectrosc. Relat. Phenom.*, 3, 381, 1974.
62. **Mahan, G. D.,** Electron Energy Loss During Photoemission, *Phys. Status Solidi*, B55, 703, 1973.
63. **Siegbahn, K., Nordling, C., Fahlman, A., Nordberg, R., Hamrin, K., Hedman, J., Johanson, G., Bergmark, T., Karlsson, S.-E., Lindgren, I., and Lindberg, B.,** ESCA—Atomic, Molecular and Solid State Structure Studied by Means of Electron Spectroscopy, *Nova Acta Regiae Soc. Sci. Ups.* IV, 20, 1967.
64. **Tougaard, S.,** Formalism for Quantitative Surface Analysis by Electron Spectroscopy, *J. Vac. Sci. Technol.*, A8, 2197, 1990.
65. **Wagner, C. D.,** How Quantitative is ESCA?—An Evaluation of the Significant Factors, in *Quantitative Surface Analysis of Materials*, McIntyre, N. S., Ed., ASTM STP 643, ASTM, Philadelphia, 1978, chap. 2.
66. **Wagner, C. D.,** *Anal. Chem.*, 44, 1050, 1972; **Wagner, C. D.,** *Anal. Chem.*, 49, 1282, 1977.
67. **Wagner, C. D., Davis, L. E., Zeller, M. V., Taylor, J. A., Raymond, R. H., and Gale, L. H.,** *Surf. Interface Anal.*, 3, 211, 1981.
68. **Nefedov, V. I., Serguskin, N. P., Band, I. N., and Trzhakovskaya, M. B.,** *J. Electron Spectrosc. Relat. Phenom.*, 2, 383, 1973.
69. **Seah, M. P.,** *Surf. Interface Anal.*, 2, 222, 1980.
70. **Powell, C. J.,** The Physical Basis for Quantitative Surface Analysis by Auger Electron Spectroscopy and X-Ray Photoelectron Spectroscopy, in *Quantitative Surface Analysis*, McIntyre, N. S., Ed., ASTM STP 643, Am. Soc. Test. Materials, Philadelphia, 1978, chap. 1.
71. **Seah, M. P.,** *Surf. Interface Anal.*, 9, 85, 1986.

72. **Mroczkowski, S. J.,** The Effect of Electron Transmission Functions on Calculated Auger Sensitivity Factors, *J. Vac. Sci. Technol.*, A7, 1529, 1989.
73. **Seah, M. P.,** Quantification of AES and XPS, in *Practical Surface Analysis,* Briggs, D. and Seah, M. P., Eds., John Wiley & Sons, Chichester, England, 1983, chap. 5.
74. **Schofield, J. H.,** *J. Electron Spectrosc. Relat. Phenom.*, 8, 129, 1976.
75. **Penn, D. R.,** *J. Electron Spectrosc. Relat. Phenom.*, 9, 29, 1976.
76. **Angevine, P. J., Vortuli, J. C., and Delgass, W. N.,** *Proc. Int. Congr., Catal.*, 6, 611, 1977.
77. **Kerkhof, F. P. J. and Moulijn, J. A.,** *J. Phys. Chem.*, 83, 1612, 1979.
78. **Windawi, H. and Wagner, C. D.,** Use of ESCA in the Characterization of Heterogeneous Materials, in *Applied ESCA,* Vol. 63, Windawi, H. and Ho, F. F.-L., Eds., Chem. Anal. Ser., Wiley-Interscience, New York, 1982, chap. 9.
79. **Fung, S. C.,** *J. Catal.*, 56, 454, 1979.
80. **Fadley, C. J., Baird, R. J., Siekhaus, W., Novakov, T., and Bergstrom, S. A. L.,** *J. Elec. Spectrosc. and Relat. Phenom.*, 4, 93, 1974; **Fadley, C. S.,** Instrumentation for Surface Studies: XPS Angular Distributions, *J. Electron Spectrosc. Relat. Phenom.*, 5, 725, 1974.
81. **Barr, T. L., Mohensian, M., and Chen, L. M.,** *Appl. Surf. Sci.*, in press.
82. **Siegbahn, K., Gelius, U., Siegbahn, H., and Olsen, E.,** *Phys. Lett.*, 32A, 221, 1970. This is also one of the introductory expositions of photoelectron diffraction.
83. **Fadley, C. S.,** Angle-Resolved X-ray Photoelectron Spectroscopy, *Prog. Surf. Sci.*, 16, 275, 1984.
84. **Feuerbacher, B., Fitton, B., and Willis, R. F., Eds.,** *Photoemission and the Electronic Properties of Surfaces,* John Wiley, New York, 1978; Cardona, M. and Ley, L., Eds., *Photoemission in Solids,* Vol. 1 and 2, Springer-Verlag, Berlin, 1978; Vol. XLIX, Plummer, E. W., and Eberhardt, W., *Rev. Adv. Chem. Phys.*, Prigogine, I. and Rice, S. A., Eds., John Wiley, New York, 1982, 533.
85. **Barr, T. L.,** Recent Advances of ESCA in Natural Passivation, paper presented at NACE National Convention, Las Vegas, April, 1990; *Corrosion 90,* NACE, Houston, 1990, Paper 296.
86. **Barr, T. L. and Yin, M. P.,** ESCA Studies of the Oxidation of Polymer Surfaces: polypropylene, in preparation.
87. **Clark, D. T. and Harrison, A.,** *J. Polym. Sci. Polym. Chem. Ed.*, 19, 1945, 1981.
88. **Briggs, D.,** Applications of XPS in Polymer Technology, in *Practical Surface Analysis,* Briggs, D. and Seah, M. P., Eds. John Wiley & Sons, Chichester, England, 1983, chap. 9.
89. **Barr, T. L.,** ESCA Studies of Naturally Passivated Metal Foils, *J. Vac. Sci. Technol.*, 14, 660, 1977.
90. **Barr, T. L.,** An ESCA Study of the Termination of the Passivation of Elemental Metals, *J. Phys. Chem.*, 82, 1801, 1978.
91. **Barr, T. L. and Hackenberg, J. J.,** Studies of the Low Temperature Oxidation of Alloys by X-ray Photoelectron Spectroscopy, Cu-Zn, *Appl. Surf. Sci.*, 10, 523, 1982.
92. **Barr, T. L. and Hackenberg, J. J.,** Determination of the Onset of the Dezincification of α-Brass Using X-ray Photoelectron (ESCA) Spectroscopy, *J. Am. Chem. Soc.*, 104, 5390, 1982.
93. **Barr, T. L.,** ESCA Studies of Metals and Alloys: oxidation, migration and dealloying of cu-based systems, *Surf. Interface Anal.*, 4, 185, 1982.
94. a) **Bloch, F.,** Double Electron Transitions in X-ray Spectra, *Phys. Rev.*, 48, 187, 1935; **Feinberg, E. L.,** Ionization of the Atom Due to β-Decay, *J. Phys.*, 4, 423, 1941; **Levinger, J. S.,** Effects of Radioactive Disintegrations on Inner Electrons of the Atom, *Phys. Rev.*, 90, 11, 1953; **Sachenko, V. P. and Demekhin, V. F.,** Satellites of X-ray Spectra, *Soviet Physics JETP*, 22, 532, 1966; **Carlson, T. A. and Krause, M. O.,** Electron Shake-Off Resulting From K-Shell Ionization in Neon Measured as a Function of Photoelectron Velocity; *Phys. Rev.*, 140, A1057, 1965; **Krause, M. O., Carlson, T. A., and Dismukes, R. D.,** *Phys. Rev.*, 170, 37, 1968; **Carlson, T. A. and Nestor, Jr., C. W.,** Calculation of Electron Shake-Off Probabilities as a Result of X-Ray Photoionization of the Rare Gases, *Phys. Rev. A*, 8, 2887, 1973. b) Aberg, T., *Phys. Rev.*, 156, 35, 1967; **Carlson, T. A. and Krause, M. O.,** Atomic Readjustment to Vacancies in the K and L Shell of Ar, *Phys. Rev.*, 137, A1655, 1965; **Carlson, T. A., Krause, M. O., and Moddeman, W. E.,** *J. Phys.*, C20, 102, 1971; **Carroll, T. X. and Thomas, T. D.,** Shake-up Spectra and Core Ionization Potentials for Formaldehyde. The Role of Electron Spin in Shake-up, *J. Electron Spectrosc. Relat. Phenom.*, 10, 215, 1977.
95. a) **Chang, J. J and Langreth, D. C.,** Deep-hole Excitations in Solids I. Fast Electron-Plasmon Effects, *Phys. Rev.*, B5, 3512, 1972; and Deep-Hole Excitations in Solids II. Plasmons and Surface Effects in X-ray Photoemission, *Phys. Rev. B*, 8, 4638, 1973. b) **Langreth, D. C.,** Born-Oppenheimer Principle in Reverse: Electrons, photons and plasmons in solids-singularities in their spectra, *Phys. Rev. Lett.*, 26, 1229, 1971. c) **Langreth, D. C.,** Singularities in the X-ray Spectra of Metals, *Phys. Rev. B*, 1, 431, 1970.
96. a) **Gadzuk, J. W. and Sunjic, M.,** Excitation Energy Dependence of Core-Level X-ray Photoemission-Sectra Line Shapes in Metals, *Phys. Rev. B*, 12, 524, 1975. b) **Gadzuk, J. W.,** Plasmon Satellites in X-ray Photoemission Spectra, *J. Electron Spectrosc. and Relat. Phenom.*, 11, 355, 1977.
97. **Manne, R. and Aberg, T.,** Koopmans Theorem For Inner Shell Ionization, *Chem. Phys. Lett.*, 7, 282, 1970.
98. **Fadley, C. S.,** Peak Intensities and Photoelectron

Cross Sections in the Sudden Approximation, *J. Electron Spectrosc. Relat. Phenom.*, 5, 895, 1974; **Fadley, C. S.,** in *Electron Spectroscopy: Theory, Techniques and Applications,* Vol. 2, Brundle, C. R. and Baker, A. D., Eds., Academic Press, New York, 1978, 1.

99. a) **Kowalczyk, S. P., Ley, L., McFeeley, F. R., Pollack, R. A., and Shirley, D. A.,** *Phys. Rev. B,* 8, 3583, 1973; **Pollack, R. A., Ley, L., McFeeley, F. R., Kowalczyk, S. P., and Shirley, D. A.,** Characteristic Energy Loss Structure of Solids from X-ray Photoemission Spectra, *J. Electron Spectrosc. Relat. Phenom.*, 3, 381, 1974; **Ley, L., McFeeley, F. R., Kowalczyk, S. P., Jenkin, J. G., and Shirley, D. A.,** Many-body Effects in X-ray Photoemission from Magnesium, *Phys. Rev. B,* 11, 600, 1975; **Kowalzyk, S. P., Ley, L., Martin, R. L., McFeeley, F. R., and Shirley, D. A.,** Relaxation and Final-State Structure in XPS of Atoms, Molecules and Metals, *Discuss. Faraday Soc.*, 7, 1975. b) **Pollack, R. A.,** Ph.D. thesis, University of California, Berkley, 1972.
100. a) **Bohm, D., and Pines, D.,** *Phys. Rev.*, 82, 625, 1951; **Pines, D. and Bohm, D.,** A Collective Description of Electron Interactions II. Collective vs. Individual Practicle Aspects of the Interaction, *Phys. Rev.*, 85, 338, 1952; **Bohm, D. and Pines, D.,** *Phys. Rev.*, 92, 609, 1953; **Pines, D.** *Phys. Rev.*, 92, 626, 1953. b) **Pines, D.,** Collective Energy Losses in Solids, *Rev. Mod. Phys.*, 28, 184, 1956. c) **Pines, D.,** *Elementary Excitations in Solids,* Benjamin Publishers, New York, 1964.
101. a) **Nozières, P. and Pines, D.,** Electron Interactions in Solids. General Formulation, *Phys. Rev.*, 109, 741, 1958. b) **Nozières, P. and Pines, D.,** Electron Interaction in Solids. Collective Approach to the Dielectric Constant, *Phys. Rev.*, 109, 762, 1958. c) **Nozières, P. and Pines, D.,** Electron Interaction in Solids. The Nature of the Elementary Excitation, *Phys. Rev.*, 109, 1062, 1958. d) **Nozières, P. and Pines, D.,** Correlation Energy of a Free Electron Gas, *Phys. Rev.*, 111, 442, 1958.
102. a) **Sunjic, M. and Sokcevic, D.,** Inelastic Effects in X-ray Photoelectron Spectroscopy, *J. Electron Spectrosc. Relat. Phenom.*, 5, 963, 1974; **Sunjic, M. and Sokcevic, D.,** On the Problem of 'Intrinsic' vs. 'Extrinsic' Scattering in X-ray Photoemission From Core Levels of Solids, *Solid State Commun.*, 18, 373, 1976.
103. a) **Doniach, S. and Sunjic, M.,** *J. Phys. C,* 3, 285, 1970. b) **Gadzuk, J. W. and Doniach, S.,** A Soluble Relaxation Model for Core Level Spectroscopy on Adsorbed Atoms, *Surf. Sci.*, 77, 427, 1978.
104. **Schaich, W. L. and Aschcroft, N. W.,** *Phys. Rev. B,* 3, 2452, 1970; **Lundqvist, B. I.,** *Phys. Condens. Matter,* 9, 236, 1969; **Sunjic, M. and Lucas, A. A.,** *Phys. Rev. B,* 3, 719, 1971; Hedin, L. and Lundqvist, S., *Solid State Phys.*, 23, 1, 1969; **Lundqvist, S. and Wendin, G.,** *J. Electron Spectrosc. Relat. Phenom.*, 5, 513, 1974; **Cederbaum, L. C. and Domcke, W.,** *J. Chem. Phys.*, 64, 603, 1976.
105. Statements to this effect have appeared quite often in the literature and text books.
106. a) **Powell, C. J. and Swan, J. B.,** Effect of Oxidation on the Characteristic Loss Spectra of Aluminum and Magnesium, *Phys. Rev.*, 118, 640, 1960; **Powell, C. J. and Swan, J. B.,** *Phys. Rev.*, 115, 869, 1959 and 116, 81, 1959. b) **Callcott, T. A. and McRae, A. U.,** *Phys. Rev.*, 178, 769, 1969; **Smith, N. V. and Spicer, W. E.,** *Phys. Rev. Lett.*, 22, 769, 1969. c) **Pireaux, J. J., Ghijsen, J., McGowan, J. W., Verbist, J., and Caudano, R.,** Surface Plasmon Spectroscopy: photoelectron spectra from adsorbates on aluminum, *Surf. Sci.*, 80, 488, 1979. d) **Sokcevic, D., Sunjic, M., and Fadley, C. S.,** Strength of Intrinsic Plasmon Satellites in XPS from Adsorbates: dispersion and lifetime effects, *Surf. Sci.*, 82, 383, 1979.
107. **Barr, T. L.,** XPS Analysis in Pt-Metal Catalysis, *ACS Div. Petrol. Chem.*, 33, 699, 1988.
108. **Parmigiani, F., Kay, E., Bagus, P. S., and Nelin, C. J.,** *J. Electron Spectrosc. Relat. Phenom.*, 36, 257, 1985.
109. **Platzman, P. M. and Wolff, P. A.,** Waves and Interactions in Solid State Plasmas, in *Solid State Phys.*, Vol. 13, Ehrenreich, H., Seitz, F., and Turnbull, D., Eds., Academic Press, New York, 1973.
110. **Ludeke, R.,** Electronic Properties of the (100) Surfaces of GaSb and InAs and Their Alloys With GaAs, *IBM J. Res. Dev.*, 22, 304, 1978.
111. a) **Froitzheim, H., Ibach, H., and Mills, D. L.,** *Phys. Rev.* B11, 4980, 1975. b) **Ibach, H. and Mills, D.,** *Electron Energy Loss Spectroscopy and Surface Vibrations,* Academic Press, New York, 1982.
112. **Ibach, H.,** *Phys. Rev. Lett.*, 24, 263, 1970; **Ibach, H.,** *J. Vac. Sci. Technol.*, 9, 713, 1972.
113. **Bohm, D. and Gross, E. P.,** *Phys. Rev.*, 75, 1851, 1864, 1949.
114. **Anderson, P. W.,** Infrared Catastrophe in Fermi Gases with Local Scattering Potentials, *Phys. Rev. Lett.*, 18, 1049, 1967.
115. **Nozières, P. and De Dominics, C. T.,** Singularities in the X-ray Absorption and Emission of Metals III: one-body theory exact solution, *Phys. Rev.*, 178, 1097, 1969.
116. **Barr, T. L., Greene, J. E., and Eltoukhy, A. H.,** *J. Vac. Sci. Technol.*, 16, 517, 1979; **Natarajan, B. R., Eltoukhy, A. H., Greene, J. E., and Barr, T. L.,** Mechanism of Reactive Sputtering of Indium 2: growth of indium oxynitride in mixed N_2-O_2 discharges, *Thin Solid Films,* 69, 217, 1980.
117. **Barr, T. L.,** An XPS Study of Si as It Occurs in Adsorbents, Catalysts and Thin Films, *Appl. Surf. Sci.*, 15, 1, 1983.
118. **Barr, T. L.,** Applications of Electron Spectroscopy to Heterogeneous Catalysis, in *Practical Surface*

Analysis, Briggs, D. and Seah, M. P., Eds., John Wiley, Chichester, England, 1983, chap. 8.
119. **Barr, T. L., Kramer, B., Shah, S. I., Ray, M., and Greene, J. E.,** ESCA Studies of the Valence Band and Loss Spectra of Semiconductor Films: ionicity and chemical bonding, *Mater. Res. Soc. Proc.*, 47, 205, 1985.
120. **Kubiak, C. J. G., Aita, C. R., Tran, N. C., and Barr, T. L.,** Characterization of Sputter Deposited Al-Nitride and Al-Oxide by X-ray Photoelectron Loss Spectroscopy, *Mater. Res. Soc.*, 60, 379, 1986.
121. **Barr, T. L. and Yin, M. P.,** ESCA Induced Loss Spectroscopy as a Means to Determine the Surface Chemistry of C-C and C-H Containing Systems, submitted to *Langmuir.*
122. **Yin, M. P., Barr, T. L., Pino, L., Giordano, N., and Antonucci, P. L.,** ESCA Studies of the Processing of C/Pt Fuel Cell Electrodes: with emphasis on XPS induced loss results, *J. Mater. Chem.*, submitted.
123. **Meldner, H. W. and Perez, J. D.,** Observability of Rearrangement Energies and Relaxation Times, *Phys. Rev. A,* 4, 1388, 1971.
124. **Müller-Hartmann, E., Ramakrishnan, T. V., and Toulouse, G.,** Localized Dynamic Perturbations in Metals, *Phys. Rev. B,* 3, 1102, 1971.
125. **Jones, W. and March, N. H.,** *Theoretical Solid State Physics,* Vol. 1, Dover Publications, New York, (John Wiley,) p. 76, 1973.
126. **Kittel, C.,** *Introduction to Solid State Physics,* 4th ed., J. Wiley & Sons, New York, 1971, chap. 9.
127. **Fuggle, J. C., Fabian, D. J., and Watson, L. M.,** Electron Energy Loss Processes in X-ray Photoelectron Spectroscopy, *J. Electron Spectrosc. Relat. Phenom.*, 9, 99, 1976.
128. **Barr, T. L.,** ESCA Studies of Metals and Alloys: oxidation, migration and dealloying of cu-based systems, *Surf. Interface Anal.*, 4, 185, 1982.
129. **Barr, T. L.,** to be published.
130. **Natarajan, B. R., Eltoukhy, A. H., Greene, J. E., and Barr, T. L.,** Mechanism of Reactive Sputtering of Indium 1. Growth of InN in Mixed Ar-N_2 Discharges, *Thin Solid Films,* 69, 201, 1980.
131. **Johnson, E. D.,** Preparations and Surface Characterization of Planar Transition Aluminas, Ph.D. Dissertation, Cornell Univ., 1985.
132. **Briggs, D.,** Applications of XPS in Polymer Technology, in *Practical Surface Analysis,* Briggs, D. and Seah, M. P., Eds., John Wiley & Sons, Chichester, England, 1983, chap. 9.
133. **Yin, M. P., Barr, T. L., and Koutsky, J.,** to be published.
134. **Galuska, A. A., Maden, H. H., and Allred, R. E.,** Electron Spectroscopy of Graphite, Graphite Oxide and Amorphous Carbon, *Applied Surf. Anal.*, 32, 253, 1988.
135. **Siegbahm, K.,** private communication.
136. **McFeeley, F. R., Kowalczyk, S. P., Ley, L., Cavell, R. C., Pollack, R. A., and Shirley, D. A.,** *Phys. Rev. B,* 9, 5268, 1974.
137. **Park, R. L., Houston, J. E., and Laramore, G. E.,** Proc. 2nd Int. Conf. on Solid Surf. 1974, *Jpn. J. Appl. Phys.*, Suppl. 2, (Part 2), 1974, 757.
138. **Weissmantel, C., Bewilogua, K., Schurer, C., Breuer, K., and Zscheile, H.,** *Thin Solid Films,* 61, L1, 1979.
139. **Liang, W. Y., and Cundy, S. L.,** *Philos. Mag.*, 19, 1031, 1969.
140. **Luries, I. G. and Wilson, J. M.,** *Surf. Sci.*, 65, 476, 1977.
141. **Tsai, Hsiao-Chu and Bogy, D. B.,** *J. Vac. Sci. Technol.*, A5(6), 3287, 1987.
142. **Rohatgi, P. K., Dahotre, N. B., Liu, Y., Yin, M. P., and Barr, T. L.,** Tribological Behavior of Al Alloy-Graphite and Al Alloy-Microcrystalline Carbon Particle Composites, in *Cast Reinforced Metal Composites,* 1988 World Mater. Congr. Proc. Ed. Fishman, S. G. and Dhinga, A. K., ASM, Chicago, IL, 367, 1988.
143. **Rohatgi, P. K., Liu, Y., Yin, M., and Barr, T. L.,** A Surface Analytical Study of Tribodeformed Aluminum Alloy 319-10 Vol.% Graphite Partical Composite, *Mater. Sci. Eng.*, A123, 213, 1990.